Ana Patrícia Martins de Jesus

Establishing a Diphtheria Toxin-sensitive system for cell ablation within the embryonic small intestine in mouse

UNIVERSIDADE DO ALGARVE

Faculdade de Ciências e Tecnologia

2016

Ana Patrícia Martins de Jesus

Establishing a Diphtheria Toxin-sensitive system for cell ablation within the embryonic small intestine in mouse

Mestrado Integrado em Engenharia Biológica

Trabalho efetuado sob a orientação da Doutora Natalia Soshnikova

e coorientação do Professor Doutor José Bragança

UNIVERSIDADE DO ALGARVE

Faculdade de Ciências e Tecnologia

2016

Establishing a Diphtheria Toxin-sensitive system for cell ablation within the embryonic small intestine in mouse

Declaração de autoria de trabalho

Declaro ser o autor deste trabalho, que é original e inédito. Autores e trabalhos consultados estão devidamente citados no texto e constam da listagem de referências incluída.

_____

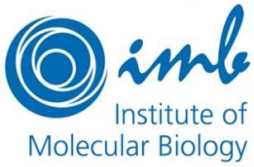

Establishing a Diphtheria Toxin-sensitive system for cell ablation within the embryonic small intestine in mouse

Ana Patrícia Martins de Jesus

2016

The work presented in this thesis was conducted at the Institute of Molecular Biology (Mainz, Germany), in the Developmental and Stem Cell Biology Laboratory, under the supervision of Dr. Natalia Soshnikova and co-supervision of Maxim Norkin.

There is no passion to be found in playing small, in settling for less than the life you are capable of.

Nelson Mandela

AKNOWLEDGMENTS

First of all, I would like to express my gratitude to my supervisors – Dr. Natalia Soshnikova, for giving me the opportunity to do my internship at the Developmental and Stem Cell Biology Laboratory of the Institute of Molecular Biology, and to Dr. José Bragança, for allowing me to give my first steps in the science world in his laboratory.

To my lab colleagues – Juri, Margarita, Lira and Maxim – thank you for receiving me so well, for all the help and companionship. To my blondie Berith, for all the good moments, delicious donuts and unforgettable memories.

To my friends who were always present, even though we were kilometers apart – Patrícia, Tatiana, Ana Raquel e Margarida.

To Eduarda, the first person I have worked with, my eternal gratitude for the all support during my time in (rainy) Germany and also for helping me keep my mental sanity during not so brighter times.

To my parents, who always gave me the freedom to design my own path and encouraged me to pursue my dreams, and my little sister, Catarina, that always knows how to put a smile on my face.

Finally, and even though a thank you is not enough, to João – who encouraged me to go abroad and never stopped believing in me when everything else was falling apart. Thank you for always being by my side.

i. ABSTRACT

The mouse small intestine possesses a highly complex structure with finger-like protrusions – villi – surrounded by invaginations called the crypts of Lieberkühn. Until it reaches its mature form, the embryonic small intestine undergoes a series of morphological and molecular changes. However, little is known about the molecular program involved in the development and establishment of the mouse small intestine.

Id2, an inhibitor of DNA binding and differentiation, has been found to play a role in several biological processes, such as stem cell maintenance and tumorigenesis, and is a plausible candidate to be involved in the mechanisms mentioned above.

The present study investigated the possible *Id2* role in the development of the mouse small intestine through the ablation of the $Id2^+$ cell population *via* Diphtheria Toxin (DT). The work conducted aimed to establish a DT-sensitive cell system for the ablation of the $Id2^+$ cell population in the mouse embryonic small intestine, and compare the genetic profiles between sorted $Id2^+$ epithelial $iDTR^-$ and $iDTR^+$ cell populations. It was also proposed to evaluate the contribution of *Id2* in the emmergence of the $Lgr5^+$ cell population.

Upon treatment of the embryos with DT, apoptosis was detected by immunohistochemistry targeting γH2AX in the $iDTR^+$ embryos, with changes in the morphology of the $iDTR^+$ embryonic small intestine also being showed by hematoxylin and eosin staining. Furthermore, upon cell sorting, $Id2^+$ cells were found to be reduced when compared to control.

Gene expression of the sorted cells by qPCR also showed a decrease in *Id2* levels. Analysis of the high-red $iDTR^+$ cell population by qPCR of a panel of genes – *Lgr5*, *PUMA*, *Ascl2*, *Wnt6*, *Wnt11*, *Sfrp5*, *Rspo1*, *Rspo3*, *Snai2*, *Smoc2*, *Id1*, *Id3*, *Kcnq1*, *Kcne3*, *TBP*, *St8sia3*, *Slc2a3*, *OneCut2* – suggests that this cell population acquires proliferative and stem cell characteristics. The analysis of the non-red $iDTR^+$ cells genetic profile also suggests a proliferative character.

Key words: Embryonic small intestine, cell ablation, Diphtheria Toxin, $Id2^+$.

ii. RESUMO

O intestino delgado de ratinho possui uma estrutura altamente complexa, apresentando protrusões – as vilosidades – rodeadas por invaginações, designadas criptas de Lieberkühn. O intestino delgado embrionário passa por uma série de alterações morfológicas e moleculares até atingir o seu estado maturo. No entanto, pouco se sabe acerca dos programas moleculares envolvidos no desenvolvimento e a maturação do intestino delgado de ratinho.

O gene *Id2*, um inibidor de ligação do DNA e de diferenciação, é descrito como possuindo um papel relevante em vários processos biológicos, nomeadamente na manutenção de células estaminais e a tumorigénese, sendo então um possível candidato a estar envolvido nos mecanismos mencionados anteriormente.

O trabalho apresentado investigou o possível envolvimento de *Id2* no desenvolvimento do intestino delgado de ratinho, através da ablação da população celular $Id2^+$ mediada pela *Diphtheria Toxin* (DT). Este projeto teve como objetivo estabelecer um sistema de células sensíveis à ação da DT para proceder à ablação da população celular $Id2^+$ no intestino delgado embrionário de ratinho, bem como comparar os perfis genéticos entre células epiteliais $iDTR^-$ e $iDTR^+$ isoladas. Outro dos objetivos propostos foi avaliar a contribuição de *Id2* no aparecimento da população celular $Lgr5^+$.

Após o tratamento dos embriões com a DT, foi detetada apoptose nos embriões iDTR+, através de ensaios de imunohistoquímica, tendo como alvo γH2AX, bem como alterações na morfologia destes embriões, detetada por *staining* com hematoxilina e eosina. Além disso, detetou-se uma redução na população $Id2^+$ em embriões $iDTR^+$, comparativamente às condições controlo.

Através de análise por qPCR, as células isoladas apresentaram um decréscimo da expressão de *Id2*. A população de células $Id2^+$ *high-red* foi analisada geneticamente para o seguinte conjunto de genes – *Lgr5*, *PUMA*, *Ascl2*, *Wnt6*, *Wnt11*, *Sfrp5*, *Rspo1*, *Rspo3*, *Snai2*, *Smoc2*, *Id1*, *Id3*, *Kcnq1*, *Kcne3*, *TBP*, *St8sia3*, *Slc2a3*, *OneCut2* –, e os resultados sugerem que esta população celular adquire características proliferativas e de células estaminais. A análise do perfil genético de células $Id2^+$ *non-red* sugere igualmente um perfil proliferativo.

Palavras-chave: Intestino delgado embrionário, ablação celular, *Diphtheria Toxin*, $Id2^+$.

iii. TABLE OF CONTENTS

iv. LIST OF ABBREVIATIONS

[^{3}H]dt	Tritiated thymidine
aa	Amino acids
APC	Adenomous Poliposis Coli
Ascl2	Achaete-scute family bHLH transcription factor 2
Bmi-1	B cell specific Moloney murine leukemia virus integration site 1
BMP	Bone Morphogenetic Protein
bp	Base pairs
bw	Body weight
CamKII	Calcium/calmodulin-dependent kinase
CBC	Crypt Base Columnar
cDNA	Complementary DNA
CK1	Casein Kinase 1
CO_2	Carbon Dioxide
DAPI	4', 6'-Diamidino-2-phenylindole
Dhh	Desert Hedgehog
Disp	Dipatched
DLL	Delta-like
DNA	Deoxyribonucleic acid
dsDNA	Double-stranded DNA
Dsh	Disheveled
DT	Diphtheria Toxin
DT-A	Fragment A of Diphtheria Toxin
DT-B	Fragment B of Diphetheria Toxin
E	Embryonic day
EF-2	Elongation factor 2
EGF	Epidermal Growth Factor
EGFR	Epidermal Growth Factor Receptor
EpCAM	Epithelial Cell Adhesion Molecule
Eph	Erythropoietin-producing hepatocellular
ESC	Embryonic Stem Cells
EtBr	Ethidium Bromide
FA	Formaldehyde

FACS	Fluorescence Activated Cell Sorting
Fw	Forward
Fzd	Frizzled
gDNA	Genomic DNA
GLP-2	Glucagon-like Peptide 2
GPI	Glycosylphophatidylinositol
Gpr49	G-protein coupled receptor 49
GSKβ3	Glycogen Synthase β3
h	Hour
H&E	Hematoxylin and eosin
HB-EGF	Heparin-binding epidermal growth factor-like growth factor
Hh	Hedgehog
HLH	Helix-loop-helix
Id1	Inhibitor of DNA binding/Inhibitor of differentiation 1
Id2	Inhibitor of DNA binding/Inhibitor of differentiation 2
Id3	Inhibitor of DNA binding/Inhibitor of differentiation 3
iDTR	inducible Diphtheria Toxin Receptor
Ihh	Indian Hedgehog
ISC	Intestinal stem cells
JAG	Jagged
Kcne3	Potassium voltage-gated channel, Isk-related subfamily, gene 3
Kcnq1	Potassium voltage-gated channel, subfamily Q, member 1
kDa	kilo Dalton
KO	Knockout
LD-PCR	Long Distance Polymerase Chain Reaction
Lgr5	Leucine-rich-repeat-containing G-protein-coupled receptor 5
LRC	Labelling Retaining Cells
LRP	LDL-related Receptor Protein
MAD	Mothers Against Decapentaplegic
MAPK	p38 Mitogen-Associated Protein Kinase
MeOH	Methanol
min	Minute
mRNA	Messenger RNA
mut	Mutant

NAD+	Nicotinamide Adenine Dinucleotide
NECD	Notch Extracellular Domain
NEXT	Notch Extracellular Truncation
NICD	Notch Intracellular Domain
NTM	Membrane-tethered Intracellular Domain
O/N	Overnight
OneCut2	One cut domain, family member 2
PCP	Planar Cell Polarity
PCR	Polymerase Chain Reaction
PFA	Paraformaldehyde
PKC	Protein Kinase C
proHB-EGF	Membrane-anchored form of HB-EGF
Ptch	Patched
PUMA	p53 Upregulated Modulator of Apoptosis
qPCR	Quantitative Polymerase Chain Reaction
Rev	Reverse
RNA	Ribonucleic acid
rpm	Rotations per minute
R-SMAD	Receptor associated SMAD
Rspo1	R-spondin 1
Rspo3	R-spondin 3
RT	Room temperature
SC	Stem cells
SDS-PAGE	Sodium Dodecyl Sulphate Polyacrylamide Gel Electrophoresis
sec	Seconds
Sfrp5	Secreted frizzled-related protein 5
sHB-EGF	Soluble form of HB-EGF
Shh	Sonic Hedgehog
Slc2a3	Solute carrier family 2 (facilitated glucose transporter), member 3
SMA	From gene *sma* from small body size
SMAD	Homologous of MAD protein from *Drosophila* and SMA protein from *Caenorhabditis elegans*
Smo	Smoothened
Smoc2	SPARC related modular calcium binding 2

Snai2	Snail family zinc finger 2
St8sia3	ST8 alpha-N-acetyl-neuraminide alpha-2,8-sialyltransferase 3
TA	Transit Amplifying
TAM	Tamoxifen
TBP	TATA-box Binding Protein
TCF/LEF	T-cell Factor/ Lymphoid Enhancer Factor
TGFβ	Transforming Growth Factor β
Wnt11	Wingless family member 11
Wnt6	Wingless family member 6
wt	Wild type

v. LIST OF FIGURES

vi. LIST OF TABLES

1. INTRODUCTION

1.1. Small intestine

The small intestine is a highly organized organ that, among other functions, serves mainly for absorptive and immunological purposes[1,2]. In mammals, the small intestine is the most proliferative and self-renewing structure and its epithelium is renovated every 4 to 5 days[3,4,5].

Starting in gastrulation and endoderm specification, this complex tissue undergoes a series of changes until it reaches its final form after the birth[2].

1.1.1. Adult small intestine

The adult intestinal tract can be described as a tube composed of three different layers – mucosa, submucosa and muscularis mucosa (**Figure 1.1**). Together, the epithelium, the lamina propria and the muscular mucosa constitute the mucosa – structurally and functionally, the intestine's most complex layer -, which is supported by the submucosa, a layer of connective tissue[6,7]. The submucosa is rich in inflammatory cells, nerve fibres, arteries and small venous channels, while the muscularis mucosa, in association with the enteric nervous system[8], is responsible for the intestine's peristaltic movements[6].

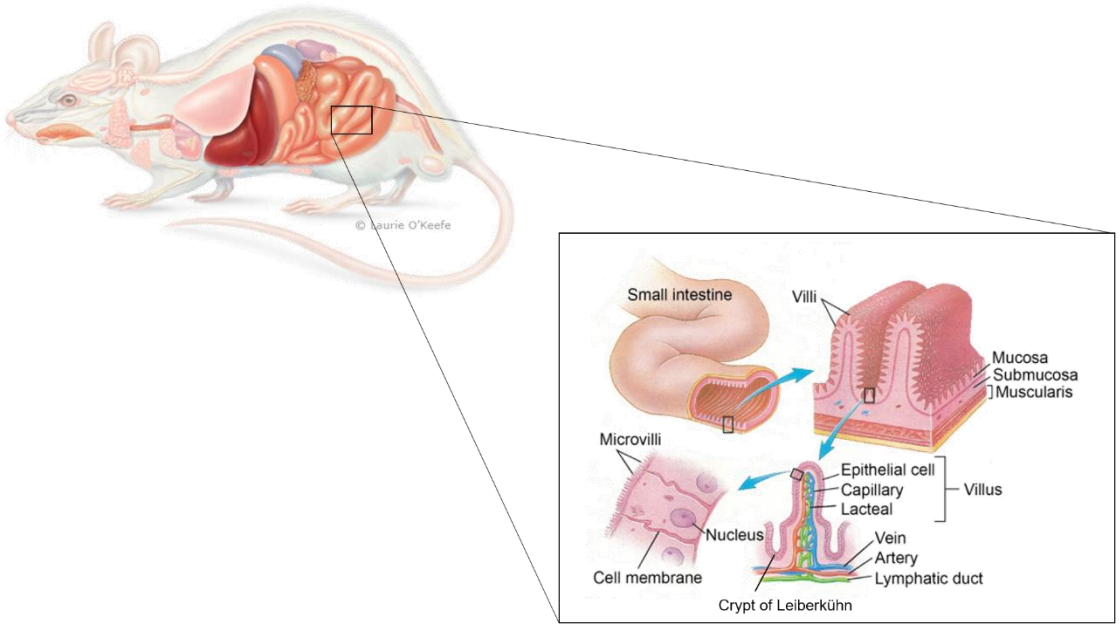

Figure 1. 1. Structure of the adult small intestine in mammals. The tubular small intestine is formed by 3 main layers of different tissues – the mucosa, the submucosa and the muscularis mucosa. These structures are oriented circumferentially around the lumen. In the mucosa, and facing the lumen, are the villi – responsible for making the small intestine the biggest surface in the body. Mouse image by ©Laurie O'Keefe (2007)[9].

The lumen, the innermost layer of the small intestine, consists of a tubular structure, in which the digested nutrients pass through, and has a very distinct morphology. It possesses finger-like protrusions, the villi[8] - due to which intestine's surface area is dramatically enlarged[1,10] -, surrounded by multiple invaginations called crypts of Lieberkühn[8] (**Figure 1.1**). Together with its characteristic morphology, the cells that populate the lumen is what allows the intestinal epithelium to carry out its function.

As the intestinal epithelial cells surround all the lumen, there are three main types of cells covering the villi – enterocytes, Goblet cells and enteroendocrine cells[1,11] (**Figure 1.2**). While the first carries out absorptive functions, the remaining are classified as secretory cells[2,12].

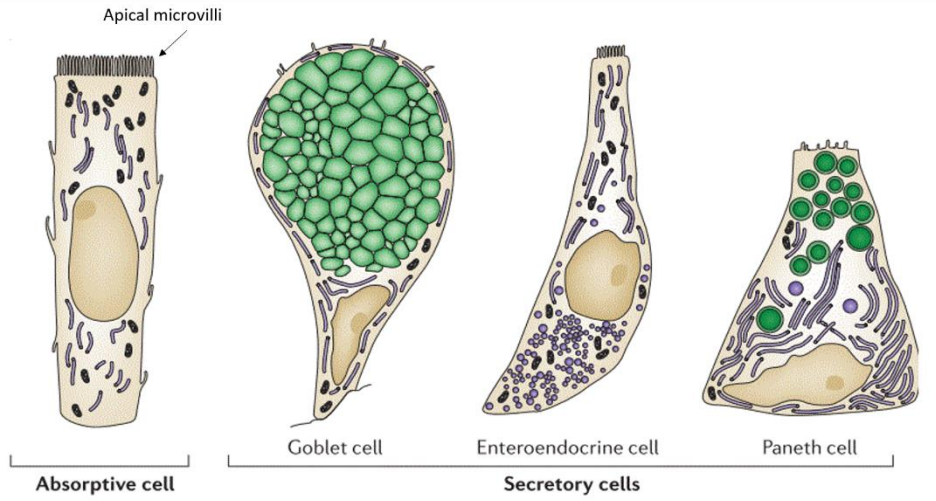

Figure 1. 2. Differentiated cells in the small intestine's epithelium. Absorptive cells are polarized and have a basal nucleus while enteroendocrine cells have neurosecretory granules. A prominent feature of Goblet and Paneth cells is their secretory granules[13] (shown in green). Image adapted from Crosnier *et al.* (2006)[12].

Enterocytes constitute more than 80% of the epithelial cells, but are mainly present at the proximal end of the small intestine. Absorptive cells, although mainly responsible for the absorption and transport of nutrients across the epithelium, also release hydrolytic enzymes[1,8]. These cells have a columnar shape, a basal nucleus and possess apical microvilli (as shown in **Figure 1.2)**, increasing their absorptive surface[13]. Goblet cells secret mucus and are found mainly at the distal end of the small intestine and in colon, where they are more needed given their lubricating role[8]. These cells are characterized by mucigen granules in their cytoplasm that will secrete mucins and other proteins. The granule contents are important for the movement

and expulsion of gut contents, as well for providing protection against shear stress and chemical damage[1]. Lastly, enteroendocrine cells, as the name suggests, are responsible for hormonal release and constitute a minor cell population (around 1%)[1,8,11]. These cells are distributed along the intestinal mucosa as intestinal cells and the hormones they secrete, such as serotonin, play an important role in the control of the gut physiological conditions[1,8,14].

Another secretory cell type found in the intestinal epithelium are Paneth cells. These cells are rich in cytoplasmic granules that, once secreted, release substances vital to the maintenance of the intestine's physiology. Among these are lysozymes, antimicrobials and defensins, which emphasises the role of Paneth cells in innate immunity and host-microbe interactions[1,8,15]. Paneth cells differ from the other differentiated cells mentioned above due to having a higher life span – they last up to 6 weeks while the others survive for only 4 or 5 days[16,15] –, and for being found at the base of the Lieberkühn crypts[1,8].

Due to the harsh conditions the intestinal epithelium is continuously exposed to, there is a need for a rapid self-renewal of the epithelial cells. This process is coordinated by the proliferative compartment found in the Lieberkühn crypts. Here, besides Paneth cells, two cell populations can be found – intestinal stem cells (ISC) and transit amplifying (TA) cells[7,16] –, the latter giving rise to 250 new epithelial cells per day[17,18]. These new epithelial cells migrate upwards – from the bottom of the crypt until the top of the villus – and undergo differentiation until they reach the crypt-villus junction[17,18]. At this point, the completely differentiated cells continue to travel upward the villi. In order to keep the balance in the number of epithelial cells, the older cells undergo apoptosis and are exfoliated at the tip of the villus, as the newly differentiated cells migrate from the crypt to substitute them. The exception are the Paneth cells, that migrate downwards and establish themselves at the bottom of the crypts[1,8, 13,15,16].

The position of each cell type along the crypt-villus axis is portrayed in **Figure 1.3**.

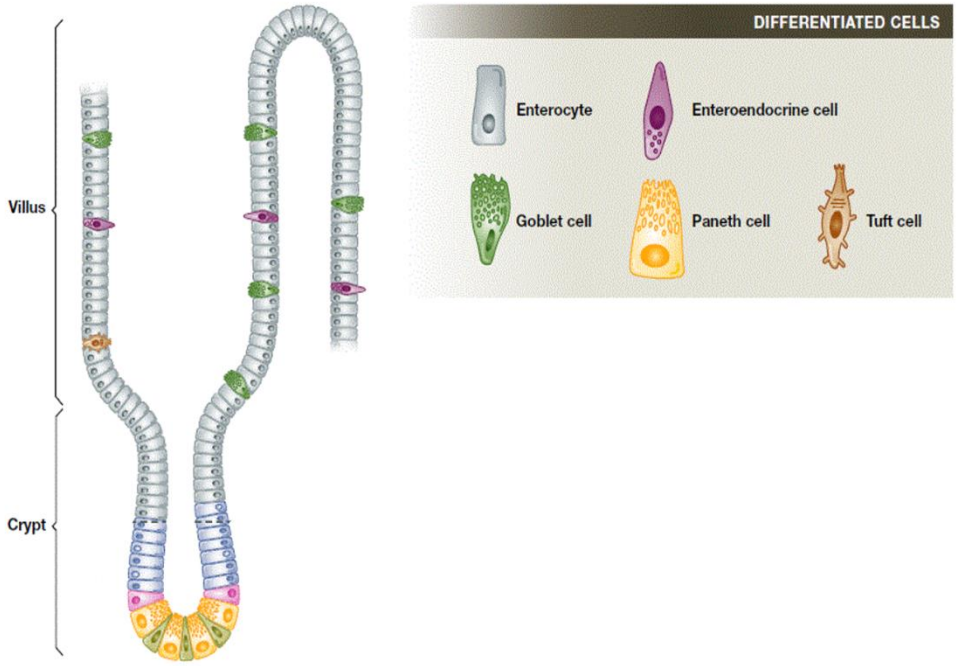

Figure 1. 3. Localization of the different cell populations in the crypt-villus axis of mouse small intestine epithelium. The crypt-villus axis is divided into two compartments: a proliferative and monoclonal one, maintained by stem cells – the crypts –, and a differentiated and polyclonal one – the villus[13]. Image from Sancho *et al.* (2015)[19].

Until it reaches the morphological structure presented in **Figure 1.3**, the small intestine undergoes a series of changes along its differentiation process from the embryonic endoderm[2].

1.1.2. Small intestine in embryos

Once all the germ layers – endoderm, mesoderm and ectoderm – are established in the early vertebrate embryo, the primitive gut tube is formed as a consequence of the series of morphogenic changes occurring in the endoderm[2,20,21].

The formation of primitive gut starts with the endoderm closure at the anterior and posterior intestinal portals, progressing towards the middle of the embryo where they will meet and form a closed tube around embryonic day (E) 8.0 and E9.0[2,20,22] (**Figure 1.4**). As the gut tube forms, the epithelium undergoes a patterning process along the anterior-posterior axis that gives rise to the foregut at the anterior region, and to the midgut and hindgut at the posterior region of the tube[7,20]. The foregut will give rise to esophagus, lungs, thyroid, liver, pancreas and stomach, while the midgut and hindgut will differentiate into the small and large intestine,

respectively[2,20]. At E9.5, the simple epithelium condenses into a pseudostratified epithelium and, from this stage until E13.5, as the tube lengthens to the size of the embryo, the mesenchyme and the lumen also increase their size[20,21,23].

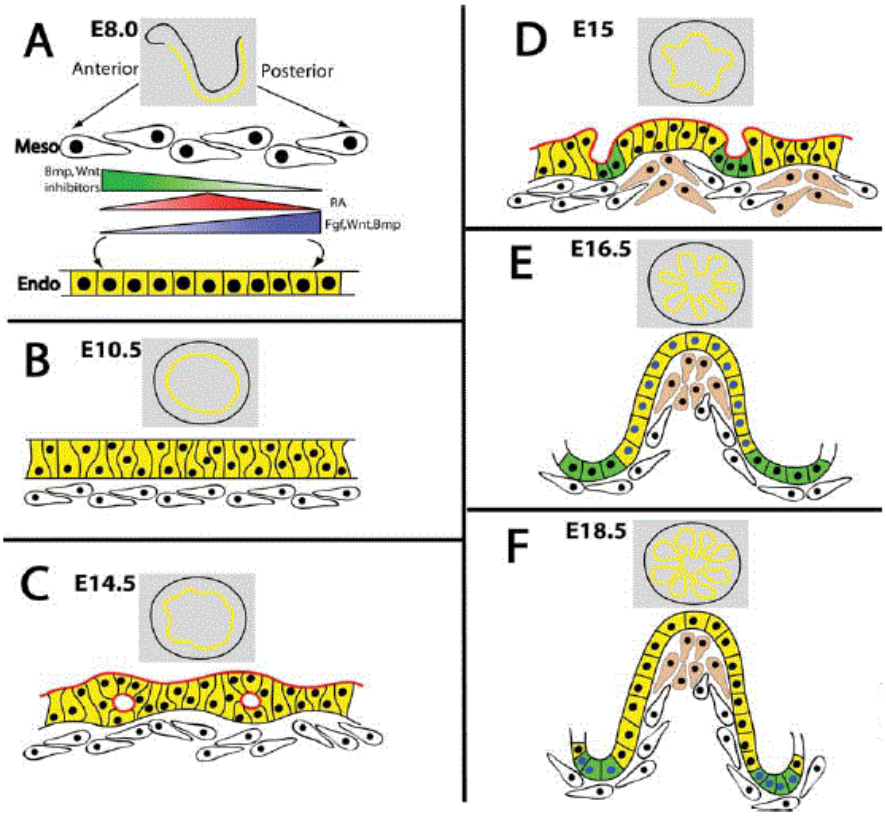

Figure 1. 4. Schematic representation of embryonic intestinal development in mouse. (A) From E8.0 to E9.5, the primitive gut tube is formed. At E10.5, the epithelial endoderm is pseudostratified (B) and after morphological changes occurred will give rise to a stratified epithelium (C). (D) Villi begin to emerge around E15.0 and are fully developed by E16.5. (E) By E18.5, the intestine has its adult morphology and the proliferative cells (green) only exist at the bottom of the crypts (F). Image adapted from Spence *et al.* (2011)[2].

With the gut tube formed, the epithelium is reorganized at E14.5. The pseudostratified epithelium undergoes morphologic changes – it changes from a tightly packed simple epithelium with nuclei at several levels to a stratified one with nuclei at the basal level[2,21]. At the same developmental day (E14.5), villi start to form due to the invagination of mesenchyme into the epithelium[7]. Both processes – villus emergence and epithelial restructuring take place in a proximal-to-distal manner[20,21].

As the villi emerges, proliferation increases at the base of the villi and becomes progressively less abundant on the villus epithelium[2,7,21]. By E17.0, proliferating cells become confined to the crypts of Lieberkühn[2,21]. Stem cells are also present in the intervillus region and, together with the proliferative cells, they will be responsible for the maintenance of the adult small intestine[21].

1.2. Stem cells

In the small intestine, homeostasis is maintained through the activity of a minor population of long-lived resident stem cells [4,5,8,24], together with the balance between stem cell proliferation and renewal with differentiation[25].

In general, stem cells (SC) are present in an organism through the embryonic stage and adult life and are characterized by two major properties – their self-renewal capacity and the ability to generate all the cell types of the organ where they reside[26].

During the embryonic development, cells of the inner cell mass of the blastocyst will give rise to all the three germ layers – endoderm, ectoderm and mesoderm. Embryonic stem cells (ESC) can be derived from the inner cell mass and retain the capacity to differentiate into all cells of the adult organism, i.e. they are pluripotent. On the other hand, adult stem cells are multipotent, since they can only self-renew and differentiate into the different cells of the specific tissue from which they were isolated[16].

1.2.1. Stem cells in adult small intestine

As mentioned in section 1.1.1, there are two cell populations in the intestine's crypt – ISC and TA cells –, which, together with Paneth cells, are responsible for the renewal of the intestinal epithelium, thus keeping homeostasis. ISC are confined to the bottom of the crypts (**Figure 1.5**) – where approximately six individual cells are present –, and are responsible to fuel the cells for epithelial renewal and are the only source of cells for the renewal of the epithelium, so its population should be kept constant[1,13].

Currently, there are two models that hypothesise how the ISC population is maintained – the Deterministic and the Stochastic model. The Deterministic model states that individual stem cells divide asymmetrically, i.e., they give rise to one stem cell, that will be kept at the bottom of the crypt, while the other cell will become a TA cell and migrate to the proliferative zone, where it will undergo proliferation cycles every 12-16 h[7,13]. While this model describes few stem cells at the niche, the Stochastic model, on the other hand, suggests that many stem

cells reside at the bottom of the crypt and that, as they divide symmetrically, stem cells produce either two stem cells (meaning no TA cells), one stem cell and one TA cell or two TA cells (meaning no daughter stem cell), which leads to an unbalance between the descendants of each stem cell lineage over time[13,27]. The Stochastic Model is also known as Niche model, as it suggests the existence of an environment at the bottom of the crypt – termed niche – that determines the "stemness" of the cells through the action of intracellular factors[13].

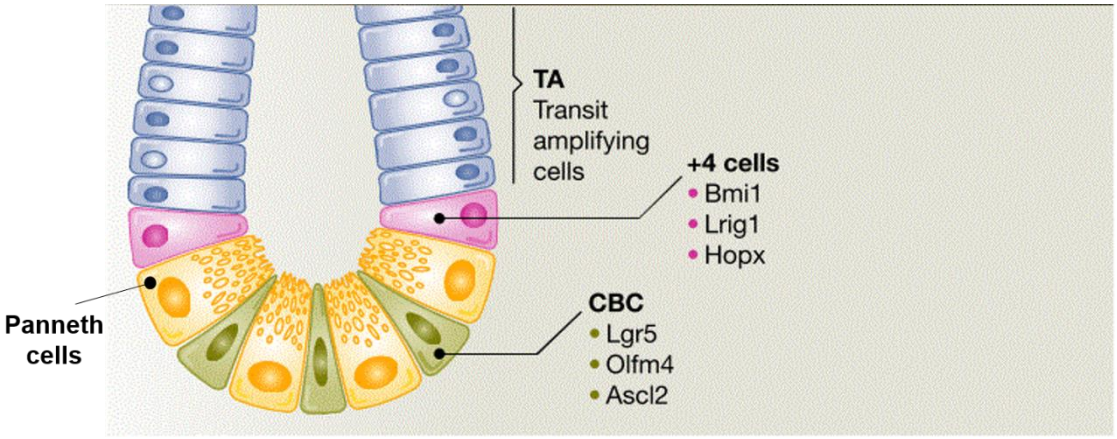

Figure 1. 5. Stem cells of the small intestine. There are two stem cell populations reported in the literature - +4 cells and Crypt Base Columnar (CBC) cells. The genetic markers of each population are also portrayed. Image adapted from Sancho *et al.* (2015)[19].

Two stem cell populations exist in the small intestine (**Figure 1.5**) – Crypt Base Columnar (CBC) cells and +4 label retaining cells (LRC) –, but their specific location within the crypt is not well known. It has been proposed that either they are located just above Paneth cells or within the fourth and fifth cells from the bottom of the crypt[28]. Currently, there are two models that describe these stem cell populations – the Classic model and the Stem Cell Zone model. The first one is based on the findings of Cairns *et al.* (1975) and Potten *et al*. (1974) and the second one in the work developed by Cheng and Leblond (1974)[29].

In 1974, Cheng and Leblond proposed that a small population of undifferentiated elongated cells located amongst Paneth cells and near the base of crypt were the cells from which all the differentiated cell types in the intestine would derive from[30]. This conclusion came after they discovered that crypts were not populated only by Paneth cell but also by actively dividing columnar cells, while doing electronic microscopy studies[31,32]. These cells - slender, immature and cycling – were called CBC cells and it was also found that they are sensitive to

tritiated thymidine ([^{3}H]dT) exposure[30,31]. The authors also reported that the surviving CBC cells would phagocyte surrounding damaged cells after [^{3}H]dT exposure. These radioactive phagosomes were initially present only in occasional CBC cells, but were latter detected within differentiated cells belonging to the four cell lineages in the intestine[18,30,31,33]. These findings were interpreted as a proof of CBC cell's stemness.

Moreover, the CBC stem cell model suggests that these stem cells have a division cycle of 24h and that their progeny moves to cell position 4-5, where they continue to divide with a daily cycle[30].

On the other hand, the Classic Model, proposed by Potten in 1974, states that stem cells reside at position +4 relative to the crypt bottom, immediately above of the highest Paneth cell in the small intestine[1,4,30,34], as shown in **Figure 1.5**. After cell tracking experiments, these authors reported that the cells at +4 position were sensitive to X and γ radiation and had labelling retaining properties - both desirable stem cell characteristics. Sensibility to radiation would prevent genetic abnormalities from being passed on to the progeny cells and the long-term DNA label retention is a result of the asymmetrical segregation of DNA, meaning that while the template DNA strands are retained in the +4 stem cells, the daughter cells inherit a newly synthetized strand[8,30,18,35]. Also called LRC, +4 cells also have an active proliferative cycle of 24 h, like CBC[35].

To note that studies conducted by Potten at the time failed to show that +4 cells can give rise to all the differentiated lineages in the intestinal crypt[36]. Also, this model is still to validate since 1) some proposed stem cell markers for this population are poorly characterized and 2) some of the already validated ones seem to mark epithelial cell populations with cellular features distinct from the LRC population described by Potten[37].

1.2.2. Stem cell markers

Although the localization of the stem cell populations in the intestine is relatively known, their identification and isolation is still a challenge. In order to overcome this, the identification of valid ISC markers is of key importance.

The list of potential ISC markers includes Lgr5, Bmi-1, Mushashi-1, m-Tert, Ascl2, Sox9 and OLFM4, among others[8,19,30,31,38]. However, with exception of Lgr5 and Bmi-1, none of the other markers have yet been related with cells capable of multi-lineage differentiation[30]. Therefore, only Lgr5 and Bmi-1 will be discussed.

Barker *et al*. (2007) reported Lgr5 (Leucine-rich-repeat-containing G-protein-coupled receptor 5), also known as Gpr49 (G-protein coupled receptor 49), as a marker for CBC cells. Lgr5 is a 7 transmembrane protein that acts as a receptor for antagonists of the Wnt pathway – the R-spondins – and also marks proliferative cells in several other adult tissues[4,35,38]. In their study, the authors showed that this marker is expressed at the bottom of the intestinal crypts of adult mice and that $Lgr5^+$ cells gave rise to long-lived clones containing all intestinal cell types. With these findings, Lgr5 was then considered the most reliable ISC marker[39,40].

On the other hand, Bmi-1 (B cell specific Moloney murine leukemia virus integration site 1) is a polycomb group protein and belongs to a group of transcriptional repressors that controls the development by the regulating of cell growth and differentiation genes[28,30,41]. The work of Sangiorgi and Capecci (2008) suggested Bmi-1 as a possible marker for +4 cells by showing that this gene consistently marks long-lived cell clones and that the ablation of the Bmi-1 cell population eliminates the epithelium of whole crypt units. Also, the location of Bmi-1 single cells was reported to be above Paneth cells, in positions +4 and +5 from the base of the crypt[28,40].

With two possible ISC populations, two questions arise: 1) Could $Lgr5^+$ and $Bmi\text{-}1^+$ cells be the same population? and 2) Which one corresponds to the genuine stem cell population?

Tian *et* al. (2011) and Yan *et al*. (2012) have reported that these markers identify two distinct populations. The first author's data suggest that Bmi-1+ cells are located upstream of $Lgr5^+$ stem cells and contribute to the replenishment of the pool of active stem cells. Also, when the cells that express Lgr5 are eliminated, the number of $Bmi\text{-}1^+$ cells increases - probably to compensate the loss – and, in this conditions, contributes to the generation of all cell types in the intestine until the Lgr5 population has recovered[42]. Moreover, Yan and colleagues showed that these two stem cell populations are functionally distinct: while $Lgr5^+$ cells have a greater contribution on maintaining the small intestine's homeostasis, $Bmi\text{-}1^+$ cells are quiescent, radioresistant and, upon injury, they rapidly proliferate in order for the epithelium to regenerate[4,43]. Together, these findings support a model where different ISC populations have separate but cooperative roles within the small intestine.

Lineage tracing experiments conducted by Barker *et al.* (2007) in Lgr5-EGFP-IRES-creERT2-LacZ mice, in which LacZ expression was induced by tamoxifen (TAM), showed that

the number of cells expressing LacZ would increase as more days passed by since the induction. This supported the $Lgr5^+$ cells capability to maintain the epithelium's self-renewing state. It was also reported the existence of epithelial cells, such as Paneth and Goblet cells, amongst the LacZ-stained clones[39]. According to these authors and their findings, $Lgr5^+$ CBC cells are the genuine intestinal stem cell population.

1.2.3. Stem cell niche

The stem cell niche hypothesis was proposed in 1978 by Schofield, who described the "niche" as a microenvironment of cells contributing to the stem cell behaviour and allows them to maintain tissue homeostasis. According to this author, the SC niche is characterized by the following properties: it provides an anatomic place to regulate stem cell number, instructs stem cells to self-renew or commit to differentiation and influences their motility[13,18,44,45,46] (**Figure 1.6**).

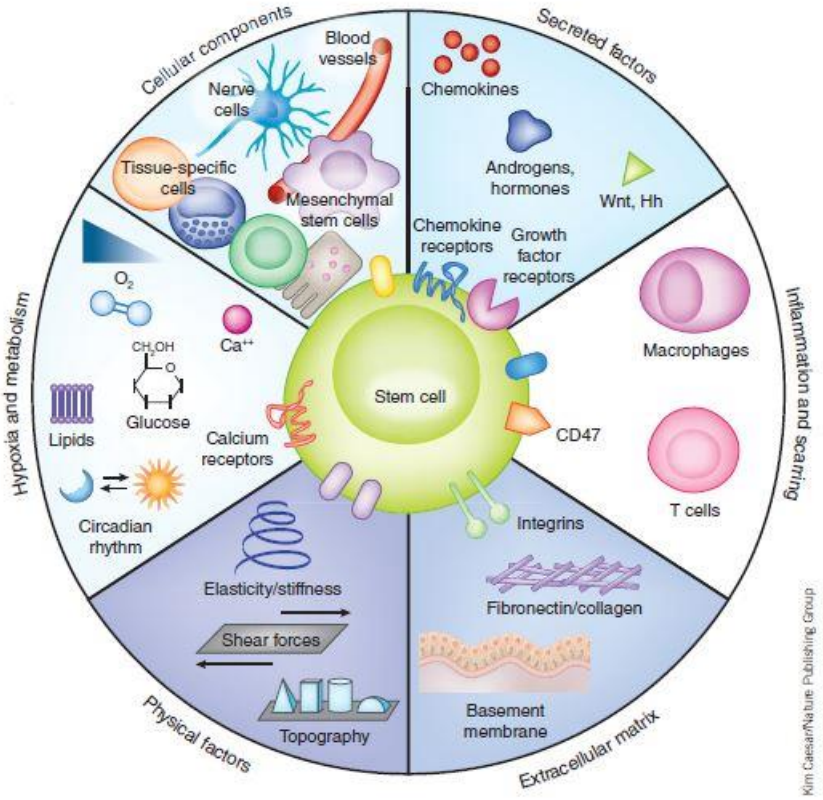

Figure 1. 6. Composition of the SC niche. Several molecular *stimuli* and cellular components take part in the maintenance of the SC niche – a complex and heterotypic dynamic structure⁴⁷⁴⁷⁴⁷. Image from Lane *et al.* (2014)[47].

Surrounding the Lieberkühn crypts, where ISC reside together with +4 cells and Paneth cells, the niche is composed by different cell types, such as myofibroblast, endothelial and neural cells, immune cells and smooth muscle cells[18,45], among other components (**Figure 1.7**).

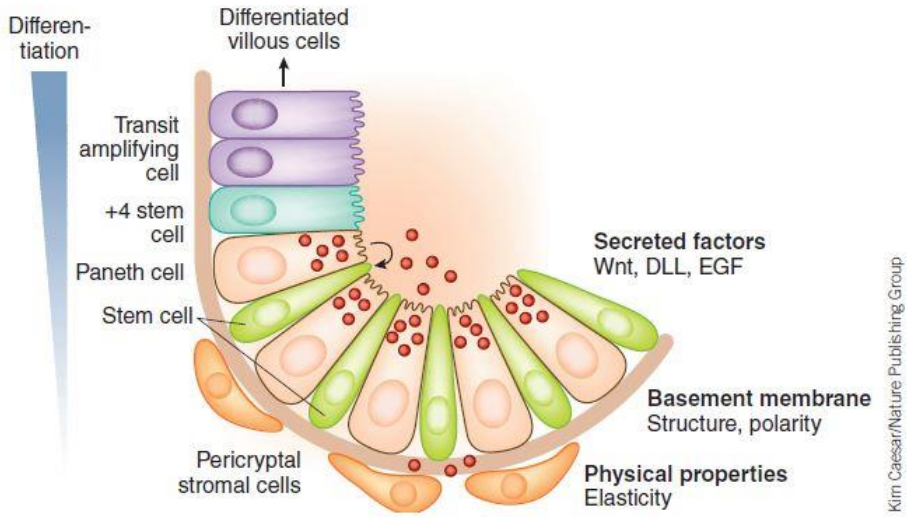

Figure 1. 7. Representation of the ISC niche. In the small intestine, Paneth cells support ISC through the segregation of Wnt3, epidermal growth factors (EGF) and Notch. Other cells types surrounding the stem cells also play a role in the maintenance of the niche. Image adapted from Lane *et al.* (2014)[47].

Paneth cells are thought to be a key component of the ISC niche, given the proximity with CBC stem cells[18] (**Figure 1.7**). Several genetic ablation and knockout studies confirmed these findings, such as the work of Sato *et al*. (2011). After the ablation of the majority of Paneth cells, these authors reported a reduction in the CBC population and also a proportional reduction in the same stem cell pool when partial ablation of Paneth cells was achieved. The remaining stem cells were always found contiguously to the remaining Paneth cells[48]. However, studies also showed that Paneth cells are only essential for the small intestine's homeostasis *in vitro* but not *in vivo*. This is supported by the studies of Kim *et al*. (2012), where CBC cells maintained their normal function when Paneth cells were completely ablated. Durand *et al.* (2012) confirmed these findings but also reported that Math1-deficient crypts required exogenous Wnt when grown in organoid culture. Together, this results point to a redundancy between Paneth cell and the stromal environment that surrounds the epithelium[18].

Located beneath the intestinal crypts, stromal cells and myofibroblast support ISC during morphogenesis, differentiation and proliferation. Studies showed that these cells express

endogenous R-spondin 3 (Rspo3) – a Wnt agonist – supporting the formation of the intestinal epithelium through the Wnt signalling pathway[45].

Another key regulator of the intestinal epithelial growth are neural cells, namely the enteric neurons. These neurons express the glucagon-like peptide (GLP)-2 receptor. GLP-2 production by a subset of enteroendocrine cells – the L cells – stimulates the proliferation of enterocytes[45,49]. The L cells can also function as a nutrient sensor[49].

Moreover, mesenchymal cells expressing Foxl1 are also reported to play a role in the niche. Aoki *et al.* (2011) showed that these cells express high levels of Rspo3 and fibroblast growth factor 2, as well as antagonists of the Bone Morphogenetic Protein (BMP) pathway. Through the ablation of Foxl1-expressing mesenchymal cells, authors reported epithelium disruption, an effect in the stem cell population by the reduction of expression of the stem cell marker Olfm4 and a reduction in Wnt signalling[50].

The maintenance of the proliferative character in the crypt, where ISC are located, and the different cell fates along the crypt-villi axis are regulated by several signalling pathways.

1.3. Cell differentiation and proliferation in the small intestine

The intestinal homeostasis, maintained by the balance between cell proliferation and differentiation, is assured by a complex network of signalling pathways, such as Wnt, BMP, Notch, Hedgehog (Hh) and Eph/Ephrin (**Figure 1.8**).

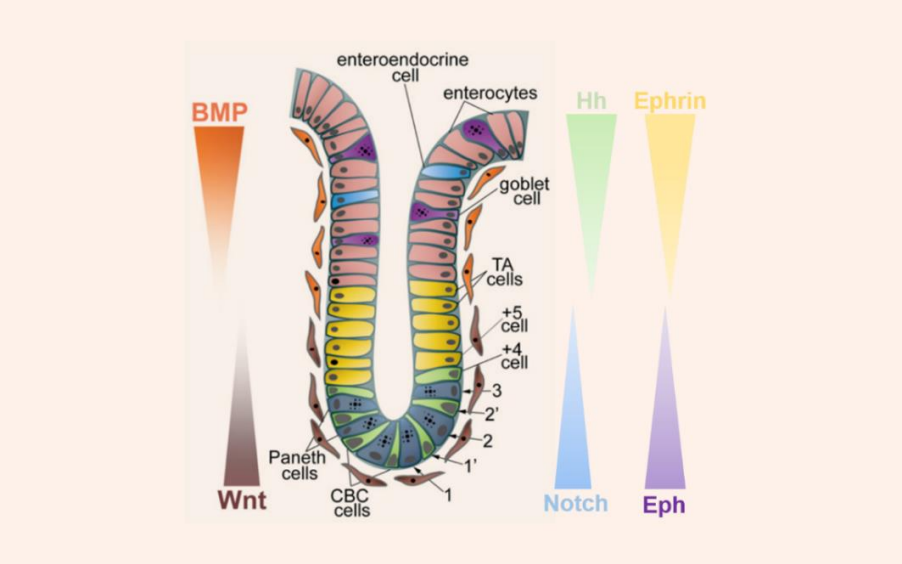

Figure 1. 8. Signalling pathways involved in the maintenance of intestinal homeostasis and their gradients of expression along the crypt-villi axis. Image adapted from Krausova and Korinek (2014)[5].

1.3.1. Wnt/β-catenin pathway

The Wnt signalling pathway is the main responsible for the proliferation of the small intestine's epithelium, and also plays a role in processes such as cell differentiation and migration, among others[1,5,51,52,53]. This signalling is ensured by 19 secreted glycoproteins of the Wnt family and its receptors – the Frizzled (Fzd) protein family, which comprises 10 members in human and mouse. The Wnt family is highly conserved through the animal kingdom and all the proteins, generally with 45 kilodalton (kDa), share conserved features essential for their function[1,30,51,52,54,55].

There are two major branches of the Wnt pathway – the canonical and the non-canonical -, being the first dependent of β-catenin, while the second is not[52].

The canonical Wnt pathway (**Figure 1.9**) activation occurs when a Wnt ligand binds to the complex formed by the seven-transmembrane Fzd receptor and its co-receptor LDL-related receptor protein (LRP) 5/6[52,55,56,57,58]. In the absence of pathway activation, β-catenin in the cytoplasm is captured by a destruction complex formed by Axin, Adenomatous Polyposis Coli (APC), Casein Kinase 1 (CK1) and Glycogen Synthase Kinase 3β (GSK3β). CK1 and GSK3β will target β-catenin for ubiquitination and proteasomal degradation through the phosphorylation of its N-terminus, thus preventing the transcription of Wnt target genes. When Wnt binds to its receptors, the intracellular part of LRP is phosphorylated by CK1γ as a consequence of the phosphorylation of Disheveled (Dsh) proteins. Axin is then recruited by

this complex and the degradation of β-catenin is avoided, leading to the accumulation of this protein in the cytoplasm. Upon translocation to the nucleus, β-catenin will displace Groucho proteins, transcriptional repressors, and interact with T-cell factor/Lymphoid Enhancer Factor (TCF/LEF), thus inducing the expression of Wnt target genes[55,57,58,59].

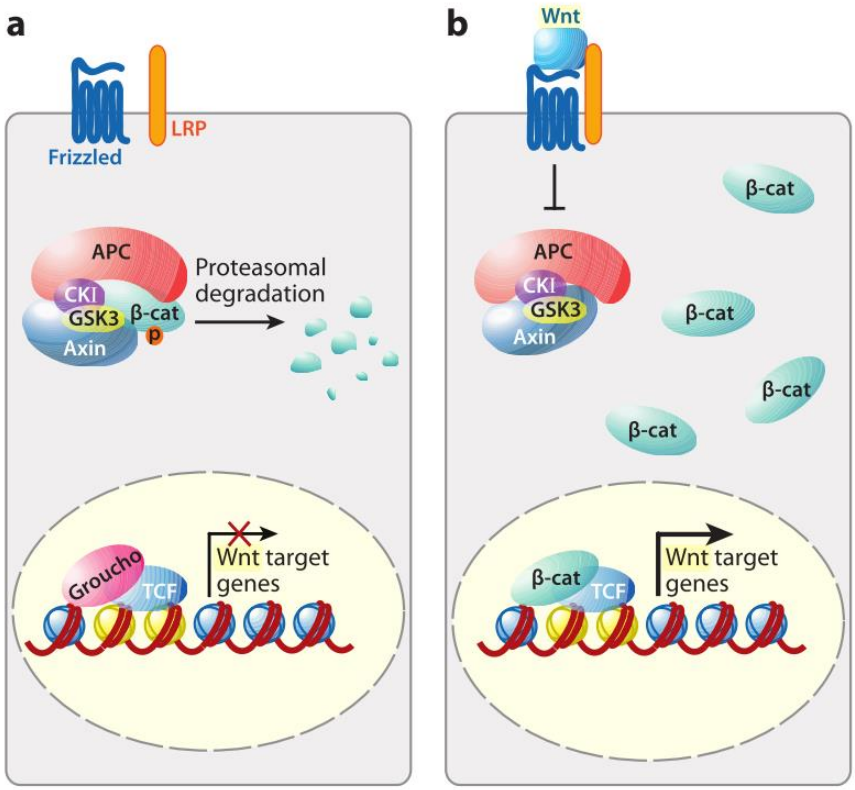

Figure 1. 9. Schematic representation of the canonical Wnt/β-catenin pathway. In the absence of the Wnt ligands Fzd and LRP5/6, β-catenin is degraded and the Wnt target genes are not expressed (a). When the canonical pathway is activated, β-catenin acumulates in the cytoplasm and, once in the nucleus, it binds to TCF/LEF to promote the expression of Wnt target genes (b)[56]. Image from van der Flier and Clevers (2009)[1].

The non-canonical pathways – Wnt/Planar Cell Polarity (PCP) and Wnt/Ca^{2+} - are less well known and its activation is independent of LRP5/6[56].

PCP controls coordinated and uniformly polarized cellular behaviours and is a critical process for many fundamental developmental processes in mammals, such as the neural tube closure and the determination of left-right asymmetry, taking part in the regulation of the actin cytoskeleton, namely the organization of polarized structures and directed migration[60,61]. Wnt signalling is required in PCP pathway, although its mechanism still remains unknown[60].

The Wnt/Ca^{2+} pathway shares some components with the PCP pathway and it's based on the finding that some Wnt molecules and Fz receptors can stimulate the intracellular release of Ca^{2+}. The calcium's release and intracellular accumulation will lead to the activation of Ca^{2+} sensitive proteins, such as protein kinase C (PKC) and calcium/calmodulin-dependent kinase (CamKII). During embryogenesis, this pathway is known to play a role in the negative regulation of dorsal axis formation, promotion of the ventral cell fate and also in heart formation[61].

Regarding the adult small intestine, the Wnt/β-catenin pathway functions as the switch between epithelial cells' differentiation and proliferation, being also essential for the maintenance of the crypt progenitor compartments[1]. Wnt is secreted by Paneth cells and the surrounding myofibroblasts and is expressed in a gradient along the crypt-villus axis, with a higher expression observed at the bottom of the crypts[51,62,63].

There are several Wnt target genes reported in the literature, such as c-Myc, involved in cell proliferation[64], Sox9, required for Paneth cells' differentiation, and Lgr5, involved in the transmission of extracellular signals[65]. Lgr5 is a receptor for R-spondins – Wnt agonists –, and this two-protein complex can associate with the complex that activates the canonical pathway, amplifying the effect of Wnt/ β-catenin signalling[51,52,58,66].

1.3.2. BMP pathway

BMPs are a group of conserved growth factors that form the largest subgroup of the Transforming Growth Factor β (TGFβ) superfamily. These factors are important morphogens that play a key role during embryogenesis and development, taking part in cell growth, apoptosis, differentiation, and also help in the maintenance of tissue homeostasis in adult organisms[58,67,68,69]. These proteins are synthetized as precursors with 400-500 amino acids (aa) and their structure is highly conserved. Once cleaved, the mature form of the protein (50-100 aa) contains seven cysteine residues. While 6 of these residues form 3 dissulfide bonds, the other cysteine is responsible for another dissulfide bond with a cysteine residue in another BMP, forming a dimer that's biologically active[67,68,69,70].

Similar to Wnt, BMP can also signal through a canonical (SMAD dependent) and non-canonical (SMAD independent) pathway[68] (**Figure 1.10**).

In the canonical pathway, the BMP receptor is a type I/II heterodimer. BMP first binds to the type I receptor and then, by affinity, the type II receptor binds to the complex and GS

domain will be phosphorylated by the type II receptor's constitutive kinase, thus converting the type I receptor into its active form[58]. Once the BMP complex is activated, it's the phosphorylation of SMAD proteins that will allow the BMP signalling. Namely, Receptor associated SMAD (R-SMAD) 1, -5 and -8 will be recruited by BMP protein complex, and once phosphorylated forms a complex with Co-SMAD4, allowing the translocation of the complex to the nucleus and the transcription of genes specifically regulated by BMPs[58,67,70,71,72].

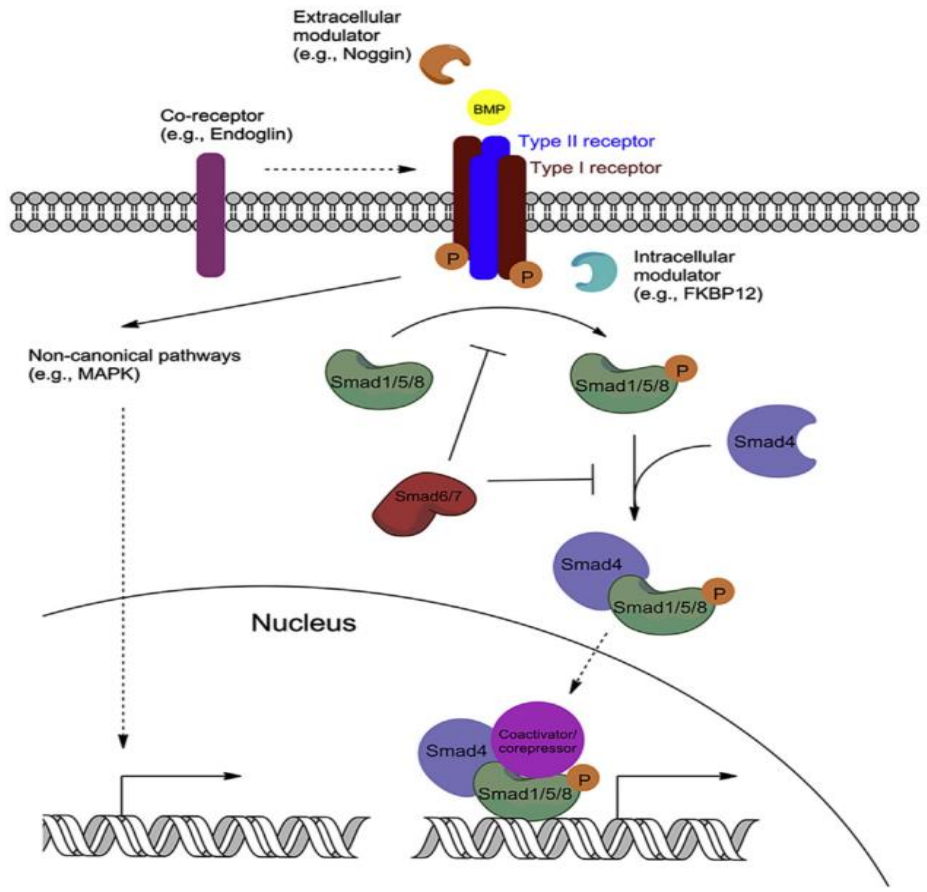

Figure 1. 10. Representation of the BMP pathway. The signal transduction initiates when BMP binds to type I or II serine/threonine kinase receptors. This association will result in the phosphorylation of R-SMADS (SMADS1, 5 and 8), that will associate with SMAD4. This complex will then translocate to the nucleus, where it further associates with coactivators or corepressors to regulate gene expression. Regulation of gene expression can also be achieved through non-canonical pathways, such as MAPK cascade. BMP signalling is modulated intracellularly (e.g., microRNAs, phosphatases and I-SMADS), extracellularly (e.g., Noggin) and also by co-receptors in the plasma membrane (e.g., Endoglin). Image adapted from Wang *et al.* (2014)[68].

SMAD-independent BMP signalling, such as MAPK (p38 Mitogen-Activated Protein Kinase) pathway, is less well known and, once it's initiated, BMPs are able to play a role on cell survival, apoptosis, migration and differentiation[67].

Depending on the pathway that interacts with BMP signalling pathway, the cellular response can change[72]. The most well studied interaction is with Wnt pathway, which contributes to the proliferation and maintenance of the epithelium in the small intestine, as stated in the previous section. In the small intestine, BMPs - produced by epithelial myofibroblasts - act as a differentiation signal and as an antagonist of Wnt signalling in the crypts, by restricting the nuclear localization of β-catenin[58,72,73].

At embryonic stages of mouse development, between E7.5 and E10.5, BMPs and their receptors are widely expressed[7]. In adult small intestine, *BMP* expression is stronger in the mesenchyme at the villus tips, while the crypts express BMP antagonists, in order to provide ISC the optimal niche for proliferation (**Figure 1.8**). This signalling is also needed for the terminal differentiation and maturation of precursors of the secretory lineage[36,58,72].

1.3.3. Notch pathway

Notch is a simple signalling pathway involved in several processes in embryonic and adult tissues, such as cell proliferation and differentiation, regulation of stem cell function and establishment of cell boundaries[1,19,25,74,75]. This pathway acts in a very unique way, given the fact that its receptors are transmembrane proteins. Thus, only the neighbour cells receive the signal – a process called lateral inhibition[25,74,76]. In mammals, there are 4 Notch receptors – Notch 1-4 –, and 5 Notch ligands, Delta-like (DLL) 1, 3 and 4, and Jagged (JAG) 1 and 2[25,74,77,78]. Both the receptors and the ligands have extracellular domains, in which EGF-like repeats are the main elements.

Notch receptors have an ectodomain termed Notch Extra-Cellular Domain (NECD) and a membrane-tethered intracellular domain (NTM). This heterodimer, which accumulates at the plasma membrane, interacts in a Ca^{2+} dependent and non-covalent manner[79].

In order to activate the Notch signalling, a series of three cleavages are needed. Once Notch is cleaved at the extracellular "S1" site, a process that occurs in the trans-Golgi network, the cell surface receptor becomes functional. Then, a second cleavage, ligand dependent, takes place, now at the "S2" site, giving origin to NEXT (Notch Extracellular Truncation), a

membrane bound activated form. Finally, NEXT is further processed at the intramembraneous "S3" and "S4" sites and the active Notch Intracelular Domain (NICD) is released[74,78,79,80,81].

NICD acts as a transcriptional regulator and will be translocated to the nucleus, where it will bind with the CSL DNA-binding protein and with the Mastermind/Lag-3 co-activator, activating the expression of Notch target genes[75,78,79]. In case NCID is absent, CSL binds to co-receptors in order to prevent the transcription of Notch target genes[78].These series of events are portrayed in **Figure 1.11**.

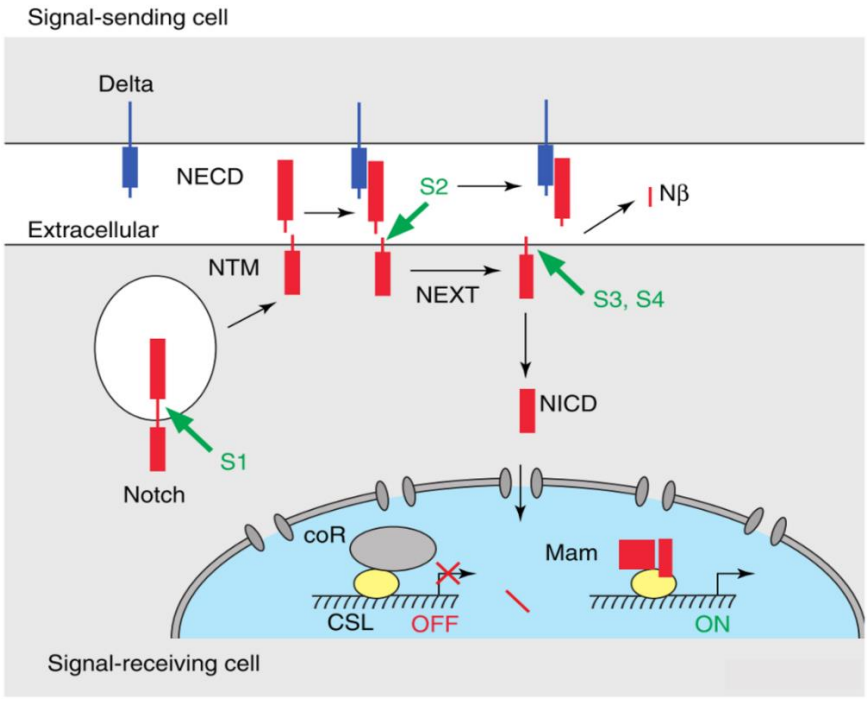

Figure 1. 11. Notch signalling pathway. Notch signalling is activated by three sequential cleavages: S2 is catalysed by the ADAM-family of metalloproteases and the S3/S4 by γ-secretase. Upon NEXT processing, NICD will translocate intro the nucleus and Nβ, a small peptide, is released[74,79]. Image adapted from Schweisguth (2004)[79].

In the adult small intestine, Notch signalling molecules are expressed in stem cells as well as in the crypt epithelial cells[7,81]. However, at embryonic stages (between E13.5 and E18.5), expression of Notch ligands and receptors was reported to occur on the mesenchyme[82].

The Notch pathway is the only one that plays two roles in the small intestine: together with Wnt, it's involved in the maintenance of cell proliferation in the crypt compartment, and it plays a major role in cell fate decisions, by inducing differentiation towards the absorptive enterocyte lineage[1,7,58].

1.3.4. Hh pathway

The Hh signalling pathway is crucial for the correct development of the embryo and its deregulation can give rise to birth defects as it plays a role in the patterning of different structures, such as the neural tube, lungs and the gastrointestinal tract. In adult organisms, Hh pathway contributes to cell differentiation, proliferation and maintenance, and thus its deregulation can lead to cancer[83,84].

In mammals, the Hh family comprises three members: Sonic Hedgehog (Shh), Indian Hedgehog (Ihh) and Desert Hedgehog (Dhh)[58,85,86]. The proteins of this family are synthetized as 45 kDa precursors that undergo autoproteolytic cleavage to produce an N-terminal signalling protein with 19 kDa with lipid modification – a palmitoyl group at its N-terminal and a cholesterol modification at the C-terminal. These modifications will control the binding of the Hh ligands to the membrane and its mobility, as well as facilitate long-range signalling despite the ligands poor solubility[83,85]. The active Hh protein secretion is mediated by two proteins – Dispatched (Disp), a multi-pass transmembrane protein, and Scube2, a secreted glycoprotein. This complex will bind to the C-terminal cholesterol group, allowing the release of Hh from the plasma membrane (**Figure 1.12 A**)[58,85,86].

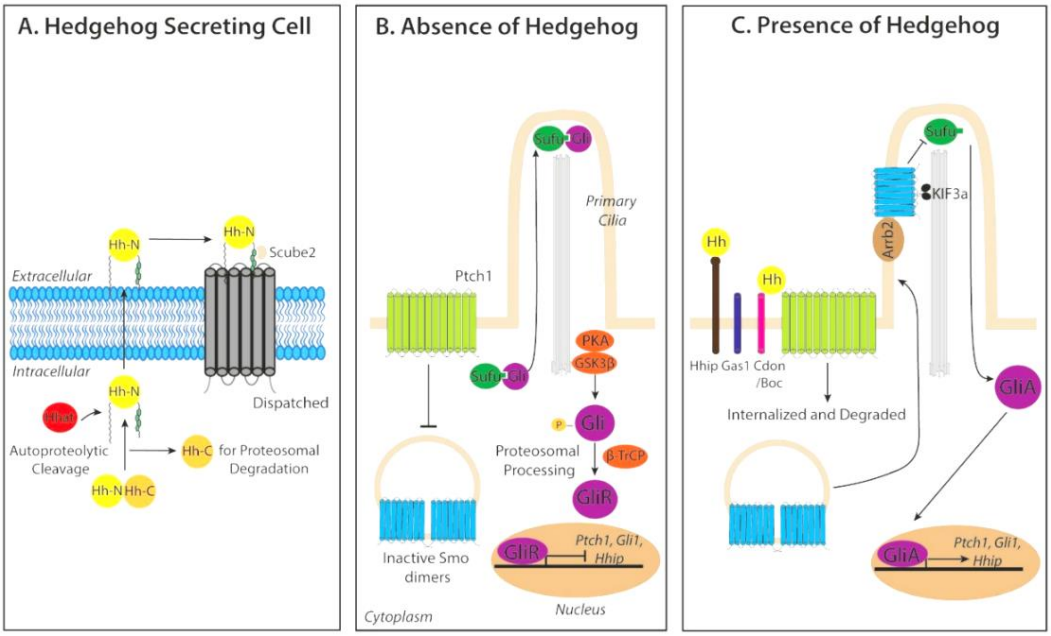

Figure 1. 12. Hh signalling pathway. The precursor of the active Hh protein undergoes some modifications until its active form is secreted with the help of proteins Disp and Scube2 (A). In the absence of Hh ligand, Ptch catalytically inhibits the activity of Smo (B). Ptch is degraded once Hh binds to it and, as a consequence, Smo is activated and the Hh signal is tranduced to the cytoplasm, allowing the transcription of Hh target genes (C)[87]. Image from Cochrane *et al.* (2015)[85].

Activation of the Hh pathway involves several cellular and molecular mechanisms (**Figure 1.12 B and C**). Hh receptor Patcher (Ptch), a 12-trasmembrane protein, inhibits Hh signalling by repressing Smoothened (Smo), a 7-trasmembrane receptor[83,84,85]. However, once Hh binds to Ptch, this complex is internalized and degraded, resulting in the accumulation of Smo in cilia and consequent Hh signalling activation[83]. Smo mediates the action of Gli proteins: in the absence of Hh ligands, Gli proteins undergo proteosomal degradation into their repressor form and will supress the expression of Hh target genes. If Smo is allowed to signal downstream, Gli proteins will act as transcription factors and regulate the target genes expression[85,86,,88].

Regarding spatial expression in the adult small intestine, *Shh* is expressed at low levels by some epithelial cells at the bottom of the crypts, while *Ihh* is expressed at the base of the villi and, at more reduced levels, at the top of the villi[58]. At embryonic stages, where Hh signalling in involved in left-right axis specification and in the regulation of villi formation, the expression of the Hh ligands varies: between E11.5 and E12.5, *Shh* and *Ihh* are expressed through the endoderm. While *Shh* expression gets downregulated by E14.5, the expression levels of Ihh don't change in the developing intestine, and by E18.5, both genes expression is confined to the intervillus epithelium[83,89]. During the small intestine's development Hh signalling acts a sensor of epithelial integrity and, together with BMP, it also establishes a gradient along the crypt-villus axis to counter-act the proliferative force driven by Wnt pathway[7,58].

1.3.5. Eph/ephrin pathway

Eph (Erythropoietin-producing hepatocellular) receptors are type I transmembrane proteins that belong to the superfamily of transmembrane Tyr kinase receptors[90,91]. These receptors are composed by three domains: an N-terminal glycosylated ligand-binding protein, a transmembrane region and an intracellular catalytic kinase domain[90]. Eph receptors are implicated in several biological processes, such as cell proliferation, adhesion and migration and cell morphology, playing a role in the spatial organization of different cell populations[91,92,93].

Ephs have high affinity to their ligands, the ephrins (Eph receptor interacting proteins), and interact with them through several sites on their N-terminal[90]. Like their receptors, ephrins are also transmembrane proteins and can be divided in two classes: class A ephrins, anchored to the membrane by glycosylphophatidylinositol (GPI), and class B, which have a

transmembrane segment and a short cytoplasmic region[93,94]. Once ligands and receptors bind, Eph clustering leads to the autophosphorylation of intracellular tyrosine residues. These residues, through the interaction with other proteins, will then trigger the downstream signalling pathway[90].

One of the prominent features of the Eph/ephrin pathway is the bidirectional signalling, meaning that both ligands and receptors are able to transduce a signalling cascade[90]. It's these Eph/ephrin bidirectional interactions that play a role in the homeostasis maintenance in the small intestine by controlling the cell positioning along the crypt-villus axis and the proliferation of progenitor cells[91]. Some of the pathway's components are targets of the Wnt/β-catenin pathway[7], which regulates the expression of a number of ephrins in differentiated cells outside the crypt in a negative manner. On the other hand, Wnt/β-catenin promotes the transcription of Ephs, and this opposite gradient is responsible for the maintenance of the proliferative and differentiated compartments in the crypt-villus axis[91,95].

As shown in the previous sections, there is a complex network of genes and pathways regulating the small intestine's development and homeostasis. It is also known that there are some proteins associated to ISC – ISC markers – but little is known about them and other putative markers. Thus, targeting specific genes can provide insights about their overall physiological functions.

1.4. Cell lineage studies

Cell lineage studies play a key role in developmental biology, since they allow to closer characterize the developmental potential of a pluripotent ESC or, in general, the capacity of one cell to give rise to its descendants[96].

Lineage tracing is one of the methods used for cell lineage studies and consists in the identification of all the progeny of a single cell. This is a key technique to understand tissue development, homeostasis and disease, and also a powerful tool to study stem cell properties in mammalian tissues, since it provides information into these cells behaviour in the context of the whole tissue or organism[97].

Although the most common techniques to perform lineage tracing experiments rely on the tamoxifen-inducible Cre-Recombinase enzyme and transgenic reporter mice[98], other methods

can be used, such as e.g. the labelling with dyes and radioactive markers, genetic mosaics or the introduction of genetic markers by transfection or viral transduction, to name a few[97].

1.4.1. Cell ablation

Targeting specific genes can provide insights into their overall physiological functions *in vivo*. However, when the aim is to gather information about the function of specific cell lineages or cell populations in whole organisms, techniques are less developed[99].

Cell ablation is one efficient method used to perform cell lineage studies and it involves the elimination of the cell population of interest. In order to achieve this, several techniques can be used, such as laser ablation, aspiration and microdissection, with the most efficient being genetic cell ablation. This technique consists in the expression of a cytotoxic gene under the control of a tissue specific promotor or a protein that triggers the death in cells sensitive to the cytotoxic products[99,100].

There are several cell ablation systems described in the literature, such as the Gfap-thymidine kinase transgenic mouse – where upon administration of the drug gancyclovir, Gfap-positive cells were ablated[101] – and the overexpression of the pro-apoptotic protein Bax in neural precursors[102]. Another substance used to achieve genetic ablation is DT (Diphtheria Toxin), where to avoid nonspecific cell damage, one of the strategies used consists in the expression of the toxin receptor in the targeted cell type. This way, the toxin is not harmful to the rest of the organism and will only ablate the specific cells in which the receptor is present at the surface[99,103].

1.4.2. Diphtheria Toxin mediated cell ablation

Diphtheria Toxin, synthetized by pathogenic strains of *Corynebacterium diphtheria*, is a single polypeptide with 535 aa and has two fragments – A and B[103,104,105]. Both them are essential for the intoxication process. Fragment B's (DT-B) role is the binding of the toxin to its cell surface receptor (HB-EGF precursor)[103,104], while DT-A – a protein with 21 kDa[105] - is responsible for the toxicity[104]. One of cytotoxic pathways described for DT is portrayed in **Figure 1.13** where, once in the cytoplasm, DT-A will catalyse the inactivation of elongation factor 2 (EF-2), which will lead to the end of protein synthesis and thus induce the apoptosis of the cell[99].

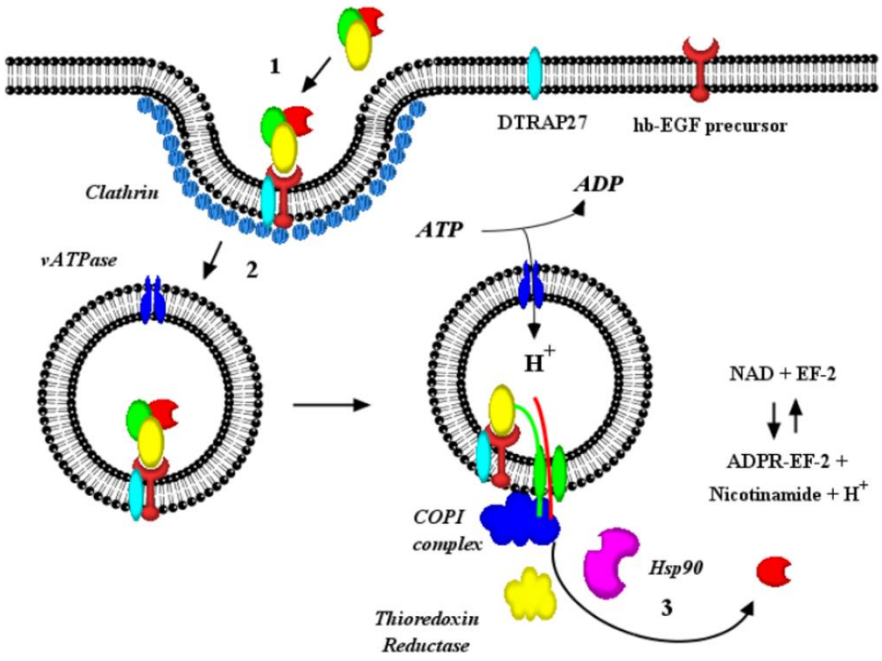

Figure 1. 13. Schematic representation of the DT entry into cells. After DT-B (yellow) binds to the HB-EGF precursor (1), the toxin is internalized into early endosomal vesicles (2). Later, and due to the acidic conditions of the late endosome, DT-A (red) is translocated to the cytosol where it catalyses the transference of the ADP-ribose moiety of nicotinamide adenine dinucleotide (NAD+) to a modified histidine residue on polypeptide chain elongation factor 2 (EF-2), inactivating it (3)[99]. Image adapted from Murphy (2011)[103].

Since DT-A is a well characterized inhibitor of protein synthesis and translation inhibition is the earliest indication of intoxication, the process described previously was taken as the only mechanism of DT toxicity[106]. However, a second cytotoxic mechanism was proposed by Chang *et al*. (1989), where they hypothesized that DT might activate a suicide pathway dependent of endogenous nucleases, similarly to other cytotoxic models described. Besides the toxin-associated deoxyribonuclease activity enhancement in the presence of Mg^{2+} and Ca^{2+}, these authors also reported that the nuclease activity was mediated by DT-A[107]. This evidence led to the conclusion that the cytolysis induced by DT is not a consequence of protein synthesis inhibition[106]. In other studies, Lee *et al*. (2005) reported that DT is able to degrade double-stranded DNA (dsDNA) through non-processive and endonucleolytic attacks, without specificity for the nucleotide sequence, and that nuclease activity can lead to the death of the target cells by itself[108].

The toxin's subunit A has high toxicity and only one molecule of this subunit in the cytosol is enough to cause cell death. Due to this, even a low expression of DT-A can ablate the target cells with high efficiency. On the other hand, if expressed non-specifically, the toxin can give rise to unwanted effects on the organism embryogenesis and morphogenesis[99]. The basic principle of this conditional cell ablation technique is portrayed in **Figure 1.14**.

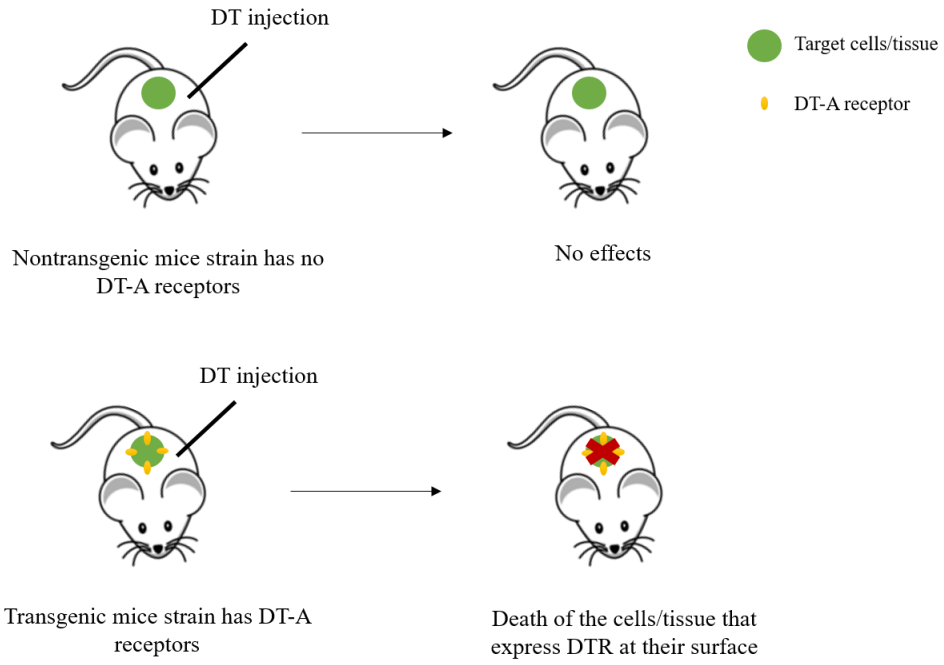

Figure 1. 14. Schematization of the DT-mediated cell ablation. Transgenic mice carry the gene that encodes the DT receptor preceded by a STOP cassette flanked by two *loxP* sites. Upon Tamoxifen administration, the STOP cassette is removed and the target cells start to express the receptor, making them sensible to the DT.

1.4.3. Diphtheria Toxin Receptor

The heparin-biding epidermal growth factor-like growth factor is a O-glycosylated protein with 22 kDa, isolated for the first time by Higashiyama *et al*. (1991)[109] from the conditioned medium of a human macrophage-like cell line[110].

HB-EGF belongs to the EGF family of growth factors, divided in four groups according to which ligand the proteins bind. In the first group, EGF, TGF-α and amphiregulin bind specifically to EGF receptor (EGFR) while the proteins of the second group, which includes HB-EGF, betacellulin and epiregulin bind to EGFR and ErbB4. The last two groups include the neuregulins (NRG1-4), where NRG1 and NGR2 bind to both ErbB3 and ErbB4, but

NRG3 and NRG4 only bind to ErbB4[111]. These proteins, along with their receptors, contribute to the development, morphonogenesis and maintenance of homeostasis in the organism[111].

When the HB-EGF binds and activates its ligands, the protein is able to participate in mitogenic, chemoattractant and cell survival activities[110]. Besides this, it also plays a role in tumour formation, heart development and maintenance, and skin wound healing[111]. HB-EGF is the only known protein of the family that plays a significant role in growth and development[110]. Several authors, such as Luetteke *et al*. (1999)[112] and Iwamoto *et al*. (2003)[113] have described that HB-EGF knockout (KO) mice died shortly after birth while KO mice for other growth factors belonging to the same family, like TGF-α, EGF and amphiregulin, did not[110,114].

Initially, HB-EGF is synthetized as a transmembrane precursor protein. The membrane-anchored form of the protein (proHB-EGF) is formed by a pro domain (propeptide and signal peptide) followed by five domains: heparin-binding, EGF-like, juxtamembrane, transmembrane and cytoplasmic, as shown in **Figure 1.15**. The soluble form of the protein (sHB-EGF), a potent mitogen and chemoattractant for a number of different cell types, is obtained through a protease cleavage[110,111].

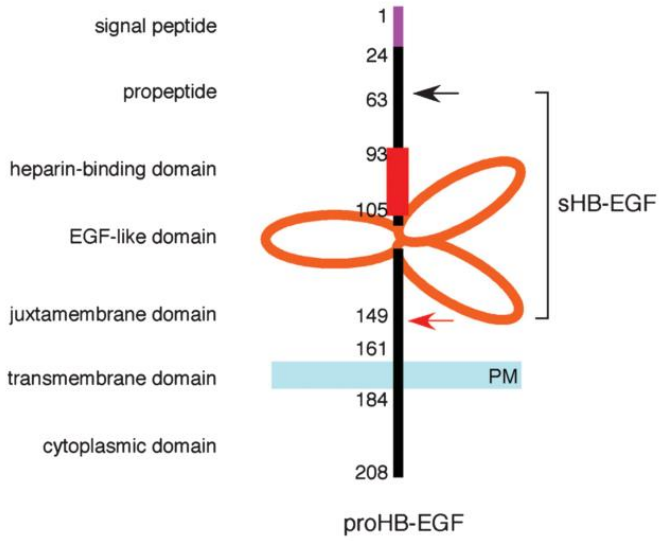

Figure 1. 15. Structure of HB-EGF protein. The mature form of HB-EGF (sHB-EGF) consists of a propeptide, a heparin binding domain and an EGF-like domain. sHB-EGF is generated by proteolytic processing at the juxtamembrane domain (red arrow). The N-terminal propeptide is also processed (black arrow), but the biological significance of this processing is not clear. Numbers in the figure indicate amino acid residues from the N-terminus. Image from Iwamoto *et al*. (2006)[114].

It's the proHB-EFG that works as the receptor for the DT-A. However, this protein/ligand recognition happens in humans, but not in mice. This is due to the 3 amino acid sequence variation between human and mouse in the EGF-like domain, being this the domain responsible for the binding of DT-A with proHB-EGF[100,110]. For this reason, the mice receptor has a lower affinity (about 10^5) to DT-A, which consequently leads to a higher DT-A resistance in mice. One of the strategies to overcome this is to create a recombinant mice strain that express a human or simian DT-A receptor (termed iDTR, inducible Diphtheria Toxin Receptor) in order to obtain specific mice cells DT-sensitive[100,104].

1.5. Id2 protein

Inhibitor of differentiation or inhibitor of DNA binding (Id) proteins belong to a highly conserved group of molecules that play major roles in various organisms, such as differentiation, cell cycle control and cell line commitment[115,116]. These proteins have a small peptide chain that possesses a helix-loop-helix (HLH) motif, and intervene in the dimerization with other basic HLH proteins, mostly E proteins. However, since Id proteins lack some basic aa essential for DNA binding, they inhibit E proteins in a negative-dominant manner by forming non-functional heterodimers, which means that genes with the E-box sequence in their regulatory elements are repressed[115,116,117].

Amongst other functions, Id proteins play an important role in stem cell maintenance, vasculogenesis, tumorigenesis and metastasis, due to their capability of inhibiting the differentiation of progenitors of different cell types, promoting the cell-cycle progression, delaying cell senescence and assisting cell migration[116].

In mammals, four Id proteins have been identified – Id1, Id2, Id3 and Id4 -, and their genes are differentially expressed in various cell types[116,118]. Id genes transcription is controlled not only by transcription factors but also through signalling pathways, such as BMP, cytokines and ligands of T cell receptors[116].

Unlike Id2, whose transcription is limited to a few cell types, being neuronal cells one of them, Id2's messenger RNA (mRNA) is ubiquitously expressed in *Mus musculus*[115,118,119]. The protein, being encoded by a gene in chromosome 12, is expressed in tissues undergoing active morphogenic activities, such as the intestine, lungs and kidneys[118]. Contrarily to what happens in other tissues, the Id2 pattern of expression does not overlap with Id1 and Id3 in tissues

derived from primitive gut. Here, Id2 is detected within the epithelium, while Id1 and Id3 expression is detected in the mesenchyme that surrounds the epithelium[118].

During gut organogenesis, Id2's mRNA is expressed in the epithelium of the gastrointestinal tract[120]. Jen *et al.* (1996) showed the expression pattern of Id2 during mouse embryonic development. By E10.5, Id2 is located in the intestinal endoderm and by E14.5, as the mesenchyme becomes gradually segregated into two areas – one will give rise to muscle layers and the cells close to the epithelium will orientate parallel to it –, Id2 is detected in the peripheral muscle cells. During villi formation, around E16.5, very low levels of Id2 expression are detected in the intestine[118]. Moreover, the Id2 gene product is thought to regulate the differentiation and cell division of enterocytes[120], since the genetic ablation of Id2 prevents the differentiation and the cell arrest of enterocytes when the crypt-villus axis is formed, and thus suggesting that this gene is involved in the lineage specific differentiation of intestinal cells[121].

2. OBJECTIVES

Until it reaches its mature form, the small intestine goes through morphologic and genetic changes during mouse embryogenesis. However, there is still not much information about the molecular programs that trigger such changes.

Plausible candidates worth further investigation are genes highly expressed in the embryonic small intestine but absent in adult ISC, and vice-versa, and genes that regulate the expression or function of signals that define the ISC identity, such as the Wnt and BMP pathways.

2.1. Project background

Previous work conducted at the Developmental and Stem Cell Biology Laboratory pointed towards a suitable candidate to study – the *Id2* gene – in order to underlie the molecular mechanisms behind the formation of a highly complex structure.

RNA sequencing of ISC and embryonic intestinal $EpCam^+$ cells showed different Id2 RNA levels in these two conditions – embryonic intestinal cells at E12.5 and E14.5 showed a similar transcriptome, while almost no Id2 RNA was detected in ISC. These results suggest a different transcriptional signature between the embryonic small intestine's epithelium and adult ISC.

Another evidence that pointed to *Id2* being a part of the molecular program responsible for the changes from the embryonic to adult stage were fluorescence activated cell sorting (FACS) experiments, where intestinal epithelial cells were isolated from Id2 wildtype (wt) and Id2 KO mouse embryos at E11.5. These results showed the appearance of an $Lgr5^+$ cell population (about 30%) in KO mice embryos, which did not occur in the wt. Wildtype mice embryos present no *Lgr5* expressing cells until E13.5, meaning that *Id2* could be involved in the induction of the expression of this ISC marker two days earlier, evidencing a possible *Id2* role in the embryonic development of the small intestine.

2.2. Goal

The goal of the present study was to perform the ablation of $Id2^+$ cells during the development of the small intestine using DT. The DT-mediated cell ablation has not been described on embryos so far, thus, it was important to establish the ablation system during mouse embryogenesis. Moreover, with the development of the cell ablation system it was then

possible to study the genetic difference between wildtype mouse embryos and Id2-ablated mouse embryos. Following the results in Id2 KO mouse embryos, one of the aims is also to gain more insight on the possible influence *Id2* might have in the appearance of the $Lgr5^+$ cell population.

3. METHODOLOGY

This study focuses on the ablation of a specific cell population during the development of the embryonic small intestine, the Id2+ cell population, as well as getting some insight about the consequences of this ablation for the surrounding cell populations.

In this experience, a mice strain expressing a Diphtheria Toxin receptor under the control of the target gene promoter was obtained, thus allowing the ablation of the cell population of interest upon administration of the toxin.

Immunostaining on histological sections was performed in order to assess the expression and location of the DT receptor, as well as the apoptosis caused by the ablation system itself. Sections were also stained in order to visualize the morphological changes derived from the treatment with the toxin.

Changes in the $Id2^+$ cell population after ablation were analyzed through FACS and some specific populations were isolated for further quantitative PCR (qPCR) analysis in order to assess the genetic differences between them.

3.1. Tamoxifen preparation and administration

Tamoxifen (Sigma) was dissolved to a final concentration of 15 mg/ml in peanut oil (Sigma) using sonication.

Pregnant female mice were anaesthetized with isoflurane (Forene® 100% (v/v), AbbVie) and 100 μg of tamoxifen per 30 g of body weight (bw) was administrated by oral gavage.

3.2. DT administration

Before injection, pregnant females were anaesthetized with isoflurane (Forene® 100% (v/v), AbbVie). 150 μl of DT (1 μg/ml, from *Corynebacterium diphtheriae,* Sigma-Aldrich) – 30 ng/ g bw – were administrated by intraperitoneal injection.

3.3. Sampling

Pregnant female mice were sacrificed by hypoxia with CO_2, followed by cervical dislocation.

Mice were dissected in order to expose the abdominal cavity and uterus was removed and placed in PBS 1x. Embryos were removed from the amniotic sac and placed in PBS 1x, where they were decapitated and organs were collected. This procedure was made under a Leica M80 (Leica Microskopie + systeme GmbH, Germany).

Embryos were then prepared for further histological experiments.

3.4. Western Blot

Liver protein extracts from previously genotyped mice were separated by SDS-PAGE. Based on the target protein size (22 kDa), a 15% acrylamide gel was chosen to separate the samples. Protein separation was made at 85 V for 5 minutes (min), so the samples could enter the gel, and after it at 120 V for 1 hour (h).

After separation, the proteins were transferred to a Immubilon®-P Transfer Membrane (Merk Millipore), previously soaked in 100% methanol (MeOH) (Carl Roth CmbH, Germany), using Trans-Blot® SD Semi-Dry Transfer Cell (BioRad). Transference was done at 75 mA for 1.5 h. In order to confirm that the transference was successful, Ponceau red was added.

The membrane was blocked with 5% milk in PBS 1x for 1 h at room temperature (RT), to prevent unspecific reactions between antibodies and the membrane. Primary antibody Goat anti-Hbegf (1:2000, Santa Cruz) was added and the membrane was left to incubate overnight (O/N) at 4ºC. After the first incubation, the membrane was washed 3 times for 5 min with PBS 1x and incubated with Donkey anti-Goat IgG-HRP antibody (1:3000, Santa Cruz) for 1 h at RT. After new washing, as previously described, a mix of 750 µl of SuperSignal® Pico Luminol/Enhancer Solution (Thermo Scientific) and 750 µl of SuperSignal® Pico Stable Peroxidase Solution (Thermo Scientific) was dropped on the membrane.

Visualization of the membrane was done using ChemiDoc™ MP System (BioRad).

3.5. Genotyping

For genotyping, a piece of ear (adult mice) or limbs/tail (embryos) was collected. To obtain gDNA, samples were treated with 75 µl of alkaline lysis buffer and put at 95ºC with agitation (Thermomixer Comfort, Eppendorf) for 20 min. After this, samples were kept at 4ºC for 20 min for inactivation, followed by the addition of 75 µl of neutralizing buffer. Finally, samples were centrifuged at 13000 rpm (HERAEUS PICO 21 Centrifuge, Thermo Scientific) for 2 min.

The genotyping was done using the Polymerase Chain Reaction (PCR) technique. Starting with a small amount of template DNA, this process allows the *in vitro* synthesis of a large amount of a specific DNA sequence. There are some compounds needed for the reaction to occur: a DNA template containing the sequence to be amplified; a DNA polymerase, which has to be thermostable to withstand this process's high temperatures; the four deoxynucleotide triphosphates (dNTPs) – adenine (A), cytosine (C), guanidine (G) and thymidine (T); and a pair of small pieces of single-stranded DNA, called primers, that are complementary to the target sequence[122].

The reaction starts with a denaturation step, which will rise the temperature up to 95ºC, denaturating the DNA template through the elimination of its secondary structures. Next, there's the annealing step in which the primers bind to the complementary DNA strain. In this part of the process, the temperature slowly decreases to temperatures between 50ºC and 70ºC. Once the biding between the primers and the DNA template is established, an elongation step takes place. The synthesis of new strands of DNA occurs at 72ºC, which is the optimal temperature of *Taq* polymerase. This enzyme will start the elongation at the 3' end of each primer, adding the dNTPs in a sequential manner, according to the DNA template. The repetition of these steps in a limited number of cycles (usually 20-35) will increase the amount of target DNA in an exponential manner, as the amount of DNA duplicates in each cycle[122].

The sequences of the primers used in the mice genotyping made along this project are shown in **Table 3.1**.

Table 3. 1. Sequences of the specific primers for genotyping, forward (Fw) and reverse (Rv), used in the amplification of gene fragments, as well as the length of the PCR product.

Gene	Primer sequence (5'→ 3')	PCR product size (bp)
dsRed	Fw: CAC CCA GAC CGC CAA GCT G Rev: GAG TCC TGG GTC CAC GGT CAC	190
***Hprt-Cre* mut**	Fw: GCG GTC CAG TAA AAA CTA TC Rev: GTG AAA CAG CAT TGC TGT CAC TT	120
***Hprt-Cre* wt**	Fw: CAC AGT AGC TCT TCA GTC TGA TAA AA Rev: TTT CTA TAG GAC TGA AAG ACT TGC TC	200
***Id2* wt**	Fw: CTT CCT CCT ACG AGC AGC AT Rev: CTC ACC TGC AAG GAC AGG AT	370
***Id2* mut**	Fw: CTC ACC TGC AAG GAC AGG AT Rev: GCT CCT GGA CAG GAA TCA AG	650
***iDTR* mut**	Fw: GAA AGT CCG TGA CTT GCA AGA GG Rev: CTC TCA GTG GGA ATT AGT CAT GCC	450
***iDTR* wt**	Fw: GGA GCG GGA GAA ATG GAT ATG AAG Rev: CCA AAG TCG CTC TGA GTT GTT ATC	650

The cycling conditions used for amplification of the gene fragments described above are shown in **Tables 3.2** to **3.6**.

Table 3. 2. PCR cycling conditions for amplification of Hprt-Cre wt and mut.

Temperature (°C)	Duration (min or seconds, sec)	Number of cycles
94	3 min	
94	25 sec	28
59	30 sec	
72	15 sec	
4	Hold	

Table 3. 3. PCR cycling conditions for amplification of iDTR wt.

Temperature (°C)	Duration (min or sec)	Number of cycles
94	3 min	
94	25 sec	28
60	30 sec	
72	30 sec	
4	Hold	

Table 3. 4. PCR cycling conditions for amplication of iDTR mut.

Temperature (°C)	Duration (min or sec)	Number of cycles
94	4 min	
94	15 sec	28
60	15 sec	
72	45 sec	
72	2 min	
4	Hold	

Table 3. 5. PCR cycling conditions for amplification of Id2.

Temperature (°C)	Duration (min or sec)	Number of cycles
94	4 min	
94	15 sec	35
58	10 sec	
72	45 sec	
72	2 min	
10	Hold	

Table 3. 6. **PCR cycling conditions for amplification of dsRed.**

Temperature (°C)	Duration (min or sec)	Number of cycles
94	1 min	
94	25 sec	31
60	30 sec	
72	40 sec	
4	Hold	

Reaction mix used in these amplifications was as described in **Table 3.7**.

Table 3. 7. Reaction mix used in amplification of interest fragments by PCR. Primers were the ones described in table 2.1. (Sigma Aldrich), 10x Thermo Pol® Reaction Buffer was from New England BioLabs® Inc., GeneAmp dNTP Blend (100 mM) from Life Technologies™, Taq Polymerase was homemade (Institute of Molecular Biologx, Germany) and gDNA was obtained from the ears of adult mice and limbs/tail of mouse embryos.

Reaction component	Volume per reaction (µl)
10x Thermo Pol® Reaction Buffer	1.5
10 mM dNTPs	0.3
100 mM Primer FW	0.1
100 mM Primer RV	0.1
miliQ water	12
Taq Polymerase	0.1

After amplification, samples were loaded into a 2% agarose gel and ran at 120 V for about 45 min. The genotyping results were visualized using ChemiDoc™ MP System (BioRad).

3.6. Histochemistry

In this study, different histochemistry techniques were used – immunostaining and staining with hematoxylin and eosin (H&E). While the first allows to determine the location, distribution and expression of a target protein on a tissue section[123], hematoxylin and eosin staining is used mainly for phenotypical characterization. In the immunostaining approach, labelling is achieved through antibodies. In this technique, a primary antibody is firstly used to bind to the target protein, and is later detected by a secondary antibody. The target protein is then localized due to the pre-labelling of the second antibody with a fluorescent molecule[123]. Hematoxylin and

eosin staining depends on the properties of the dyes – hematoxylin, a blue-purple colour reagent that stains nucleic acids, and pink eosin, that stain proteins in a nonspecific manner[124,125]. This technique allows the observation of a range of cytoplasmic, nuclear and extracellular matrix, providing key structural information[124].

3.6.1. Tissue processing

Embryos collected as described in section 3.1 were prepared for cryosections and paraffin sections.

3.6.1.1. Cryosections

Embryos were fixed in 1% formaldehyde (FA, Sigma-Aldrich) at 4 ºC for 20 min. After two washes with PBS 1x for 5 min, embryos were equilibrated in 30% sucrose (Sigma Aldrich, Germany) solution O/N and embedded in cryo medium (Surgipath FSC22 Blue Frozen Section Compound, Leica).

Sections with a thickness of 10 μm were prepared with Leica Cryostat CM3050S (Leica Microskopie + System GmbH, Germany) and mounted in SuperFrost Ultra Plus® glass slides. The samples were kept at -80ºC until further experiments.

3.6.1.2. Paraffin sections

Collected embryos were fixated in 2% paraformaldehyde (PFA, Sigma-Aldrich) O/N and washed twice with cold PBS 1x for 10 min each. For dehydration, embryos were incubated at RT for 15 min in 50% and 70% MeOH (in PBS 1x), and then transferred to 100% MeOH (Carl Roth GmbH, Germany) and incubated O/N at 4 ºC. Paraffin embedding of the mouse embryos begun after the incubation in two changes of xylol (Carl Roth GmbH, Germany) for 10 min each, after which the embryos were transferred to paraffin at 58 ºC O/N and the blocks were prepared in Leica EG1150 H Paraffin Embedding Center (Leica, Microkopie + System GmbH, Germany).

The blocks were sectioned (10 μm sections) in a Leica RM 2255 Microtome (Leica Microskopie + System GmbH, Germany), mounted in SuperFrost Ultra Plus® glass slides and kept at 4ºC. Before any histological procedure, the sections were placed at 58ºC during 1 h for the paraffin to melt.

3.6.2. Immunostaining

Cryosections were equilibrated in PBS 1x and fixation was done with 1% FA for 10 min. After two washings with PBS 1x for 3 min each, tissue sections were blocked with 5% (in PBS 1x) of animal serum (**Table 3.8**), with special attention to the species of origin of the serum, which should be the same in which the secondary antibody was produced, for 1 h at RT.

Table 3. 8. Composition of the blocking solutions for each one of the target proteins - EpCam, HB-EGF and H2AX.

Target protein	Composition	Animal serum
EpCam	- 50 µl of 0.1% Triton-X - 250 µl of 100% animal serum - 700 µl of PBS 1x	Goat
HB-EGF		Donkey
H2AX	- 50 µl of 100% animal serum - 1 drop of M.O.M™ Mouse IgG Blocking Reagent (Vector Laboratories, Inc) - 38.5 µl of AffiniPure Fab Fragment Donkey Anti-mouse IgG (H+L) (Jackson ImmunoResearch Laboratories, Inc.) - 850 µl PBS 1x	Donkey

After blocking, the samples were incubated with the primary antibody in blocking serum (**Table 3.9**) O/N at 4ºC. Then, samples were washed with PBS 1x 3 times for 5 min and incubated with the secondary antibody (**Table 3.9**) for 1 h at RT. Following the incubation with the secondary antibodies, samples were washed as previously described, embedded in Shandon IMMU-MOUNT™ (Thermo Scientific) mounting medium and allowed to dry at RT, covered with a cover slip and sealed with nail polish.

Imaging was performed in AF7000 widefield system (Leica).

Table 3. 9. Composition of the primary and second antibody solutions used in the detection of the target proteins EpCAM, HB-EGF and H2AX.

Target protein	Composition	Primary Antibody	Secondary Antibody
EpCAM	- 1 µl of antibody - 50 µl of 100% goat serum - 950 µl PBS 1x	Anti-Mouse 326 (EpCam) PerCP-eFluor® 710 (0.2 mg/ml, eBioscience®)	Alexa Fluor® 568 Goat Anti-Rat IgG (H+L) (2mg/ml, Life Technologies™)
HB-EGF	- 1 µl of antibody - 50 µl of 100% donkey serum - 950 µl PBS 1x	Goat Policlonal Human Anti-Hbegf (0.2 mg/ml, R&D Systems™)	Alexa Fluor® 647 Donkey Anti-Goat IgG (H+L) (2mg/ml, Life Technologies™)
H2AX		Mouse Anti-Histone H2AX (Ser 139) (1 mg/ml, Millipore)	Alexa Fluor® 488 F(ab') Donkey Anti-Mouse IgM (H+L) (2mg/ml, Invitrogen™)

3.6.3. Hematoxylin and eosin staining

Once the paraffin was melted in the sections of the mouse embryos, as mentioned in section 3.6.1.2, they were rehydrated through the following steps: 2 changes of xylol and 2 changes of 100% ethanol, each with a 5 min duration, followed by a decreasing series of ethanol dilutions – 70%, 50% and 30% ethanol – for 2 min each and finally in distilled water for 5 min.

In order to carry out the H&E staining, paraffin sections were stained in a hematoxylin solution (MORPHISTO) for 2 min, washed in warm running tap water for about 30 sec, and, to terminate the hematoxylin staining, rinsed in distilled water, followed by 10 dips in a 95% alcohol solution. Counterstaining then followed with an eosin Y aqueous solution (Sigma-Aldrich) for 5 min. Dehydration was done through 95% alcohol for 1 min, followed by 2 changes of 100% alcohol of 5 min each. Samples were then cleared in 2 changes of xylene, 5 min each, mounted with Roti® medium (Carl Roth GmbH, Germany) and covered with cover slips.

Imaging was performed in DM2500 microscope (Leica).

3.7. Isolation of intestinal cells

3.7.1. Isolation of epithelial cells

Once the embryos were isolated, as described in section 3.3, they were dissected to isolate the small intestine, under a Leica M80.

Small intestine was placed in a tube with 500 µl PBS 1x and 1.5 µl of collagenase (50 mg/ml) and left to digest for 10 min at 37ºC on a Thermomixer compact (Eppendorf AG, Germany), at 800 rpm. After digestion, 500 µl of PBS 1x were added and samples were centrifuged at 3000 rpm for 3 min ((HERAEUS PICO 21 Centrifuge, Thermo Scientific) to wash. Supernatant was removed and another washing step was performed. After washing steps, anti-EpCAM (Anti-Mouse 326 (EpCam) PerCP-eFluor® 710, 0.2 mg/ml, eBioscience) antibody solution (5 µl of antibody in 1 ml of 2% goat serum) was added and samples were mechanically crushed, in order to increase the antibody's area of action, followed by incubation covered from light for 15 min at RT in a table-shaker See-Saw Roker SSL4 (Stuart Scientific, GB). To remove the excess EpCam antibody that didn't bind to the cells, 1 ml of PBS 1x was added and samples were centrifuged for 3 min at 3000 rpm, supernatant was removed and the cell pellet was ressuspended in 300 µl of PBS 1x.

Cell sorting was performed in High Speed Sorter BD Aria III Sorp and cells were sorted for qPCR analysis – 500 cells from each sample were sorted in 7 µl of buffer (1 µl of RNase inhibitor in 19 µl of dilution buffer).

3.8. Genetic analysis

In order to compare the genetic profiles between embryos that had the Id2+ cell population ablated and the embryos that hadn't, both cDNA synthesis and amplification were done using SMART-Seq v4 Ultra Low Imput Kit for Sequencing (Clontech Laboratories, Inc.). The protocols are briefly described in the points below and all the reagents used were supplied by the kit.

3.8.1. cDNA synthesis and amplification

To obtain cDNA from the samples previously sorted, cells were transferred to a 0.2 ml RNase-free PCR tube and nuclease-free water was added up to 9.5 µl. 1 µl of 10x Reaction Buffer (**Table 3.10**) was added and samples were vortexed and incubated at RT for 5 min.

Table 3. 10. Composition of 10x Reaction Buffer.

Reagent	Volume (µl)
10x Lysis Buffer	19
RNase Inhibitor	1

In order to set up the control and test samples, the guidelines described in **Table 3.11** were followed.

Table 3. 11. Guidelines for sample preparation.

Components	Volume (µl)
10x Reaction Buffer	2
Nuclease-free water	Up to 8.5
Diluted Control RNA	-
Sample	1 – 9.5
Total volume	10.5

Samples were maintained on ice and 2 µl of 3' SMART-Seq CDS Primer II A (12 µM) were added to the samples, followed by incubation in a TProfessional Trio Thermocycler (Biometra) at 72ºC for 3 min. Immediately after the incubation, samples were kept on ice for 2 min.

The Master Mix (**Table 3.12**) for the synthesis of first-stranded cDNAwas prepared at RT.

Table 3. 12. Master Mix solution composition used for first-strand cDNA synthesis.

Reagent	Volume per reaction (µl)
5x Ultra Low First-Strand Buffer	4
SMART-Seq v4 Oligonucleotide (48 µM)	1
RNase Inhibitor (40 U/µl)	0.5
Total volume per reaction	5.5

SMARTScribe Reverse Transcriptase (2 µl per reaction) was added to the mix prior to its use, and 7.5 µl of the Master Mix were added to each tube. Samples were preheated to 42ºC and amplification was done using the program described in **Table 3.13**.

Table 3. 13. Conditions used in first-strand cDNA synthesis.

Temperature (ºC)	Duration (min)
42	90
70	10
4	Hold

Amplification of cDNA was carried out by Long Distance PCR (LD-PCR). This technique allows the amplification of larger DNA fragments, which cannot be amplified using routine PCR methods or reagents[126].

Once cDNA was synthetized, all the reagents needed for its amplification – in order to increase the quantity of genetic material available for further work – except the enzyme, were put on ice and the following Master Mix was prepared (**Table 3.14**).

Table 3. 14. Composition of the Master Mix solution used for cDNA amplification.

Reagent	Volume per reaction (µl)
2x SeqAmp PCR Buffer	25
PCR Primer II A (12 µM)	1
SeqAmp DNA Polymerase	1
Nuclease-free water	3
Total volume per reaction	30

In a fresh tube, 30 µl of Master Mix were mixed with 20 µl of first-stranded cDNA and the mixture was vortexed and spinned.

cDNA amplification was performed in TProfessional Trio Thermocycler (Biometra) using the conditions described in **Table 3.15**.

Table 3. 15. Conditions used in cDNA amplification.

Temperature (ºC)	Duration	Number of cycles
95	1 min	
98	10 sec	16
65	30 sec	
68	3 min	
72	10 min	
4	Hold	

3.8.2. Quantitative PCR

Genetic analysis of the cells collected in section 3.6 was done by qPCR.

Genes that take part in cell proliferation, apoptosis and stem cells markers, among others, were analysed. The sequences are shown in **Table 3.16** and the Master Mix composition is described in **Table 3.17**.

Table 3. 16. Specific primer sequences of the genes analysed by qPCR and corresponding annealing temperatures.

Gene	Primer sequence (5'→ 3')	Annealing temperature (ºC)
Ascl2 (Achaete-scute family bHLH transcription factor 2)	Fw: GGA CGC AAT AAG CTA AGC ATC TG Rev: CCT GGG ACC CCG TAC CAG TCA	61
EpCam (Epithelial Cell Adhesion Molecule)	Fw: TCC TTC CGG GGT ACT GGA AT Rev: TGA CTC ACC CGC CCCA	58
Id1 (Inhibitor DNA binding/Inhibitor of differentiation 1)	Fw: GCT GAA CTC GGA GTC TGA AG TCG Rev: CCG TTC AGG GTG CTG AGC	60
Id2 (Inhibitor DNA binding/Inhibitor of differentiation 2)	Fw: CTC TCC CAA TCT TTT GCA GGC Rev: GCA CTG GTT GTC TGA AAT AAA GCA	57
Id3 (Inhibitor DNA binding/Inhibitor of differentiation 3)	Fw: TGC AGC GTG TCA TAG ACT ACA TCC Rev: GAG CTC AGC TGT CTG GAT CG	60
Kcne3 (Potassium voltage-gated channel, Isk-related subfamily, gene 3)	Fw: GTG GGA CAT CCA CGA AGA GA Rev: TCC CGT TGG AAG TCT CCA TA	56

Kcnq1 (Potassium voltage-gated channel, subfamily Q, member 1)	Fw: TGG AAG ACA AGG TGA CAC AAC TG Rev: GAC AGC AGC TGG TGG AGC AT	59
Lgr5 (Leucine rich repeat containing G protein coupled receptor 5)	Fw: GCA AAC TTC CCA GAG CTC AA Rev: CCC CAA ATG CAC AAC ACT GG	56
OneCut2 (One cut domain, family member 2)	Fw: GGA CGC AAT AAG CTA AGC ATC TG Rev: CCT GGG ACC CCG TAC AGT CA	60
PUMA (p53 Upregulated Modulator of Apoptosis)	Fw: CCT CAA CGC GCA GTA CGA GC Rev: CTC CAT TTC TGG GG CTC CAG G	62
Rspo1 (R-spondin 1)	Fw: CAG TCC TGC ACA ATG TGA AAT GAG C Rev: CGG AAA CCG CAC AGC TTC C	60
Rspo3 (R-spondin 3)	Fw: CAG CGA AGA ATG CAT CCT AAT GTC AG Rev: CTG GGC TTA CAT GAC AAA CAG CC	61
Sfrp5 (Secreted frizzled-related protein 5)	Fw: CTG GAC AAC GAC CTC TGC AT Rev: CAT CTG TTC CAT GAG GCC AT	56
Slc2a3 (Solute carrier family 2 (facilitated glucose transporter), member 3)	Fw: CAT CTC CAT TGT CCT CCA GC Rev: CAA TCG TGG CAT AGA TCG GT	56
Smoc2 (SPARC related modular calcium binding 2)	Fw: CCA TCC ACC GGA TAC TGC TG Rev: GTT GCT CAT ACC TTG TGG AGG	59
Snai2 (Snail family transcriptional repressor 2)	Fw: ACA CTG CTG CCA AAC CAT TTC Rev: TAG GCG TGG CTA TTA ACC GT	56
St8sia3 (St8 alpha-N-acetyl-neuraminide alpha-2,8-sialyltransferase 3)	Fw: TAA AGG TCC AGT TGG CTT GG Rev: CGT TTG GGT GAC AGG TGT TT	55
TBP (TATA-box Binding Protein)	Fw: CAG GAG CCA AGA GTG AAG AAC AAT CC Rev: CTG GGA AGC CCA ACT TCT GC	61
Wnt11 (Wingless-type MMTV integration site family, member 11)	Fw: TGG AGC GAT GTC ACT GCA AG Rev: AGA TTT GGG GGC AGA TTG GG	58
Wnt6 (Wingless-type MMTV integration site family, member 6)	Fw: CGA GGA GAA CTG TCT GTG CC Rev: AGA CGC CTG ACA ACT AAG CC	59

Table 3. 17. Master Mix used in genetic analysis by qPCR. Primers are the ones described in table 3.13 (Sigma Aldrich) and 2x SYBR® Master Mix is from Life Technologies GmbH.

Reaction component	Volume per reaction (µl)
2x SYBR® Master	5
Primer Fw (3 mM)	1
Primer Rev (3 mM)	1
Template cDNA	0.02
Nuclease-free water	Up to 10

Table 3.18 describes the conditions used in amplification of the qPCR reactions of the analysed genes.

Table 3. 18. Amplification conditions used for qPCR reactions.

Temperature (ºC)	Duration (min or sec)	Number of cycles
95	10 min	
95	15 sec	40
60	1 min	
95	15 sec	
60	1 min	

All samples were run in triplicates and results were treated using Livak's normalization method.

3.8.3. Statistical analysis

Graphics and statistical analysis were done using GraphPad Prism® (version 6.0) software. Statistical differences were evaluated with Student's t test.

4. RESULTS AND DISCUSSION

In order to gain insight about the cell ablation system studied, morphological, cytometric and genetic approaches were used. Immunostaining was used to confirm the DT receptor expression and to assess apoptosis, while histological staining allowed to visualize the phenotype of the embryonic small intestine. Cytometric and genetic experiments were performed in order to obtain a more detailed insight into the genetic profile of some cell populations and also into the efficiency of the DT-mediated ablation system of $Id2^+$ cells.

4.1. Sampling

To perform the studies presented in this work, collection of mouse embryos and isolation of their internal organs was required. The typical morphology of a whole mouse embryo at developmental stage E14.5, and its internal organs, is presented on **Figure 4.1**.

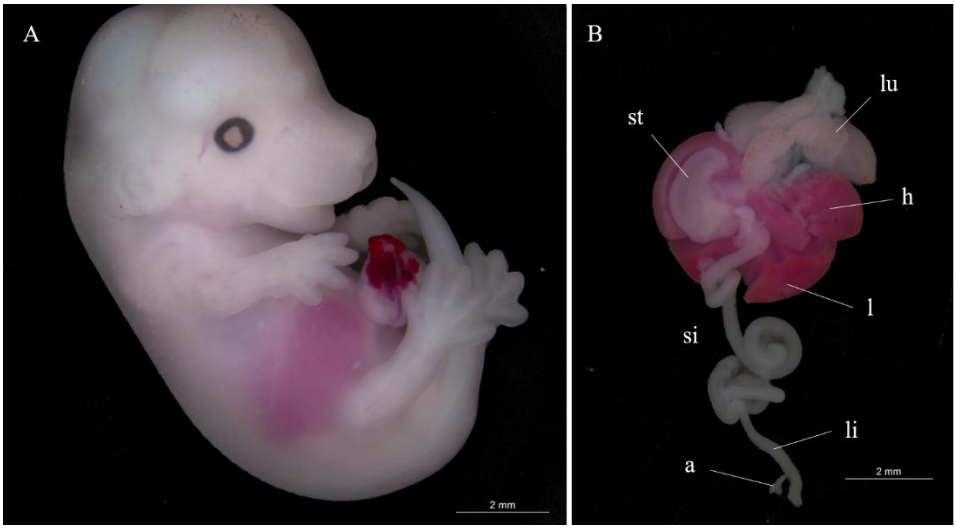

Figure 4. 1. Mouse embryo at E14.5 (A) and its internal organs (B). The internal organs dissected included lungs (lu), liver (l), small intestine (si), stomach (st), as well as heart (h), large intestine (li), appendix (a) and kidney (not visible in the picture). Scale bars correspond to 2 mm. Pictures taken in Leica MF205 FA microscope.

4.2. Establishment of the inducible system

The iDTR ablation system consists in the expression of the DT receptor (HB-EGF, also known as iDTR) under the control of the specific promoter of a gene of interest, causing the death of the cells that express the receptor upon treatment with DT. This system was an important tool in this study given its versatility, since the system can be activated at the developmental stage of interest, and specificity for the target cells. Thus, we first investigated

the functional properties of the iDTR system *in vivo* by testing whether the expression of the DT receptor confers the small intestine's cells the sensitivity to DT, resulting in their death.

In order to do so, the mice strain chosen was $Hprt^{Cre}$iDTR. In their genome, these mice harbour both the STOP cassette, which is flanked by two *loxP* sites, and the gene that encodes for iDTR under the control of a ubiquitous promoter. Therefore, after homologous recombination mediated by the Cre enzyme, all cells will express the DT receptor at their surface.

Crossings to obtain $Hprt^{Cre}$iDTR progeny were either performed with the male parent harbouring the Cre enzyme and the female the iDTR gene, or the other way around, in order to determine whether this would influence the results (**Table 1**). However, when the Cre enzyme was from the male parent no phenotypical differences were detected, between DT-sensitive and non-sensitive cells treated with DT, by H&E staining (data not shown). This lack of phenotypical differences observed in the first two crossing might have been related to the parent carrying the mutation for the Cre enzyme. Maternal or paternal transmission of this enzyme has some influence, since in some mouse strains the enzyme activity is stronger if its inherited from the mother[127,128].

Table 4. 1. Time points between TAM administration, DT injection and mouse dissection in HprtCre x iDTR crossings done along this project.

	Time points		
Crossing	**TAM**	**DT**	**Dissection**
1. $Hprt^{Cre}$ male x iDTR female	E13.5	E15.5	E16.5
2. $Hprt^{Cre}$ male x iDTR female	E13.5	E14.5	E15.5
3. $Hprt^{Cre}$ female x iDTR male	E9.5	Not treated	E16.5
4. $Hprt^{Cre}$ female x iDTR male	E11.5	E13.5	E14.5

4.2.1. iDTR expression in Hprt^{Cre}iDTR mice

Before any further experiments, it was necessary to determine whether the DT receptor was being expressed in the *in vivo* system. For this purpose, protein lysates were prepared from liver cells collected from Hprt^{Cre}iDTR mice previously genotyped for the presence of iDTR. Positive and negative samples were analysed by Western Blot targeting iDTR. (**Figure 4.2**).

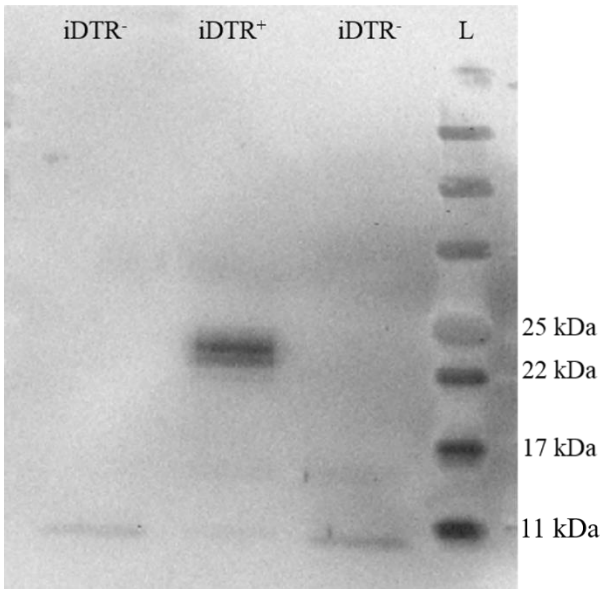

Figure 4. 2. Western Blot analysis of Hprt^{Cre}iDTR mice liver protein lysates targeting for HB-EGF on a 15% acrylamide SDS-PAGE transferred to a PVDF membrane. Samples were blotted with primary antibody Goat anti-Hbegf (1:2000) and secondary antibody Donkey anti-Goat IgG-HRP (1:3000). Lysates from negative and positive DT receptor mice are shown as iDTR$^-$ and iDTR$^+$, respectively. L corresponds to the ladder Color Prestaned Protein Standard, Broad Range (11-245 kDa) from New England BioLab® Inc.

Results from the Western Blot on HB-EGF confirmed the genotyping results (**Figure 4.2)**. However, a more intense band was detected around 23 kDa, along with several others with a molecular weight between 22 and 25 kDa, in the iDTR$^+$ sample. Besides the membrane-anchored form of HB-EGF (DT receptor), the secreted form of the protein is also processed at multiple sites in the N-terminal portion, rendering the secretion of multiple forms of HB-EGF with different molecular weights[129]. Therefore, some of the bands observed by Western Blot may be related to these secreted forms, or are post-translational modified forms. The band detected with 11 kDa in all samples could be due to unspecific binding of the antibody.

These results indicate that the homologous recombination was successful, meaning that the STOP cassette was removed and, as a consequence, the gene that encodes the DT receptor was transcribed and the protein synthesized.

4.2.2. Genotyping

Once it was determined that the DT receptor was expressed in Hprt^{Cre}iDTR mice, further experiments were conducted in this strain. Prior to these, litters were genotyped in order to choose the suitable embryos to carry on the work. The genotyping results from embryos treated with the toxin are shown in **Figure 4.3**. DT non-treated embryos were already genotyped (data not shown).

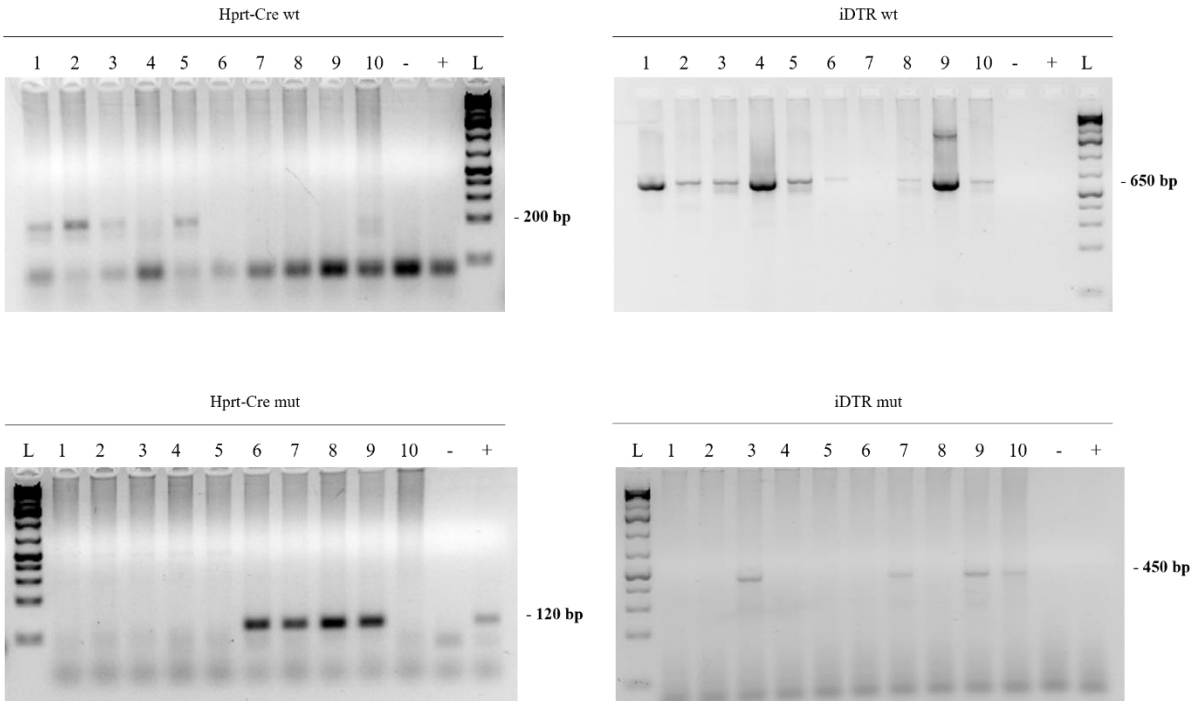

Figure 4. 3. Genotyping results of Hprt^{Cre}iDTR embryos treated with DT, for *Hprt-Cre* wt (200 bp), *iDTR* wt (650 bp), *Hprt-Cre* mut (120 bp) and *iDTR* mut (450 bp), on a 2% agarose gel in 1x TAE stained with ethidium bromide (EtBr). (-) and (+) are the negative and positive controls of the PCR reaction. wt – wildtype. mut – mutant. L corresponds to the ladder GeneRuler 1Kb Plus DNA Ladder.

Genotyping for the wildtype form of the gene works as a positive control for the presence of DNA, since the presence of a band is expected for every embryo, allowing to perceive if there is DNA in the collected samples.

According to these results, only 2 embryos (embryos 7 and 9) would have the DT receptor ubiquitously expressed, given the fact that they are the only two positive for the mutant

forms of *Hprt-Cre* and *iDTR*. Embryos 8 ($iDTR^-$) and 9 ($iDTR^+$) from the DT treated condition were used in further experiments.

4.2.3. DT receptor localization and cell death assessment

For a better assessment of the distribution of the DT receptor – iDTR – within the embryonic small intestine and determine if there was cell death upon DT treatment, immunostaining against HB-EGF and γH2AX was performed, respectively. In this assay, 4 conditions were studied: embryos iDTR negative and positive, both treated with and without DT. DT^- embryos were collected at E16.5 and DT^+ at E14.5. The time points (**Table 4.1**) were: TAM at E9.5 for $iDTR^-$ embryos, and TAM at E11.5 and DT at E13.5 for $iDTR^+$ embryos. This difference between the developmental stages will not have an impact on the results, since the assays performed with the $Hprt^{Cre}$iDTR strain were just to evaluate if the system worked in mouse embryos.

Samples were also counterstained with 4', 6-diamidino-2-phenylindole (DAPI), a blue fluorescent dye, that binds strongly to adenine-thymine-rich regions, staining preferentially dsDNA and allowing the visualization of nucleus morphology and apoptosis[130].

Immunostaining against the DT receptor (HB-EGF) is shown in **Figure 4.4**. No fluorescence is detected on $iDTR^-$ embryos (**Figure 4.4 A** and **E**), meaning that the receptor is not expressed in these conditions, as expected. $iDTR^+$ embryos show fluorescence all over the small intestine section (**Figure 4.4 I** and **L**), due to the ubiquitous expression of the receptor in this strain.

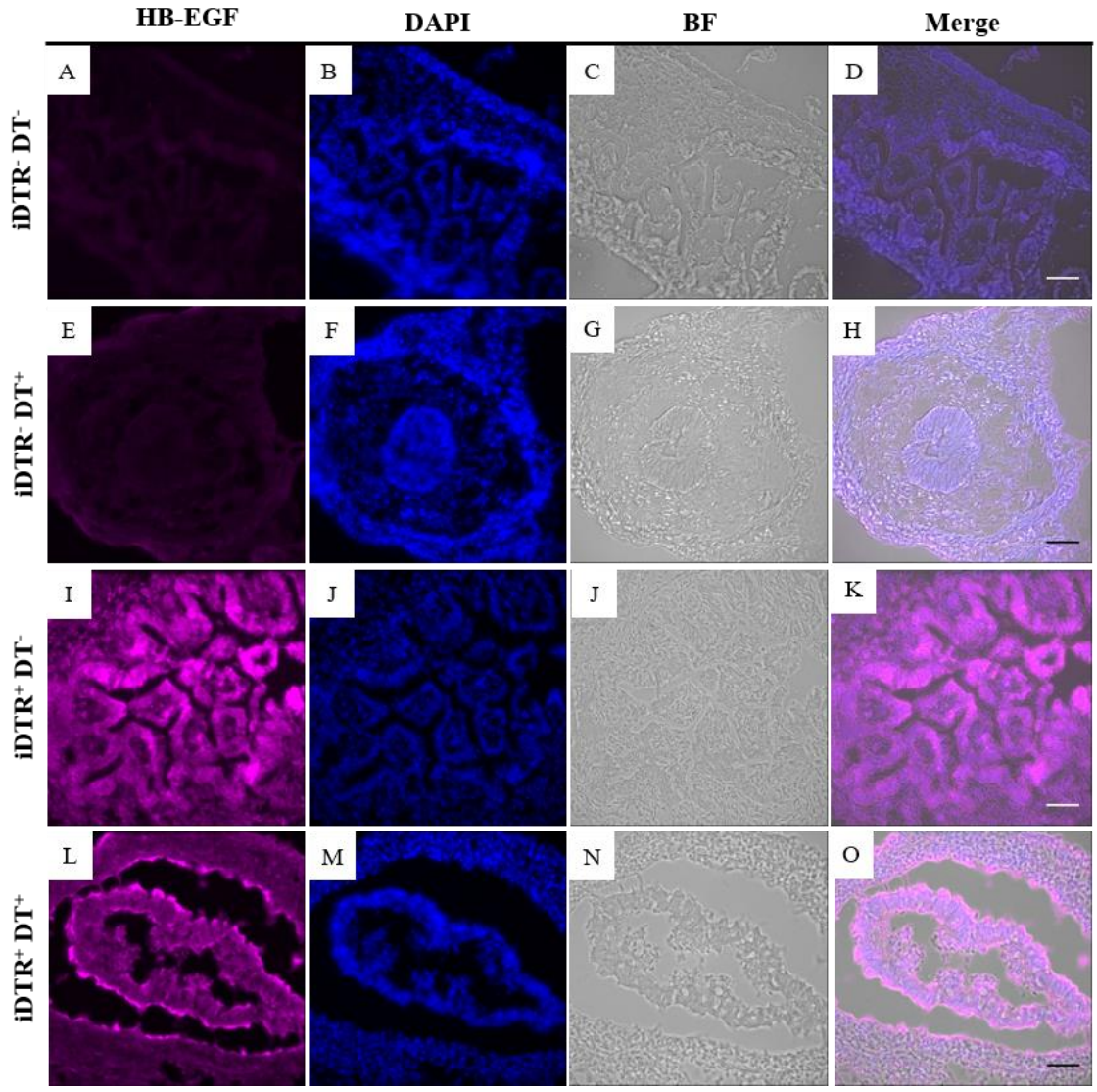

Figure 4. 4. Immunostaining against HB-EGF in 10 µm cryosections from Hprt^{Cre}iDTR mouse embryos. HB-EGF (magenta) and DAPI (blue) stainings are presented in the first and second columns (from left to right), respectively. Bright-field (BF) images are shown in the third column and merge of all the pictures on the last one. Scale bars correspond to 10 µm.

To assess cell death within the embryonic small intestine in the 4 different conditions, samples were stained against γH2AX (**Figure 4.5**). Once cells are exposed to DNA-damaging agents, like radiation or genotoxic compounds, histone H2A variant H2AX will be phosphorylated into γH2AX due to the appearance of double-stranded breaks. This staining is sensitive for the analysis of DNA damage due to the fast and abundant phosphorylation of H2AX, as well as its correlation with each double-stranded break[131,132].

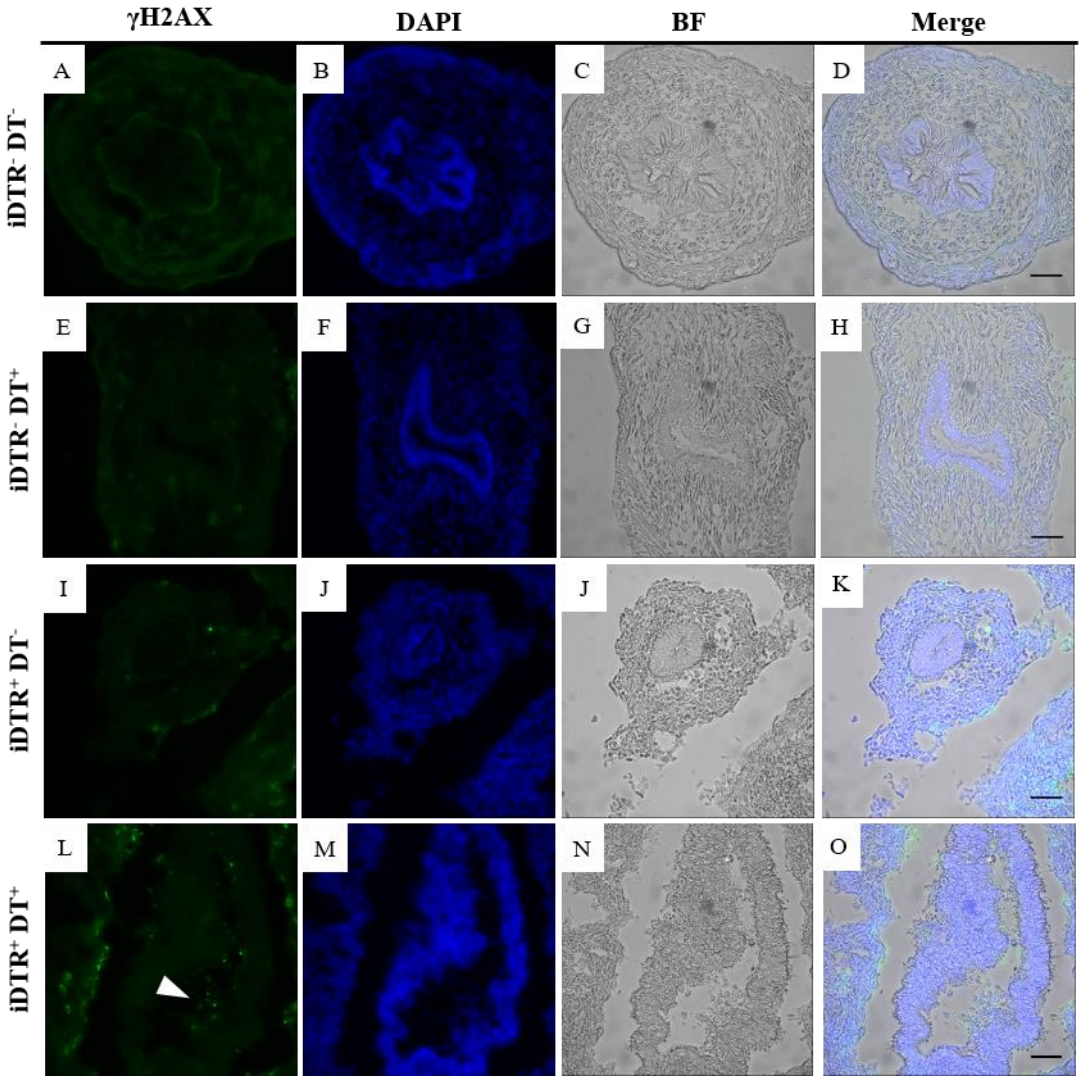

Figure 4. 5. Immunostaining against γH2AX in 10 µm cryosections from Hprt^{Cre}iDTR mouse embryos. γH2AX (green) and DAPI (blue) stainings are presented in the first and second columns (from left to right), respectively. The white arrow indicates the apoptotic sites. Bright-field (BF) images are shown in the third column and merge of all the pictures on the last one. Scale bars correspond to 10 µm.

Apoptosis was not detected in iDTR$^-$ negative embryos – DT$^-$ and DT$^+$ (**Figure 4.5, A and E**, respectively) –, as expected. The sample positive for the DT receptor (**Figure 4.5, L**) presents some apoptotic sites at the small intestine's lumen (white arrow), evidencing the action of the toxin in the DT-sensitive cells. However, some residual fluorescence is also observed in the iDTR$^+$DT$^-$ embryo (**Figure 4.5, I**), but it is most likely due to auto-fluorescence.

4.2.4. Embryo morphology

In order to see how DT affects the morphology of the embryo, hematoxylin and eosin staining was performed on sections (**Figures 4.6** and **4.7**). Besides the small intestine, the morphology of the lungs is also shown (third line in both figures), since these two organs share a similar tissue composition – epithelium and mesenchyme.

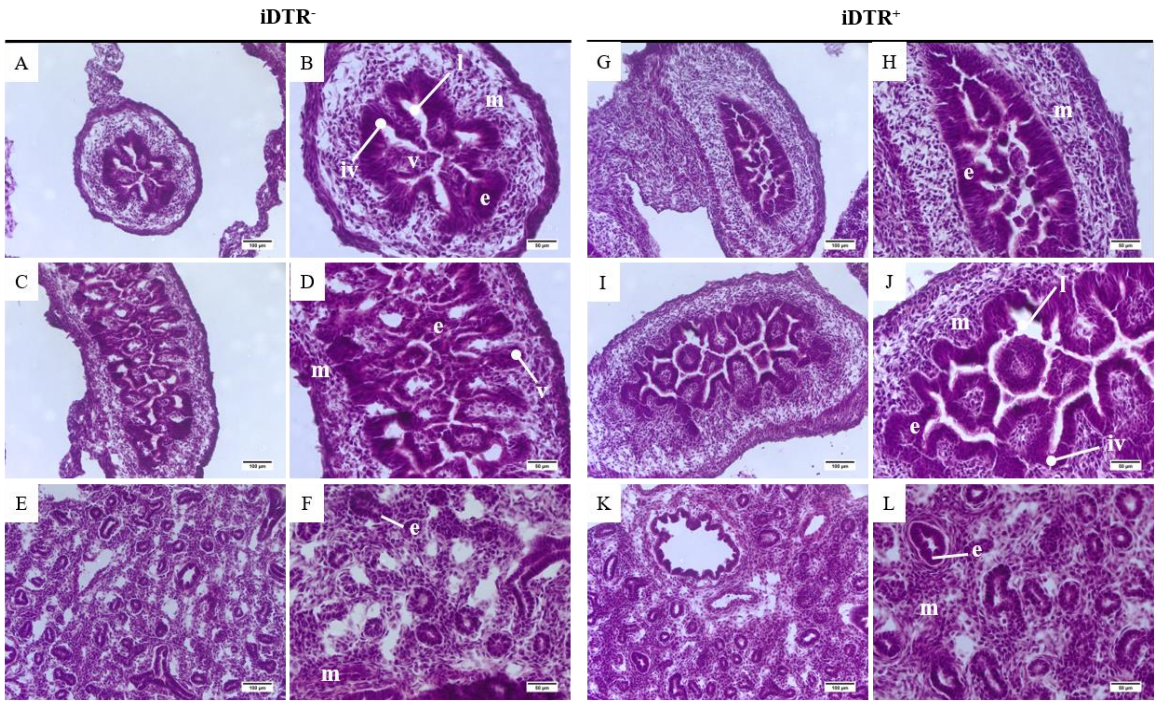

Figure 4. 6. Histology of small intestine and lungs from mouse embryos at E16.5 non-treated with DT. 10 µm cryosections were stained with hematoxylin and eosin. Embryo DT receptor negative (iDTR$^-$) is shown on the left panel and the positive (iDTR$^+$) on the right. Images A-D and G-J show the small intestine; E-F and K-L show the lungs. At this stage, the small intestine presents a more complex structure: e – epithelium, iv – inter-villus region, l – lumen, m – mesenchyme, v - villi. Scale bars on A, C, E, G, I and K are 100 µm; on B, D, F, H, J and L are 50 µm.

Comparing both embryos (iDTR$^-$ and iDTR$^+$) without the DT treatment, both showed a normal development for this embryonic stage. At E16.5 villi are already fully developed and these structures can be seen, together with the inter-villus regions, on **Figure 4.6 B**.

The lungs also present a normal morphology for this developmental stage.

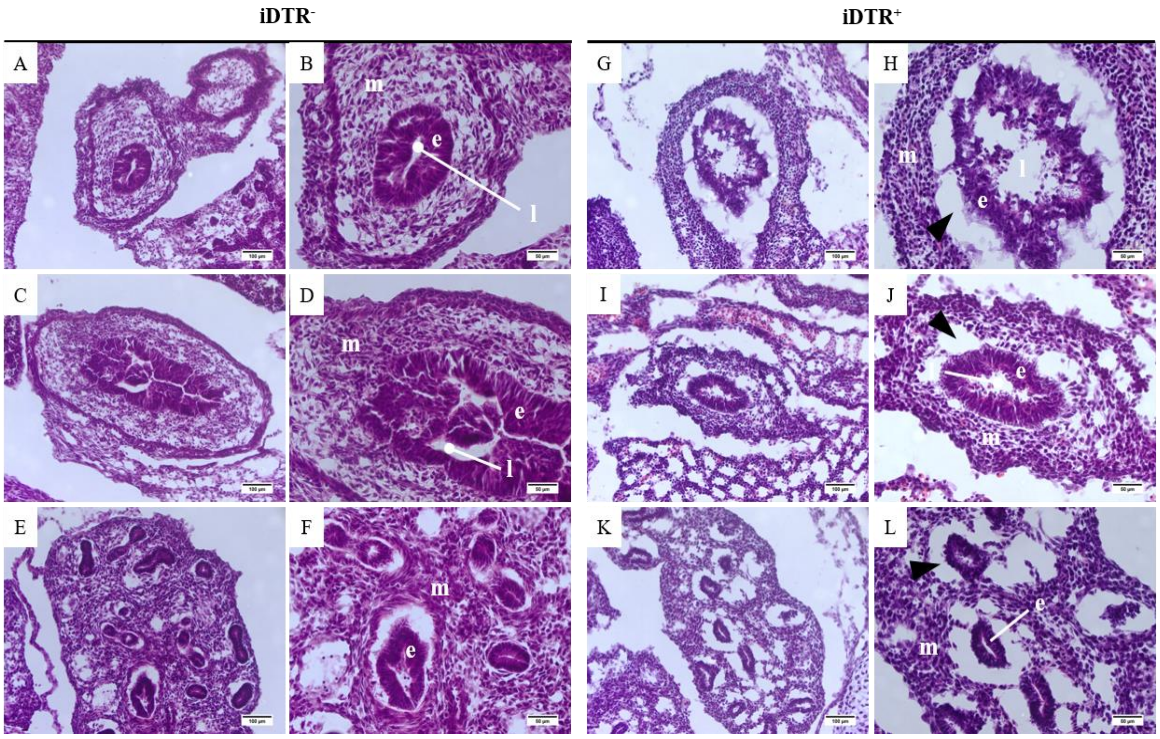

Figure 4. 7. Histology of small intestine and lungs from Hprt^{Cre}iDTR mouse embryos at E14.5 treated with DT. 10 µm cryosections were stained with hematoxylin and eosin. Embryo DT receptor negative (iDTR$^-$) is shown on the left panel and the positive (iDTR$^+$) on the right. Images A-D and G-J show the small intestine; E-F and K-L show the lungs. At this stage, the small intestine presents a more complex structure: e – epithelium, l – lumen, m – mesenchyme. Black arrows indicate the detachment between the epithelium and the mesenchyme. Scale bars on A, C, E, G, I and K are 100 µm; on B, D, F, H, J and L are 50 µm.

Embryos treated with DT showed a different scenario. While the small intestine of iDTR$^-$ embryos presents a morphology similar to those of the control embryos portrayed in **Figure 4.6**, the small intestine of iDTR$^+$ embryo shows drastic changes in its phenotype (**Figure 4.7, G-L**). The most prominent feature in this condition is the detachment between the epithelium and the mesenchyme (indicated by black arrows), observable not only on the small intestine (**Figure 4.7, H and J**) but also in the lungs (**Figure 4.7, L**). Interestingly, a population of distinct cells is visible on the histological sections of DT receptor positive embryo exposed to the toxin (**Figure 4.8**). These cells are likely to be white blood cells, since DT is able to penetrate the cells that express the receptor, causing an inflammatory response, and as a consequence, the organism activates its defence mechanisms against the toxin.

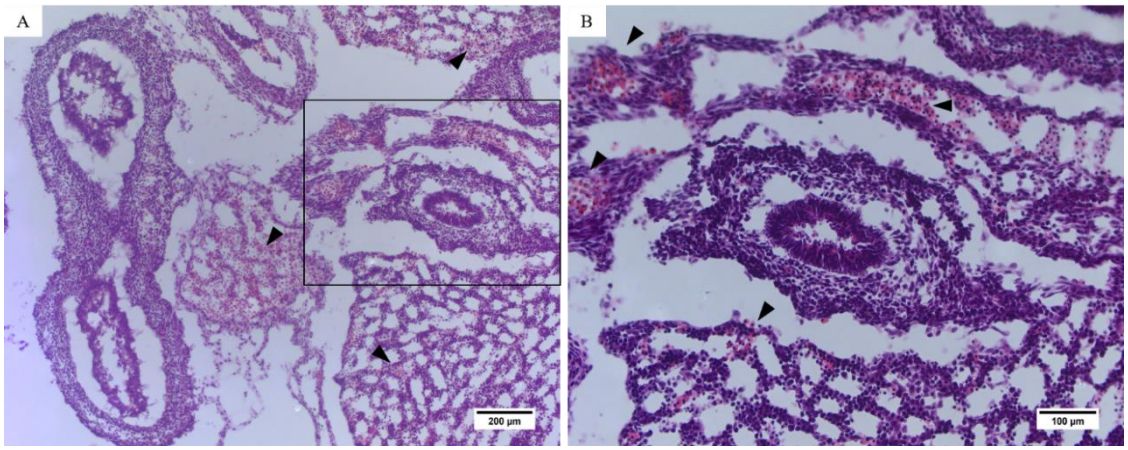

Figure 4. 8. Histology detail of small intestine from Hprt^{Cre}iDTR mouse embryos at E14.5 treated with DT. Black arrows indicate what could be white blood cells. B is the augmentation of the zone inside the box in A. Scale bars are 200 µm and 100 µm in A and B, respectively.

These assays allowed to conclude about the global efficiency of the system, using a generic mouse strain. Based on the immunostaining results, the DT receptor was only expressed in iDTR^{+} mice and apoptosis was detected only in mice that expressed the receptor and were treated with the toxin.

Histological analysis showed that both embryos not treated with DT (iDTR^{-} and iDTR^{+}) and the iDTR^{-} embryo treated with DT had the same phenotype. These results indicate that 1) neither the receptor nor the toxin are harmful to the embryo by themselves and 2) the apoptosis and phenotype observed in the iDTR^{+} embryo treated with DT is due to the interaction between the toxin and the receptor.

4.3.Ablation of Id2 positive cells

4.3.1. Establishment of conditions

As mentioned in **section 2**, the main goal of this project was the ablation of Id2^{+} cells and the study of its consequences within the embryonic small intestine. The mice strain used was Id2^{Cre}iDTR (**Annex 1**), where only cells that are Id2 positive will express the DT receptor at their surface, thus being the only cells sensitive to the toxin's action.

The evaluation of the expression of the receptor and cell death focuses within the embryonic small intestine at E14.5 is shown in **Figures 4.9** and **4.10**, respectively. Embryos used in this assay were previously genotyped (data not shown), and Id2^{+}iDTR^{+} embryos – treated and untreated with DT – were used. During the analysis of the slides by fluorescence

microscopy, it was observed that the receptor was mostly expressed in the anterior section of the embryonic small intestine compared the posterior section, being this differences portrayed in the **Figure 4.9**. The anterior section of the small intestine corresponds to the portion that goes from the beginning of the gut tube until the middle, and the posterior section to the remaining portion, right before the appendix (**Annex 2**). Morphologically, the anterior section of the embryonic small intestine is larger than the posterior, and the latter presents a more roundish shape, as seen in the figure below.

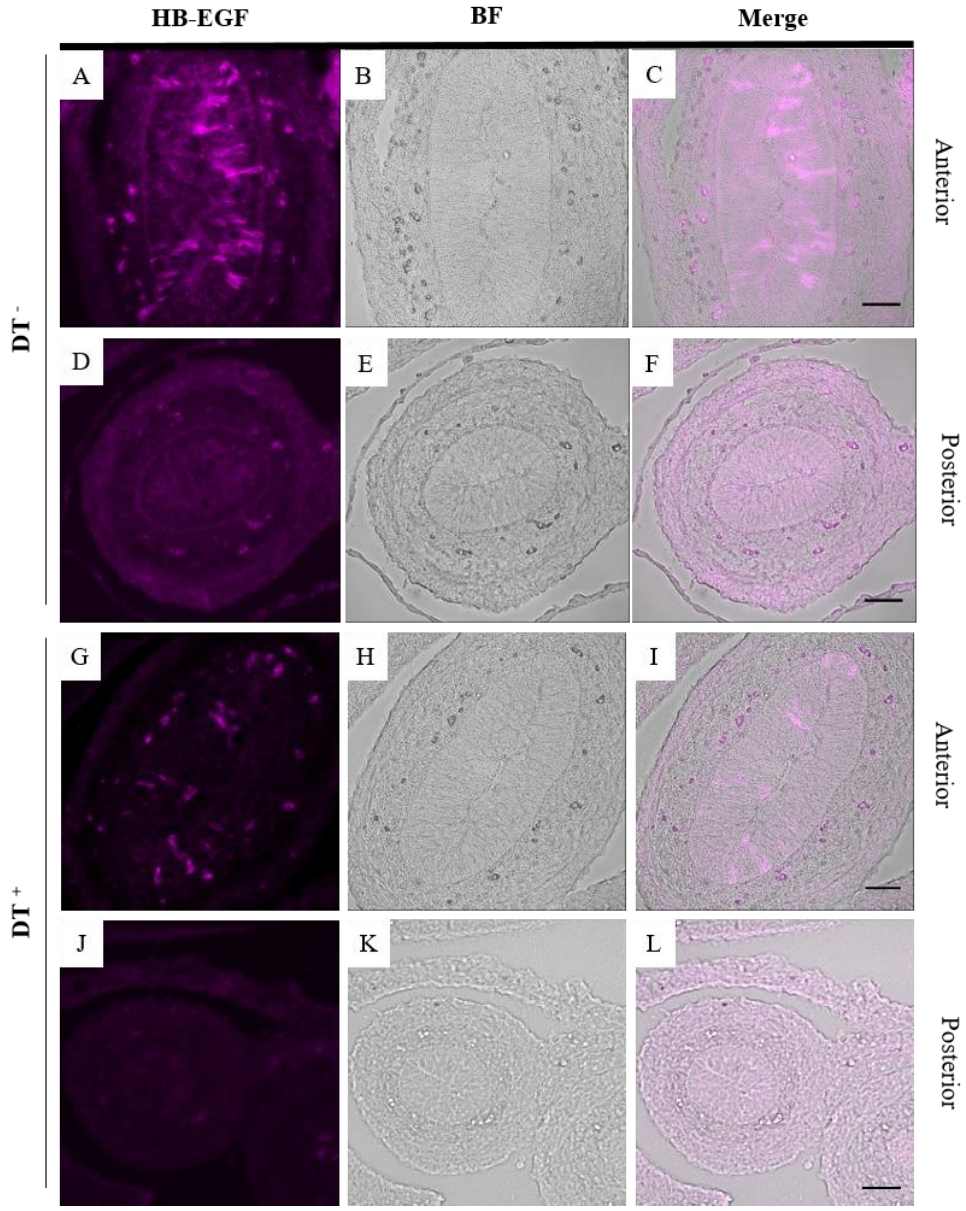

Figure 4. 9. Immunostaining against HB-EGF in 10 µm sections from Id2^{Cre}iDTR mouse embryos at E14.5, embedded in paraffin. Expression of the DT receptor in the different sections of the embryonic small intestine – anterior and posterior – is shown. Female mouse was treated with TAM at E11.5 and DT at E13.5. Bright-field (BF) images are shown in second column and the merge of all the pictures in the last one. Scale bars correspond to 10 µm.

The figure above shows fluorescence in the epithelium of the embryonic small intestine, indicating that the DT receptor is being expressed in this strain, independently of the DT treatment. Russell *et al.* (2004) described that *Id2* is expressed in the epithelial cells during the embryonic development of the small intestine, but not in the mesenchyme[121,133]. Even though there are some fluorescent zones in the mesenchyme in **Figure 4.9 A** – maybe due to unspecific binding –, most of the cells expressing *Id2* are localized in the small intestine's epithelium, as stated in the literature.

The fact that $Id2^{+}$ cells expressing the receptor are only visible in the anterior section of the small intestine (**Figure 4.9 A** and **G**), might indicate that *Id2* is mostly expressed on the anterior portion of the embryonic small intestine. There is also an observable difference between the number of cells expressing the DT in the anterior sections. In **Figure 4.9 G**, there is less expression of the DT receptor detected compared to **Figure 4.9 A**, possibly due the fact that this embryo was treated with DT and, as consequence, cell death occurred.

Regarding the posterior portion (**Figure 4.9 D** and **J**), the receptor was not detected, even though what appears to be auto-fluorescence was.

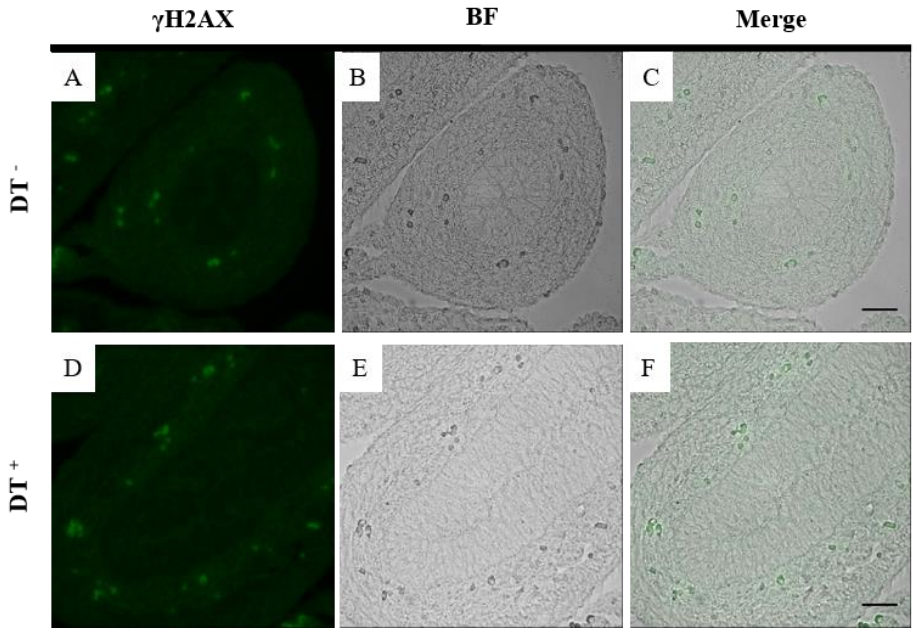

Figure 4. 10. Immunostaining against γH2AX in 10 µm sections from $Id2^{Cre}$iDTR mouse embryos at E14.5 embedded in paraffin. Female mouse was treated with TAM at E11.5 and DT at 13.5. Bright-field (BF) images are shown in second column and the merge of all the pictures in the last one. Scale bars correspond to 10 µm.

Once the receptor was detected, it was important to verify if the toxin could cause cell death in the samples expressing the DT receptor. Regarding cell death, only auto-fluorescence was detected (**Figure 4.10 A** and **E**), meaning that a 2-day interval between the treatments with TAM and DT is not enough to induce apoptosis. These results are supported by the embryonic small intestine's morphology portrayed in **Figure 4.11**, where no phenotypic changes can be observed between both conditions.

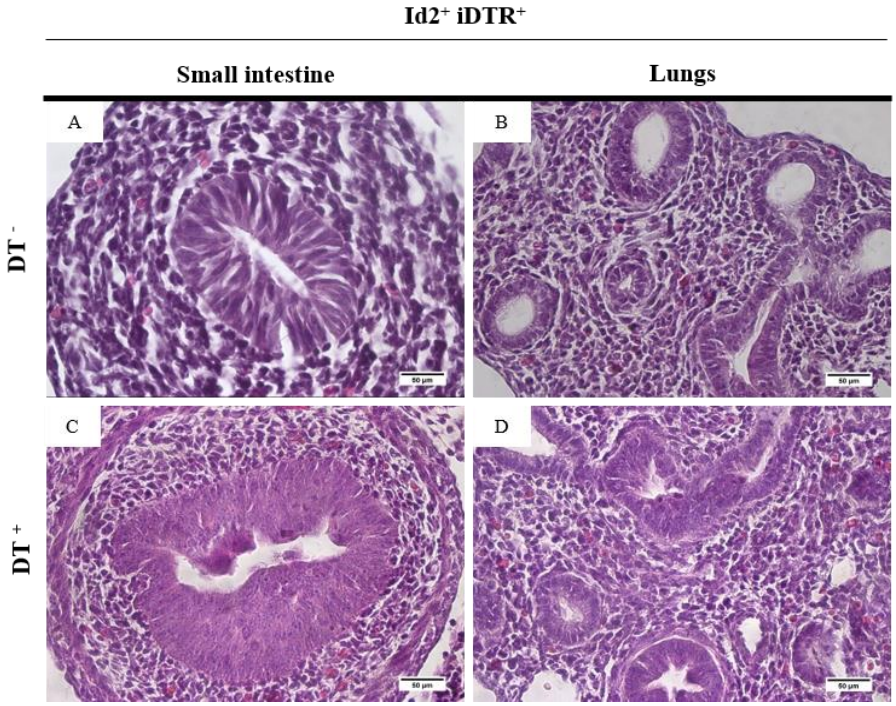

Figure 4. 11. Histology of small intestine and lungs in 10 µm sections from Id2^{Cre}iDTR mouse embryos at E14.5, treated and not treated with DT, embedded in paraffin. Sections were stained with hematoxylin and eosin. Female mouse was treated with TAM at E11.5 and DT at 13.5. Scale bars correspond to 50 µm.

Given the previous results, and in order to assess if the time interval had an effect in the toxin's action, the assays were repeated but the time point between TAM and DT administration was increased to 5 days. Embryos were genotyped and a double negative (iDTR^{-} DT^{-}) and a double positive (iDTR^{+}DT^{+}) embryo were taken for further experiments. Immunostaining and morphology assays are shown in **Figures 4.12** to **4.14**.

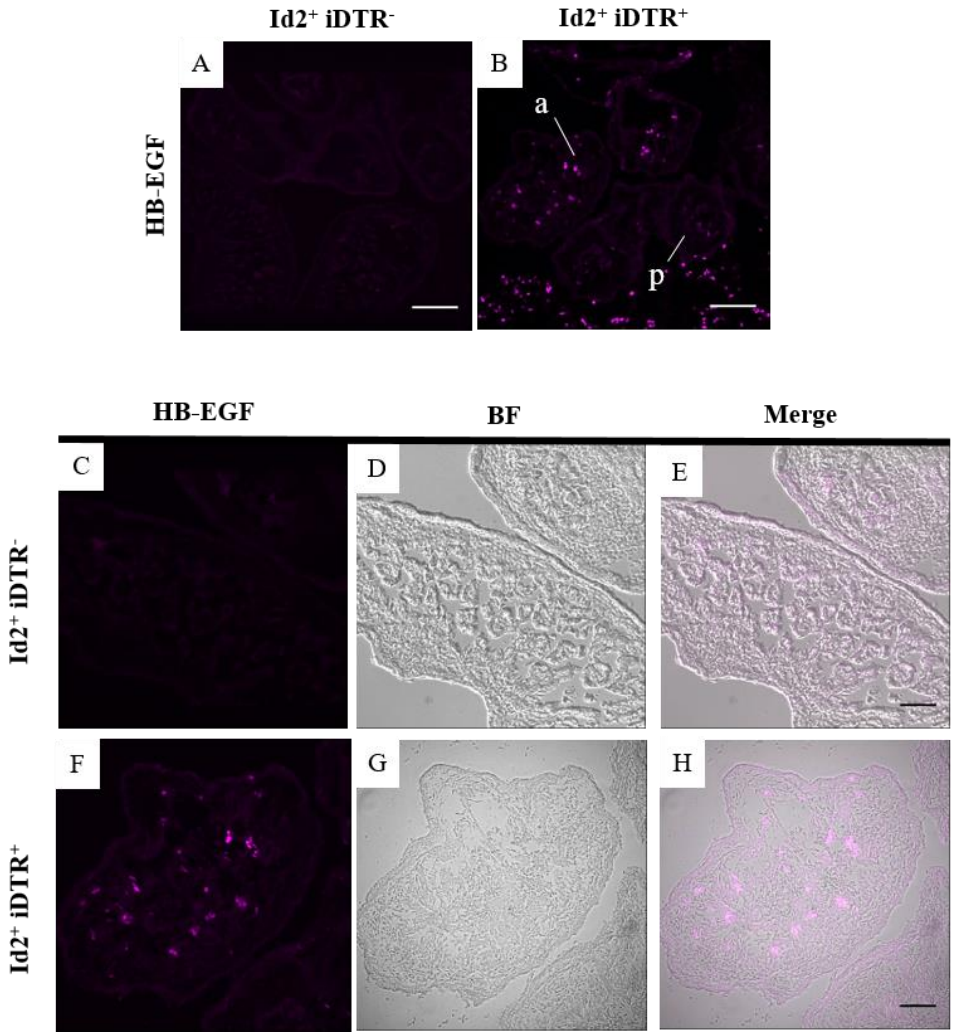

Figure 4. 12. Immunostaining against HB-EGF in 10 µm sections from Id2^{Cre}iDTR mouse embryos at E15.5 embedded in paraffin. Female mouse was treated with TAM at E8.5 and DT at E13.5. A and B are an overview of the embryonic small intestine section. The remaining pictures present the anterior portion of the embryonic small intestine. Bright-field (BF) images are shown in second column and the merge of all the pictures in the last one. a – anterior. p – posterior. Scale bars correspond to 50 µm in A and E, and 20 µm in the remaining pictures.

Similar to what is described in **Figure 4.9**, fluorescence correspondent to the receptor expression is mainly observed in the anterior part of the small intestine (**Figure 4.12 B**). The presence of the DT receptor in the sections from the embryonic small intestine was only detected in samples genotyped positively for iDTR (**Figure 4.12 B and F**), with dispersed fluorescent zones visible in the epithelium. This scattered fluorescent can be related to the efficiency of the homologous recombination induced by TAM so, even though the embryo is iDTR$^+$, not all the epithelial cells could be expressing the DT receptor. Also, since this assay was performed after the treatment with the toxin, it's expected to be less signal since some cells may have died.

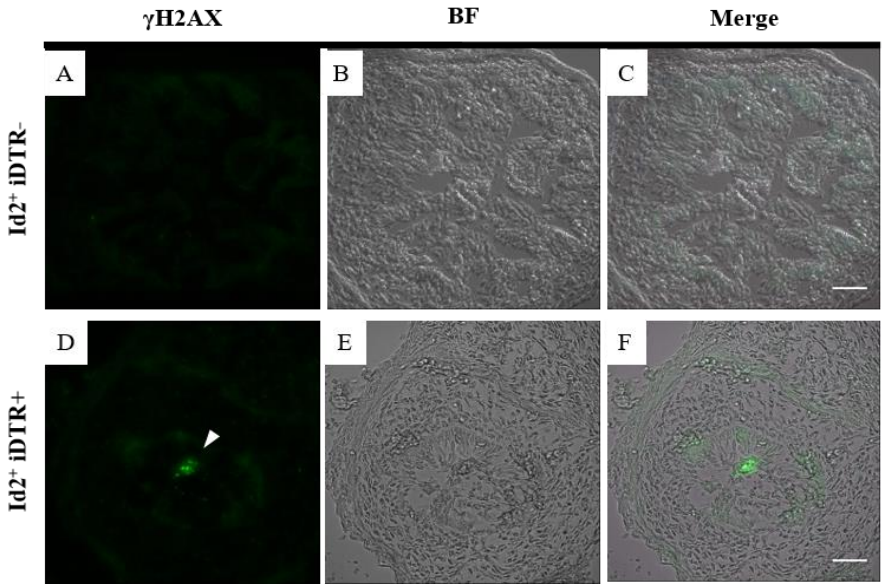

Figure 4. 13. Immunostaining against γH2AX in 10 µm sections from Id2^{Cre}iDTR mouse embryos at E15.5 embedded in paraffin. Female mouse was treated with TAM at E8.5 and DT at E13.5. The white arrow indicates the apoptotic zone. Bright-field (BF) images are shown in second column and the merge of all the pictures in the last one. Scale bars correspond to 10 µm.

Apoptotic zones were detected in the small intestine's lumen (**Figure 4.13**) by immunostaining against γH2AX, indicating that with 5 days between the treatment with TAM and DT some cells start to undergo the apoptotic process.

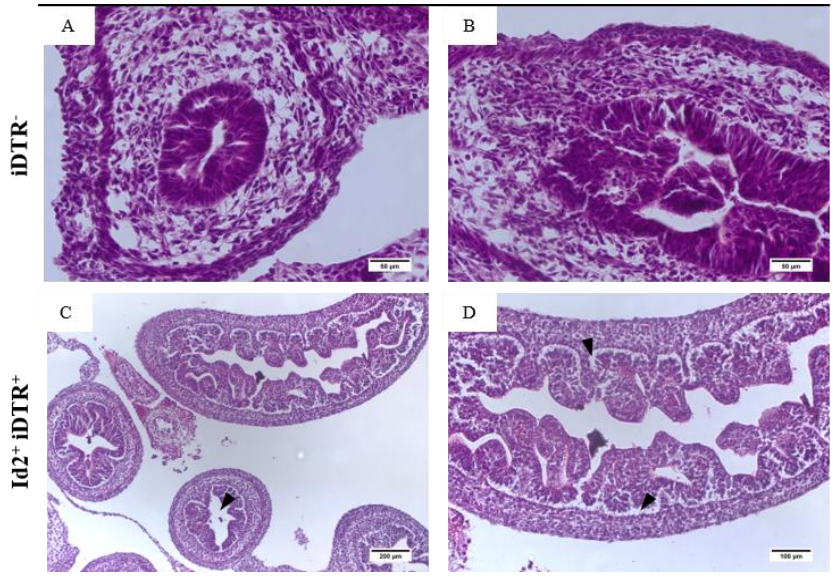

Figure 4. 14. Comparison between the histology of small intestine in 10 µm cryosections from (A-B) Hprt^{Cre}iDTR mouse embryos at E14.5 and (C-D) Id2^{Cre}iDTR mouse embryos at E15.5 embedded in paraffin, treated with DT. (A-B) Female mouse was treated with TAM at E11.5 and DT at E13.5. (C-D) Female mouse was treated with TAM at E8.5 and DT at E13.5. Posterior (A) and anterior portions (B and D) of embryonic the small intestine are portrayed. Both portions are presented in C. Prominent characteristics, such as areas of detachment and lumen enlargement, are indicated by the black arrows. Scale bars correspond to 50 µm in A and B, 200 µm in C and 100 µm in D.

The phenotype of $Id2^{Cre}$iDTR mouse embryos treated with DT is presented in **Figure 4.14**. The morphology of the $Id2^{+}iDTR^{+}$ embryos was compared with $iDTR^{+}$ treated with DT from the $Hprt^{Cre}$iDTR litter, used as a negative control. Even though the phenotype is not as drastic as the observed in $Hprt^{Cre}$iDTR embyros upon DT treatment, $Id2^{Cre}$iDTR embryos present a detachment between the small intestine's epithelium and the mesenchyme (indicated by the arrows in **Figure 4.14 D**). The lumens size also appears to have increased (indicated by the arrows in **Figure 4.14 C**). All this features are not present in **Figure 4.14** A and **B**, where a normal morphology of the embryonic small intestine is presented.

Compared with the first assays performed with $Id2^{Cre}$iDTR embryos, these results indicate that the labelling of $Id2^{+}$ cells is efficient at E8.5. The modifications observed by DT action might be due to the increase of time between its injection and the collection of the embryos, giving the toxin more time to take action.

However, immunostaining - together with fluorescence microscopy – is a detection method with low efficiency. The percentage of labelled cells detected is very low – approximately 10% – and these results are influenced by the time gap between the TAM administration and mouse opening. Due to this, by the time this assay is done it's not the $Id2^{+}$ progenitor cells that are labelled, but its descendants.

4.3.2. Isolation of intestinal epithelial cells

In order to overcome the limitations of immunostaining and gain more insight on the DT-mediated ablation of $Id2^{+}$ cells, further work was conducted using a new strain: $Id2^{Cre}dsRed^{+/-}Lgr5^{GFP}$iDTR mice (**Annex 3**). Besides the histochemical analysis, this system allowed to measure the percentage of $Id2^{+}$ cells, since they would show red fluorescence, giving a more precise idea of the efficiency of the method used to ablate the $Id2^{+}$ cells – besides the DT receptor, some *Id2* positive mouse embryos will also express *dsRed*, which encoded for a red fluorescent protein.

Immunostainings to assess the expression of the receptor and apoptosis in this new strain are shown in **Figure 4.15**.

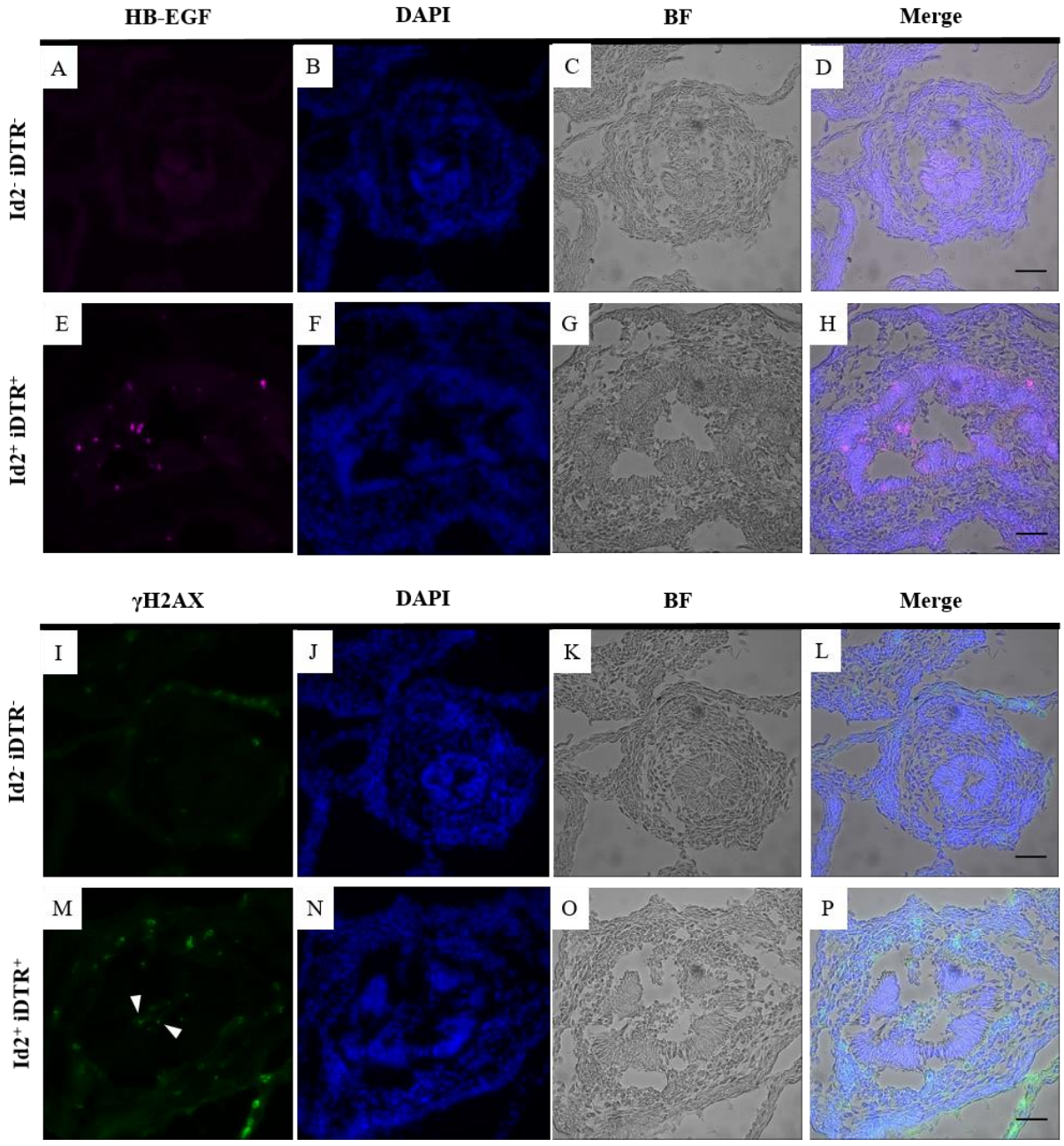

Figure 4. 15. Immunostaining against HB-EGF and γH2AX in 10 µm cryosections from Id2^{Cre}dsRed$^{+/-}$ Lgr5^{GFP}iDTR mouse embryos, treated with DT, at E13.5. Female mouse was treated with TAM at E8.5 and DT at E12.5. (A to H) Immunostaining against HB-EGF. (I to P) Immunostaining against γH2AX. Apoptotic sites are indicated by the white arrows. Bright-field (BF) images are shown in the third column and merge of all the pictures on the last one. Scale bars correspond to 10 µm.

These stainings show the expression of the DT receptor in the epithelium of the Id2^{+} iDTR^{+} embryo (**Figure 4.15 E**), as well as apoptosis in the small intestine's lumen in the same conditions (**Figure 4.15 M**). Receptor is not expressed in the double negative sample and, regarding the staning against γH2AX, only auto fluorescence was detected (**Figure 4.15 A and I**, respectively).

Once the receptor's expression and apoptosis were detected in this strain, work progressed to the isolation of intestinal epithelial cells.

To do so, and besides the embryonic small intestine, lungs were collected. This organ was observed under a microscope to detect red fluorescence, given the fact that if the embryo is positive for *dsRed*, lungs will present red fluorescence (**Figure 4.16**). This method allows the rapid selection of the embryos that should undergo sorting. After sorting, embryos were genotyped in order to determine which ones were expressing the receptor and which of the embryos presenting red fluorescence on the lungs were positive for *Id2* and *dsRed*. (**Figure 4.17**).

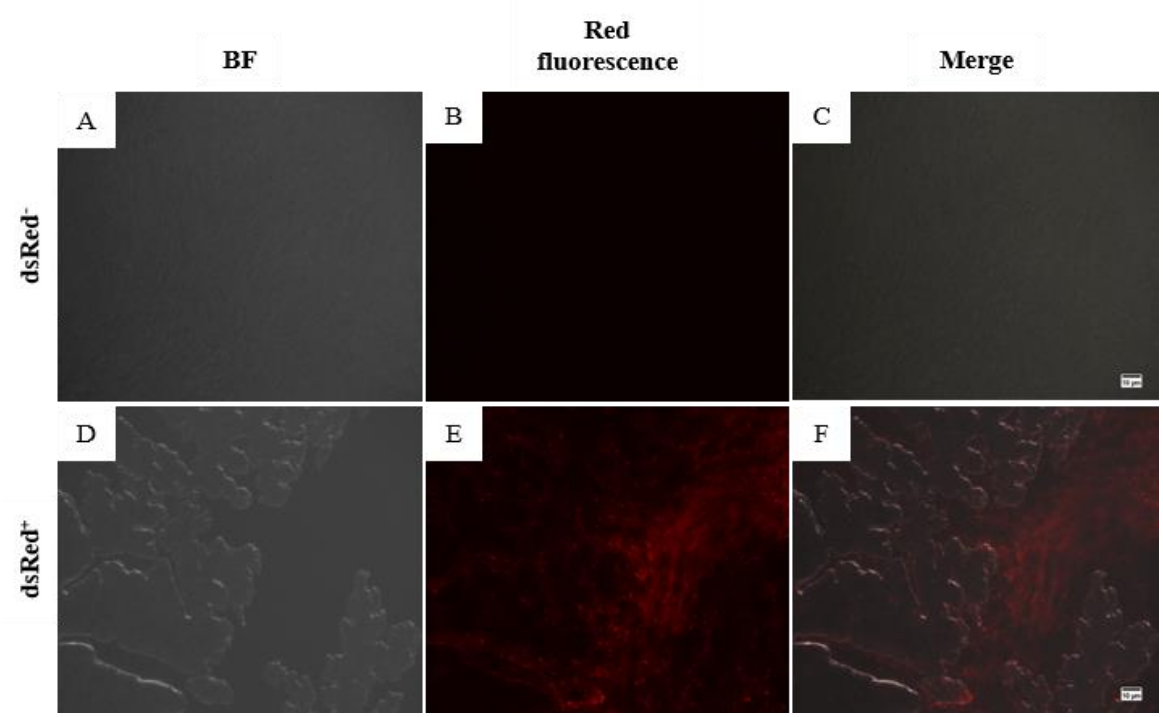

Figure 4. 16. Red fluorescence detected in lungs from Id2^{Cre}dsRed$^{+/-}$Lgr5^{GFP}iDTR mouse embryos, treated with DT, at E14.5. Pictures show lungs from an embryo negative (A-C) and positive (D-F) for *dsRed*. BF – bright field. Pictures taken in a Leica IL LED microscope. Scale bar corresponds to 10 µm.

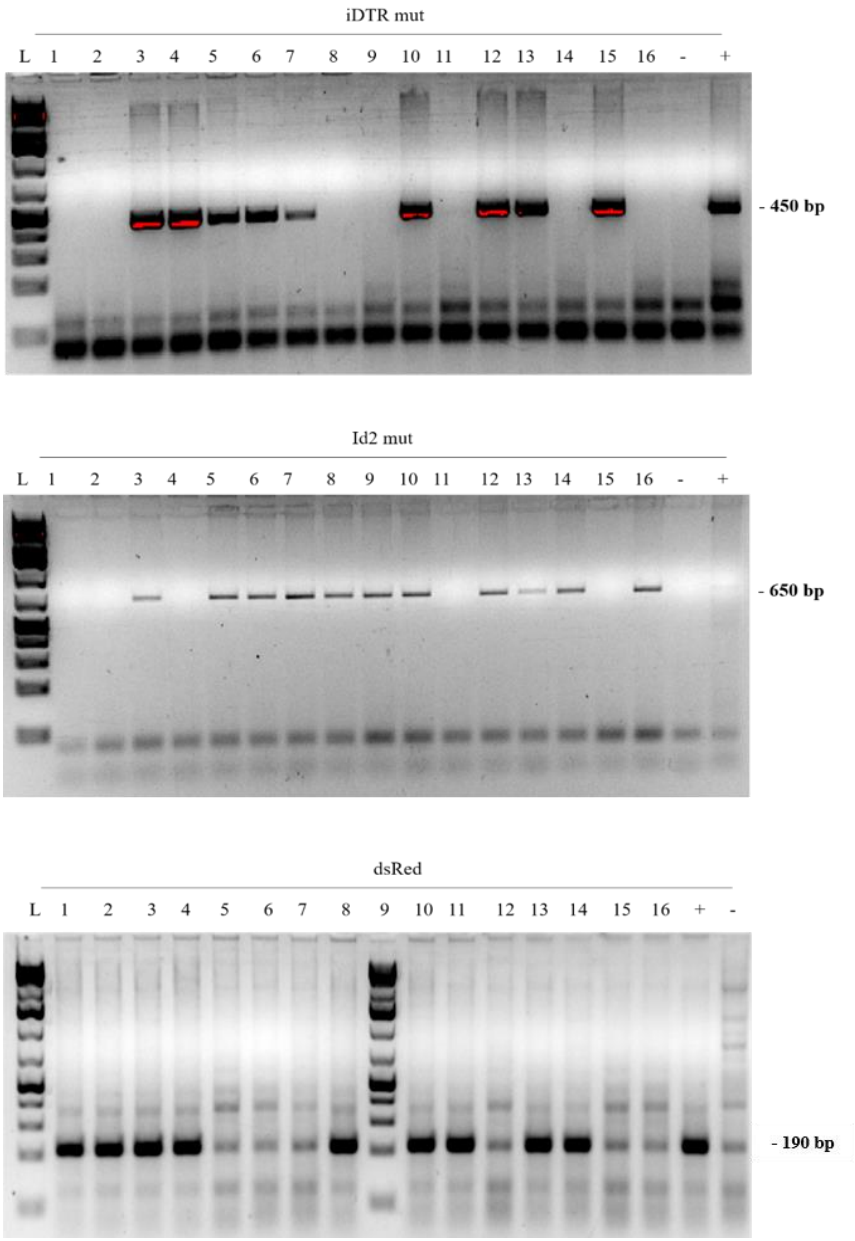

Figure 4. 17. Genotyping results of Id2^{Cre}dsRed$^{+/-}$iDTR embryos treated with DT, for *iDTR* mut (450 bp), *Id2* mut (650 bp) and *dsRed* (190 bp), on a 2% agarose gel in 1x TAE stained with EtBr. (-) and (+) are the negative and positive controls of the PCR reaction. mut – mutant. L corresponds to the ladder GeneRuler 1Kb Plus DNA Ladder.

From 16 embryos, 7 were double positive (Id2^{+}iDTR^{+}) but only 3 were triple positive (Id2^{+}iDTR^{+}dsRed^{+}) – embryos 3, 10 and 13.

Intestinal epithelial cells from mouse embryos were isolated by FACS. In order to isolate the target cells, samples were stained with EpCam antibody, given the fact that this protein is present in the intestinal epithelium. Cells were co-stained with DAPI to discriminate

between live and dead cells. Only cells positive for EpCam were gated to be analyzed for red fluorescence by flow cytometry (**Figure 4.18**).

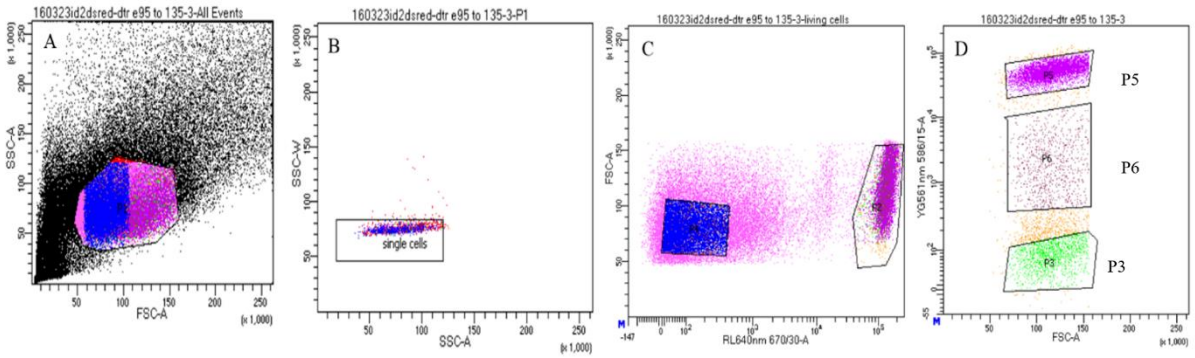

Figure 4. 18. Strategy used in the isolation of epithelial intestinal cells. Cells were co-stained with DAPI in order to discriminate between living and dead cells (A). Duplets were discarded and only single cells were taken for further analysis (B). Through EpCam staining, single cells were divided into epithelial cells (EpCam$^+$, right gate) and mesenchymal cells (EpCam$^-$, left gate) (C). Finally, EpCam$^+$ cells were sorted for red fluorescence. Non-red (P3), red (P6) and high-red EpCam$^+$ cells (P5) (D).

In this conditions – 2-day interval between the administration of TAM and DT, and dissection a day after toxin administration – only one (embryo 10) out of the 3 triple positive embryos showed a decrease in the red cells percentage (**Figure 4.19**). Non-red and high-red EpCam$^+$ cells from the triple positive (embryo 10) and from an Id2$^+$iDTR$^-$dsRed$^+$ sample (embryo 8) were collected for further genetic analysis by qPCR.

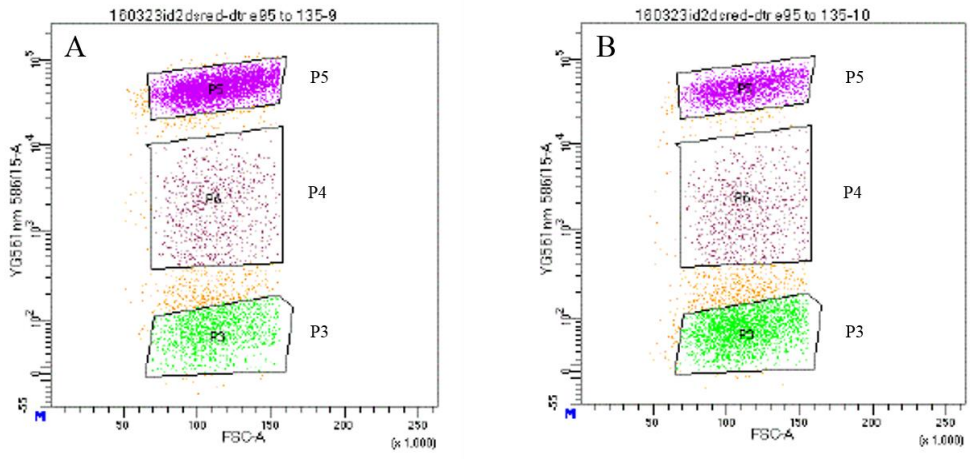

Figure 4. 19. Red epithelial cells from embryonic small intestine sorted at E13.5. (A) Id2$^+$iDTR$^-$dsRed$^+$ embryo. (B) Id2$^+$dsRed$^+$iDTR$^+$ embryo. P3 – Non-red epithelial cells. P4 – Red epithelial cells. P5 – High-red epithelial cells.

The percentage of epithelial red cells on the iDTR^{-} sample (**Figure 4.19 A**) was 65.5%, while on the triple positive (**Figure 4.19 B**) was 36.6% – approximately 30% less.

As mentioned above, only 1 out of 3 triple positive embryos showed a decrease in the red cells percentage. To see if both the percentage of labeled and ablated cells would increase, a new experimental setup was established – labeling with TAM was done at E7.5 and DT was injected during 3 consecutive days (E8.5 to E11.5). Dissection was done 3 days after the last toxin injection (E14.5).

However, in this litter, 7 out of 13 embryos were not alive at the time of the collection. Furthermore, according to genotyping results (**Figure 4.20**), the DT-sensitive embryos were among the dead pups, so only iDTR^{-} samples were taken for cell sorting (**Figure 4.21**).

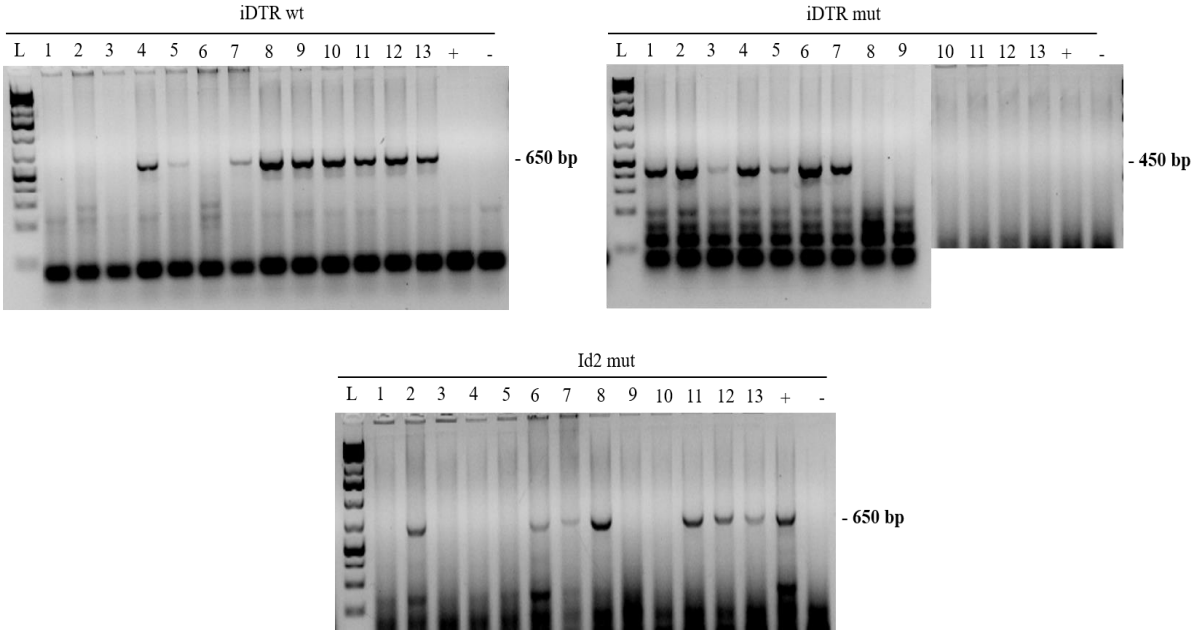

Figure 4. 20. Genotyping results of Id2^{Cre}dsRed$^{+/-}$iDTR embryos treated with DT, for *iDTR* wt (650 bp), *iDTR* mut (450 bp) and *Id2* mut (650 bp), on a 2% agarose gel in 1x TAE stained with EtBr. Embryos 1 to 7 were dead inside the mother's womb at the time of the collection. (-) and (+) are the negative and positive controls of the PCR reaction. wt – wildtype. mut – mutant. L corresponds to the ladder GeneRuler 1Kb Plus DNA Ladder.

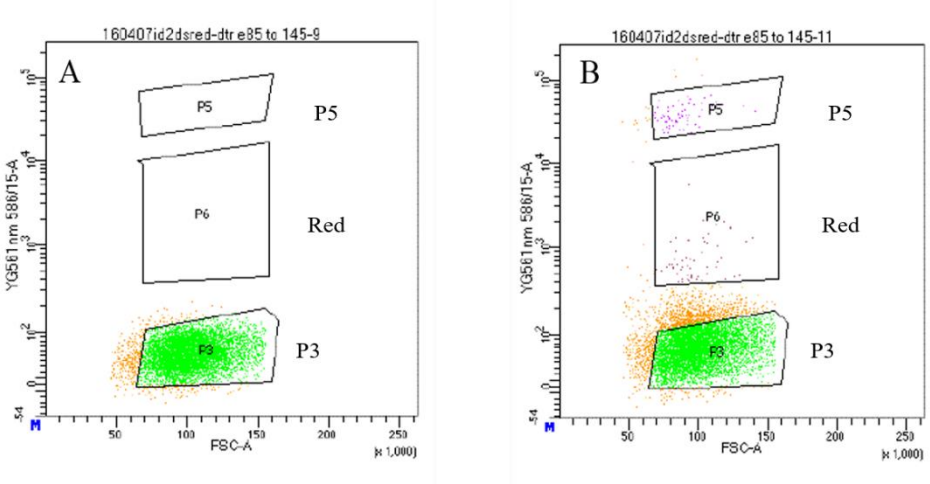

Figure 4. 21: Red epithelial cells from embryonic small intestine sorted at E14.5. (A) Id2^{-}iDTR^{-}dsRed^{-} embryo. (B) Id2^{+}dsRed^{+}iDTR^{-} embryo. P3 – Non-red epithelial cells. P4 – Red epithelial cells. P5 – High-red epithelial cells.

As expected, no red cells were detected by FACS in the negative sample (**Figure 4.21 A**), which was in accordance with the genotyping results that had identified this sample as Id2 negative and thus it did not have the *dsRed* cassette on its genome. On the sample positive for *Id2* and *dsRed*, only 1% of the analyzed cells were red (**Figure 4.21 B**), suggesting that the homologous recombination was not efficient.

Even though Danielian *et al*. (1998) reported that a single injection of 2 mg of TAM – similar to the dose administrated – at E8.5 led to a rapid loss of embryos[134], TAM was not the cause of death of the embryos, since it only occurred in iDTR^{+} embryos. This means that the three consecutive DT injections were most likely the cause of death of 53% of the litter. The lethality could be due to 1) the toxin's action itself, given its toxicity or 2) since *Id2* is expressed in other tissues than the epithelium of the small intestine during embryonic development – thus the DT receptor will be expressed in those other tissues as well –, the consecutive treatment with DT might have ablate Id2^{+} cells at a larger scale, and taken together, it caused the inviability of the iDTR^{+} embryos.

Due to the previous results, in the third crossing that was carried out to produce Id2^{Cre}dsRed$^{+/-}$Lgr5^{GFP}iDTR progeny, TAM was administrated at a later time point – E11.5. Thus, DT was injected at E13.5 and dissection performed 3 days later, at E16.5. Embryo genotyping results are showed in **Figure 4.22**. To note that all the embryos were viable at the time of collection.

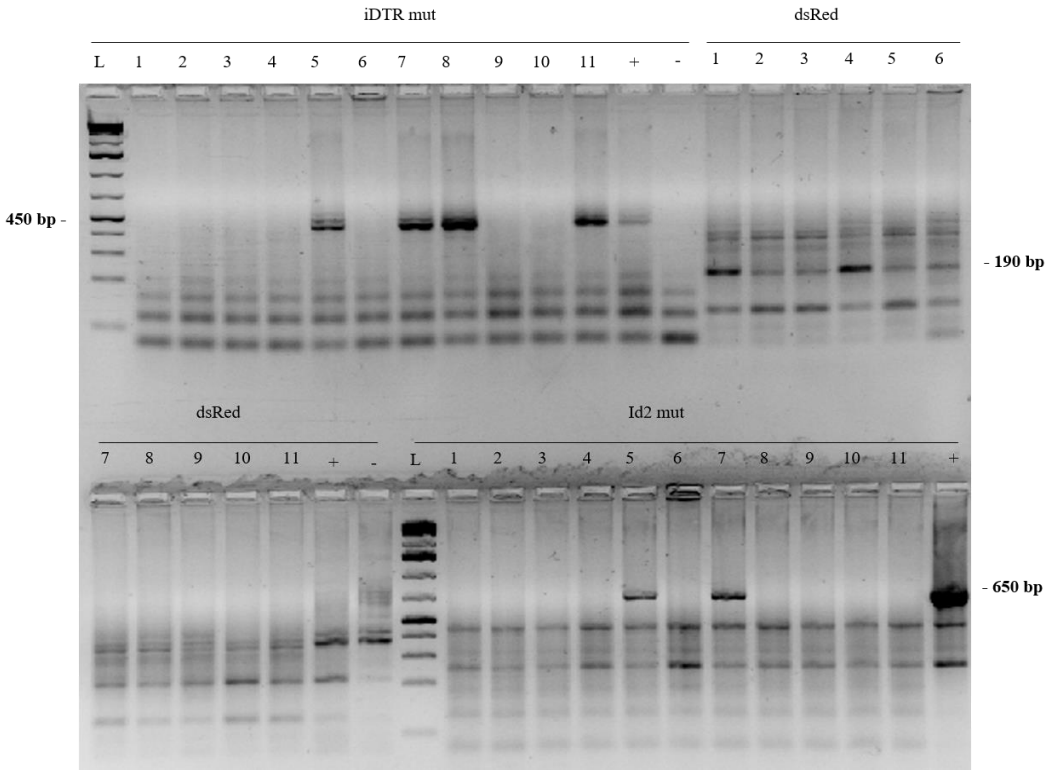

Figure 4. 22. Genotyping of Id2^{Cre}dsRed$^{+/-}$Lgr5^{GFP}iDTR embryos treated with DT, for *dsRed* (190bp), *Id2* mut (650 bp) and *iDTR* mut (450 bp), on a 2% agarose gel in 1x TAE stained with EtBr. (-) and (+) are the negative and positive controls of the PCR reaction. mut – mutant. L corresponds to the ladder GeneRuler 1Kb Plus DNA Ladder.

The embryos were dissected, the small intestines collected and divided in anterior and posterior (**Annex 2**). Epithelial cells of each of the sections of the embryonic small intestine were isolated and samples were sorted for red cells (**Figure 4.23**).

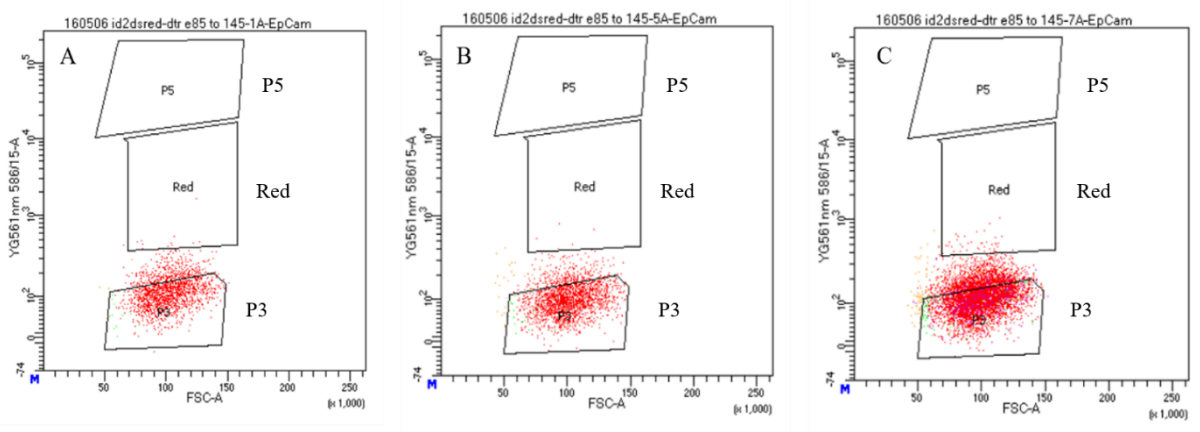

Figure 4. 23. Sorted red epithelial cells from small intestine of mouse embryos at E16.5. (A) Id2^{-}iDTR^{-}dsRed^{-} embryo (triple negative). (B) and (C) Id2^{+}dsRed^{-}iDTR^{+} embryo (double positive). P3 – Non-red epithelial cells. Red – Red epithelial cells. P5 – High-red epithelial cells.

According to genotyping (**Figure 4.22**), none of the embryos were triple positive ($Id2^{+}iDTR^{+}dsRed^{+}$), since none of them presented the bands for all the 3 gene fragments analyzed. These results were further confirmed by FACS, where no red cells were detected (**Figure 4.23**).

Besides the red fluorescence, the strain used in these assays – $Id2^{Cre}dsRed^{+/-}Lgr5^{GFP}iDTR$ – has a gene that encodes for the green fluorescent protein (GFP) under the control of the *Lgr5* gene promoter. Due to this, if an embryo is positive for *Lgr5*, it will present green fluorescence. Sorting showed changes in the green cell percentage and, given this, they were analyzed to verify if the DT in DT-sensitive embryos would have any effect in this green cell population. A representation of the gates used to assess the percentage of green cells is shown in **Figure 4.24**.

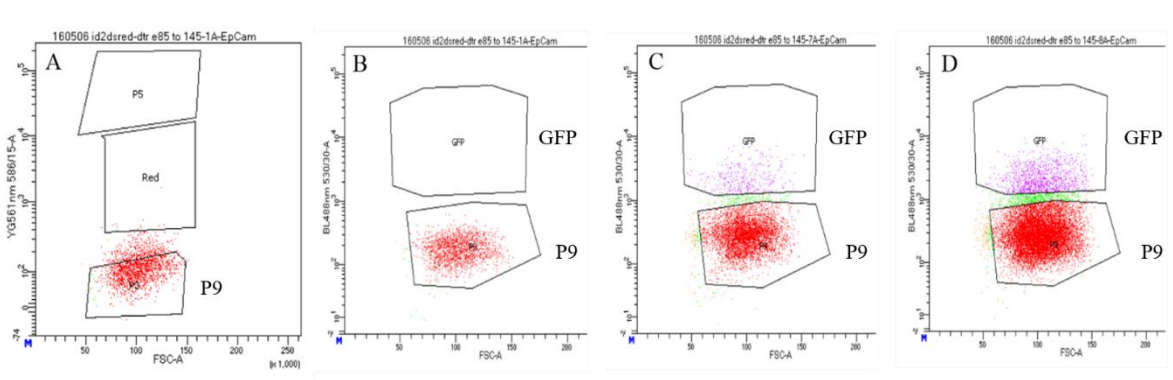

Figure 4. 24. Sorted green epithelial cells from small intestine of mouse embryos at E16.5. (A) Cells from gate P9, non-red epithelial cells, were sorted and analysed for green fluorescence (GFP). (B) $Lgr5^{-}$ embryo. (C) $Id2^{+}Lgr5^{+}iDTR^{+}$. (D) $Id2^{+}Lgr5^{+}iDTR^{-}$ embryo.

The effect of $Id2^{+}$ cell ablation in the $Lgr5^{+}$ cell population can already be observed in **Figure 4.24**, where the $iDTR^{+}$ embryo has less green cells than the $iDTR^{-}$ (**Figure 4.24, C and D**, respectively). To have a better understanding of the influence of the Id2 ablation in the green cell population, percentages between $iDTR^{-}$ and $iDTR^{+}$ embryos, both for the anterior and posterior portions of the embryonic small intestine, were compared (**Figure 4.25**).

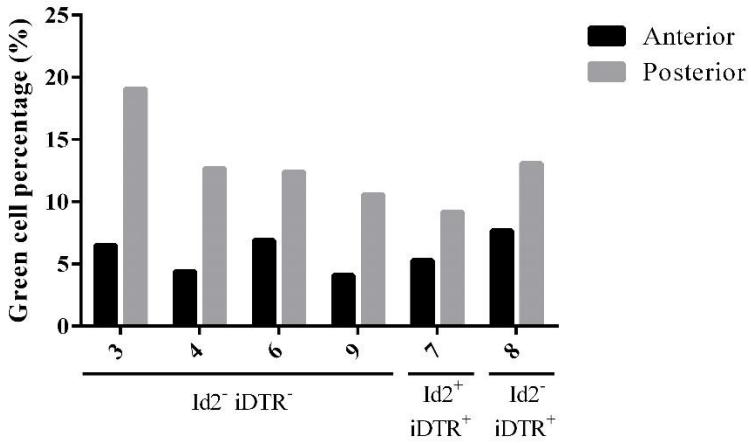

Figure 4. 25. Green cell percentage in Lgr5 positive mouse embryos collected at E16.5 obtained by FACS analysis of different sections – anterior and posterior – of the small intestine.

The cells from the posterior section of the embryonic small intestine express more *Lgr5*, as higher percentages of green cells were found in the cell preparation from this section when compared with the values observed from the anterior embryonic small intestine (**Figure 4.25**). The $Id2^{+}iDTR^{+}$ embryo showed a green cell percentage of 5.3% and 9.2% - in anterior and posterior, respectively – against the 7.7% and 13.1% presented by $Id2^{-}iDTR^{+}$. In double negative samples (embryos 3, 4, 6, 9), the green cells percentages range from 4.1% to 6.9% in anterior and from 10.6% to 19.1% in the posterior embryonic small intestine. These results show that the green cell percentages presented by $Id2^{+}iDTR^{-}$ embryos are within the range of the negative controls and so, the difference in the $Lgr5^{+}$ cell population observed in $Id2^{+}iDTR^{+}$ is due to the toxin's action. This evidences the existence of a possible correlation between the $Id2^{+}$ and $Lgr5^{+}$ cells, even though it was not possible to detect changes in the red $Id2^{+}$ cell population, and compare the changes between both populations.

In order to have stronger red cell signal, further crossings were done with one of the parents being homozygous for dsRed ($dsRed^{+/+}$). Also, this litter had a three-day break between TAM (E11.5) and DT (E14.5) treatments. Embryos were collected at E15.5. Genotyping was performed in the collected embryos and results are shown in **Figure 4.26**. The gates used for sorting of the red cells are the ones described previously in **Figure 4.18**.

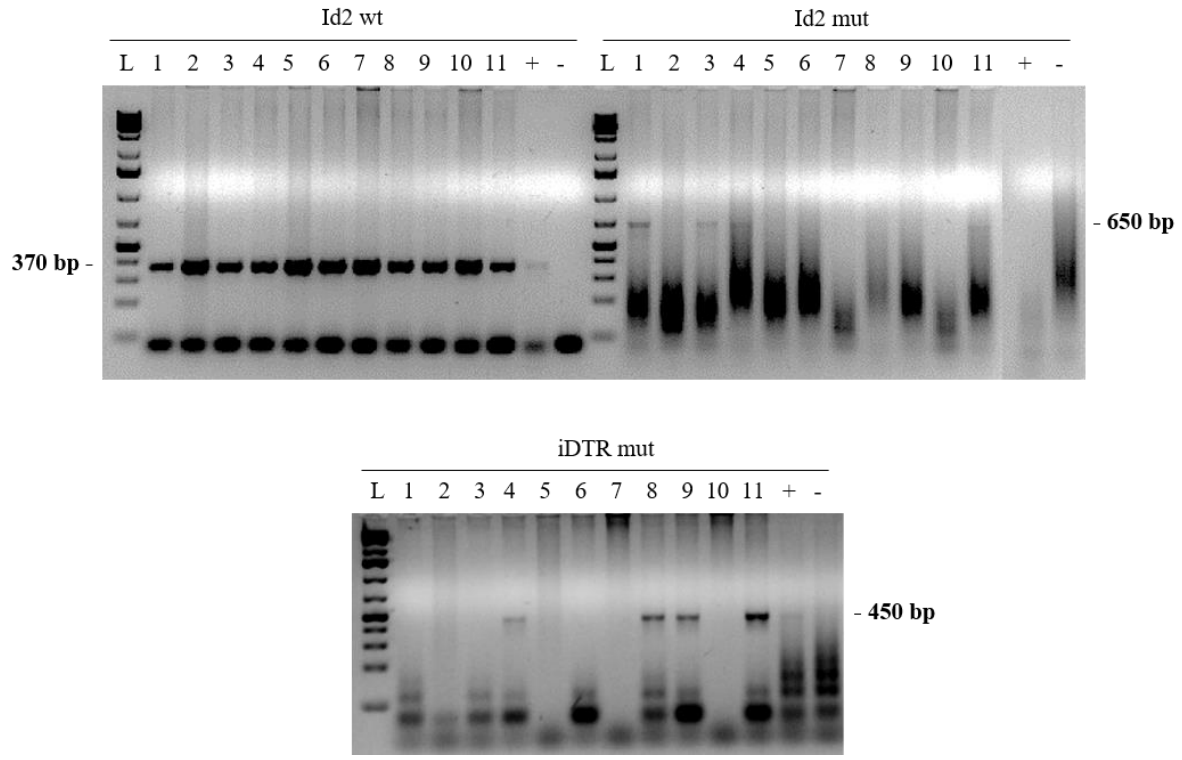

Figure 4. 26. Genotyping of Id2^{Cre}dsRed$^{+/+}$Lgr5^{GFP}iDTR embryos treated with DT, for *Id2* wt (370 bp), *Id2* mut (650 bp) and *iDTR* mut (450 bp), on a 2% agarose gel in 1x TAE stained with EtBr. (-) and (+) are the negative and positive controls of the PCR reaction. wt – wildtype. mut – mutant. L corresponds to the ladder GeneRuler 1Kb Plus DNA Ladder.

Genotyping results (**Figure 4.26**) show that only two out of 11 embryos were double positive for Id2 and iDTR (embryos 4 and 11), since just this 2 present bands for the mutant form of Id2 and iDTR. All of the mouse embryos collected were analyzed by FACS to detect the presence of red fluorescent cells (Id2^{+} cells) and embryos 1 to 4, as well as 11, were positive for red fluorescence. However, only 1, 3, 4 and 11 were positive for *Id2* mut. This means that, between these 4 embryos, theoretically only embryos 4 and 11 will show a decrease in the Id2 red cell population due to the action of DT.

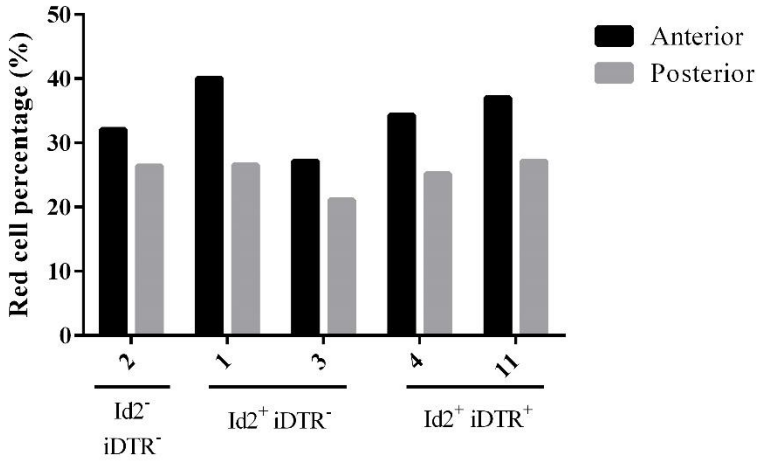

Figure 4. 27. Red Id2$^+$ cells percentage in mouse embryos collected at E15.5 obtained by FACS analysis of different sections – anterior and posterior – of the small intestine.

Overall, the posterior part of the embryonic small intestine shows less percentage of Id2$^+$ red cells (**Figure 4.27**), indicating that *Id2* can be more expressed in the anterior section. However, the embryo that shows less percentage of red cells both in anterior and posterior section of the small intestine – embryo 3 – is only positive for *Id2* mut, meaning that the Id2$^+$ cell ablation mediated by the toxin was not successful in this assay. This is further supported by the fact that both Id2$^+$iDTR$^+$ embryos – 4 and 11 – presented about the same red cell percentages as the embryos that don't express the DT receptor.

The percentage of Lgr5$^+$ green cells in the different embryo's small intestine sections (anterior and posterior) was also analyzed by FACS and are shown in **Figure 4.28**.

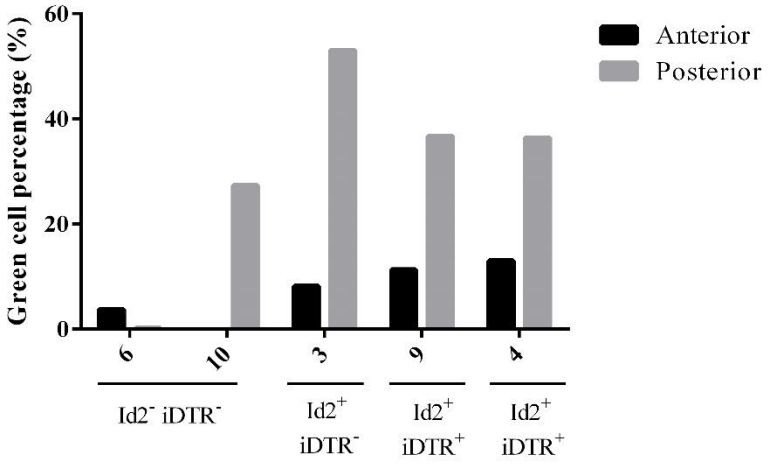

Figure 4. 28. Green cell percentage in Lgr5 positive mouse embryos collected at E15.5 obtained by FACS analysis of different sections – anterior and posterior – of the small intestine.

Similarly, to what was observed on **Figure 4.25**, cells expressing *Lgr5* were found to be expressed in higher amount in the posterior section of the embryonic small intestine in this litter (**Figure 4.28**). Also, iDTR$^+$ embryos show less green cells in the posterior section when compared to embryo 3, which is iDTR$^-$, evidencing once more the possible influence of *Id2* in the Lgr5$^+$ population.

Since the intervals between the treatment with TAM and DT might influence the number of labeled and ablated cells, the time points should ideally be as close as possible. Due to this, and following the previous results, the interval between TAM and DT treatment was shortened to one day – TAM was administrated at E13.5, DT injected at E14.5 and dissection of the pregnant females performed at E16.5. Embryo genotyping, red Id2$^+$ cell and green Lgr5$^+$ cell percentages by FACS are shown in **Figures 4.29** to **4.31**, respectively.

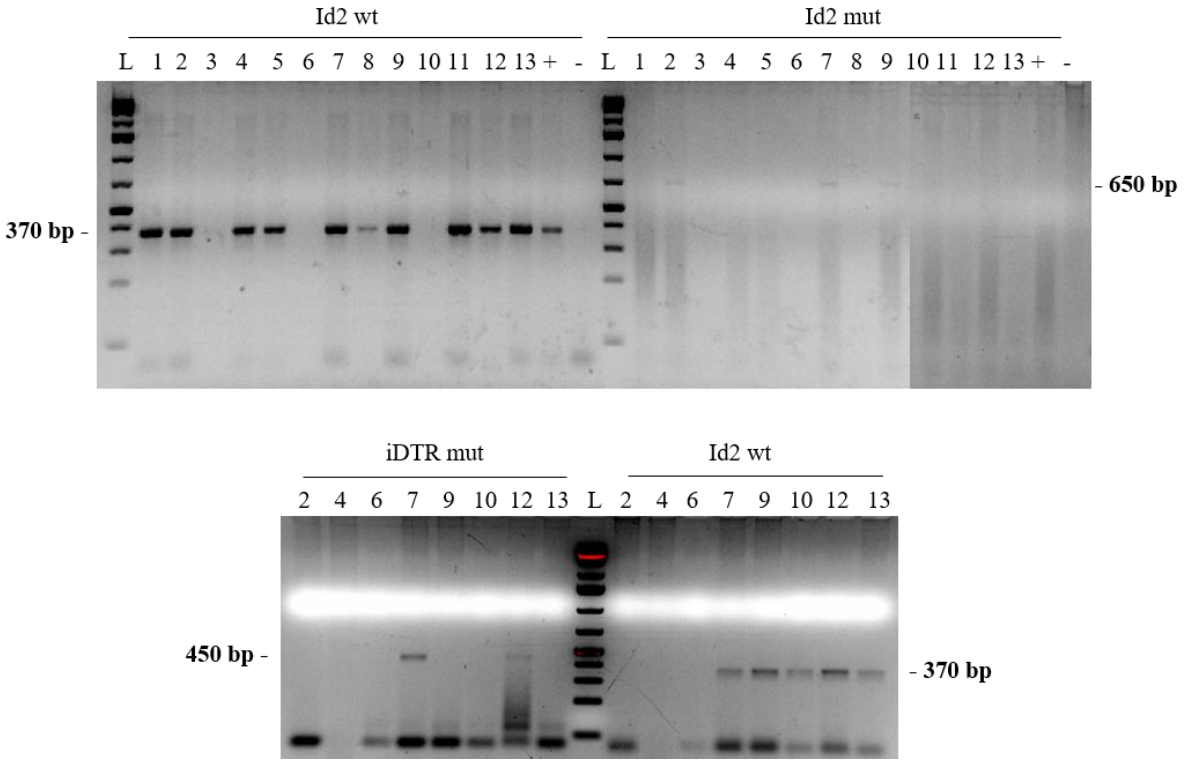

Figure 4. 29. Genotyping of Id2^{Cre}dsRed$^{+/+}$Lgr5^{GFP}iDTR embryos treated with DT, for *Id2* wt (370 bp), *Id2* mut (650 bp) and *iDTR* mut (450 bp), on a 2% agarose gel in 1x TAE stained with EtBr. (-) and (+) are the negative and positive controls of the PCR reaction. wt – wildtype. mut – mutant. L corresponds to the ladder GeneRuler 1Kb Plus DNA Ladder.

According to genotyping, one out of 13 embryos is double positive for *Id2* and *iDTR* (embryo 7). Embryos 2 and 9 are positive for *Id2* and embryo 12 was positive only for *iDTR*.

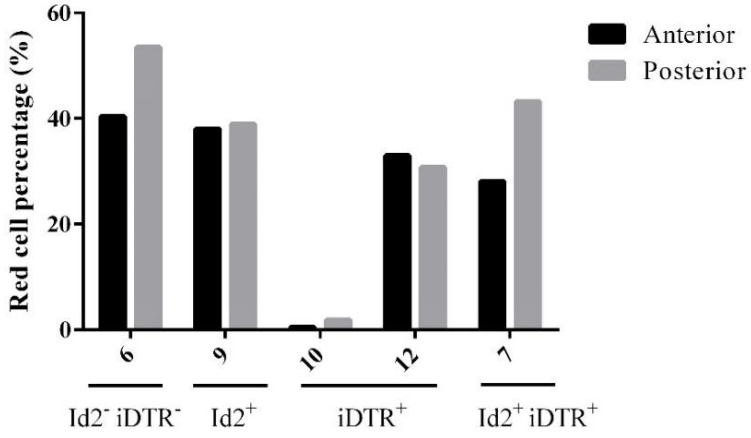

Figure 4. 30. Red Id2^{+} cells percentage in mouse embryos collected at E16.5 obtained by FACS analysis of different sections – anterior and posterior – of the small intestine.

Analyzing the FACS results for the $Id2^+$ red fluorescent cells (**Figure 4.30**), it is possible to observe that one-day interval between TAM and DT treatment led to a decrease in the red cell percentage on the embryonic small intestine's epithelium in the $Id2^+iDTR^+$ (embryo 7), when compared with the double negative (embryo 6), indicating that in this conditions the embryos were susceptible to the DT's action. Embryos found to be $iDTR^+$ (embryos 10 and 12) also show a lower amount of red cells, given the fact that these embryos have the DT receptor being expressed. Regarding embryo 10, the percentages observed – 0.5% in anterior and 1.8% in posterior – have a great difference compared to embryo 12. Given the fact that in this progeny, upon homologous recombination, the gene that encodes for *dsRed* is under the control of the *Id2* specific promoter, it was expected that only $Id2^+$ cells presented red fluorescence. Given this, either the red cell percentages of embryo 10 are an artifact caused by some *dsRed* leakage or this embryo is also $Id2^+$. However, this cannot be inferred since when the genotyping for *Id2* mut was done (**Figure 4.29**), embryo 10 had no band for *Id2* wt, meaning that no genetic material was amplified possible due to insufficient DNA amount, even though when the genotyping for *iDTR* was performed it showed a band in the *Id2* wt controls.

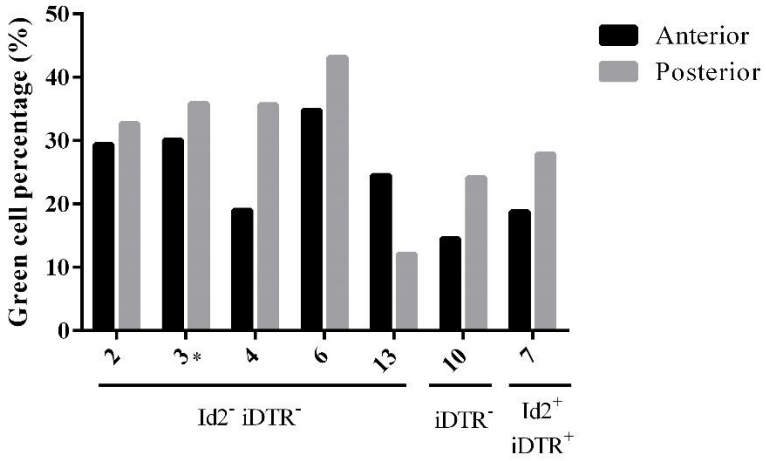

Figure 4. 31. Green cell percentage in Lgr5 positive mouse embryos collected at E16.5 obtained by FACS analysis of different sections – anterior and posterior – of the small intestine. Embryo 3 is indicated with (*) because genotyping was inconclusive.

As with the previous litters, $Lgr5^+$ green cells were analyzed by FACS and the results are presented in **Figure 4.31**. Overall, with exception of embryo 13, there are more green $Lgr5^+$ cells on the posterior section of the embryonic small intestine. However, even though the $Id2^+iDTR^+$ embryo (embryo 7) shows less green cells compared with most of the double

negatives (embryos 2, 3, 4, 6 and 13), the values are very similar to the ones presented in the iDTR$^-$ negative embryo, and thus no conclusions can be drawn.

As mentioned previously the time points between TAM administration, DT injection and embryo collection should be as close as possible, such as one day between each one, with special attention to the gap between TAM and DT – the bigger the interval, higher is the chance to label Id2$^+$ descendants and not its progenitors. Although it's reported in the literature that significant recombination is still observable between 24 and 48 h after TAM administration[135], Robinson *et al*. (1991) stated that TAM peak levels occurred between 3 and 6 h after oral administration[136]. These authors also reported that the half-life of TAM in mice is 11.9 h[136], which means that TAM levels at this organism are null roughly 24 h later its administration.

However, the establishment of this ideal time points was not achieved during the execution of this project, since some of the female mice got abortions. From 9 Id2^{Cre}dsRed$^{+/-}$ Lgr5^{GFP} x iDTR crossings, 3 of the females had an abortion the day after DT was injected. Although the abortions happened after the injection of toxin, the remaining mice treated in the same conditions had no complications to achieve the desired gestational stage, so these occurrences might be due to the antiestrogen activity of TAM. Similar events were reported by Danielian *et al*. (1998)[134], where pregnancies failed shortly after TAM injection, even though this was stated to happen after three consecutive TAM administrations.

4.3.2.1. Genetic analysis of intestinal epithelial cells

We evaluated the genetic differences between Id2$^+$ high-red intestinal epithelial cells between both conditions – DT receptor negative and positive – in order to assess the influence of the DT-mediated ablation in the cells genetic programs. Genetic analysis was conducted in embryonic small intestine collected at E13.5 from embryos treated with TAM at E10.5 and DT at E12.5.

The following genes were analyzed: *Id1*, *Id2*, *Id3*, *Lgr5*, *Wnt6*, *Wnt11*, *PUMA*, *Rspo1*, *Rspo3*, *Snai2*, *Smoc2*, *Sfrp5*, *Kcnq1*, *TPB*, *Kcne3*, *St8sia3*, *Slc2a3*, *OneCut*. *EpCam* was used as the housekeeping gene, since it is constitutively being expressed in the embryonic small intestine epithelium. Results are shown in **Figures 4.32** and **4.33**.

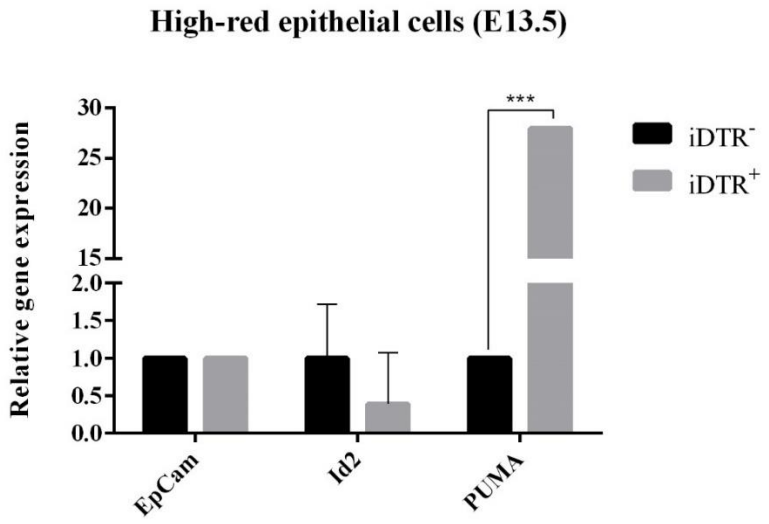

Figure 4. 32. Gene expression analysis of *Id2* and *PUMA* in high-red intestinal epithelial cells collected at E13.5. Results are shown as mean ± SEM, with N=3. Statistical significance was evaluated with Student's t test. *** corresponds to $p<0.0001$.

Results of gene expression presented in **figure 4.32** show a reduction in *Id2* expression levels in the red cells isolated from the iDTR$^+$ mouse embryos, even though not statistically significant. These results might be due to the fact that ablation of Id2$^+$ cells was not completely achieved. It is important to note the increase in PUMA expression – an apoptotic marker[137] – in these cells expressing the DT receptor, thus induced to die after the treatment with DT. Protein synthesis inhibition caused by the toxin's penetrance into the cells iDTR$^+$ will activate a p53-dependent apoptosis, in which *PUMA* is a key mediator[137,138].

During FACS only living cells (DAPI$^+$) were collected for further analysis and there were still 36.6% of high-red cells detected in the embryos treated with DT (**Figure 4.19 B**). Together with the fact that *Id2* expression level in the epithelial cells treated with DT is not null, this could mean that the cells analyzed by qPCR are the descendants of Id2$^+$ cells initially labeled, that survived the DT-mediated ablation.

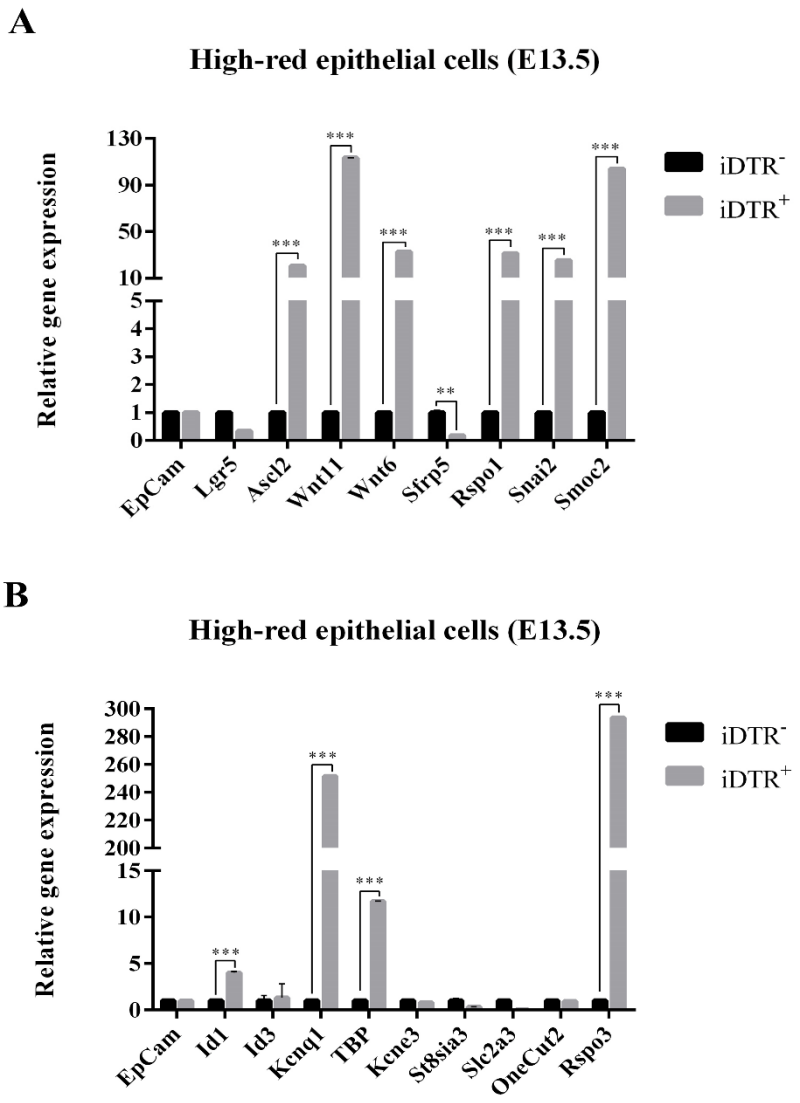

Figure 4. 33. Gene expression analysis of (A) *Lgr5, Ascl2, Wnt11, Wtn6, Sfrp5, Rspo1, Snai2, Smoc2*, (B) *Id1, Id3, Kcnq1, TBP, Kcne3, St8sia3, Slc2a3, OneCut* and *Rspo3* in high-red intestinal epithelial cells collected at E13.5. Results are shown as mean ± SEM, with N=3. Statistical significance was evaluated with Student's t test. ** corresponds to p<0.001 and *** to p<0.0001.

Besides *PUMA*, the following genes also showed statistical differences between both conditions: *Ascl2*, *Wnt6*, *Wnt11*, *Sfrp5*, *Rspo1*, *Snai2*, *Smoc2* (**Figure 4.33 A**) *Id1*, *Kcnq1*, *TBP* and *Rspo3* (**Figure 4.33 B**).

Ascl2 – a a basic HLH transcription factor that binds do the Lgr5 promoter[139] – and *Lgr5* showed opposite expression tendencies – an unexpected behaviour since they are both ISC markers. A similar finding was described by Mustata *et al*. (2013) when analyzing the genetic profile of organoids and spheroids[140], which requires further analysis. Even though the principal driver of *Ascl2* expression is the presence of Wnt/Rspo1 signalling[141] (and both are

upregulated in high-red epithelial iDTR$^+$ cells), there could be two reasons for the opposite behaviour of *Lgr5* regarding *Ascl2*. Either 1) *Lgr5* is being expressed but not transcript, which would require further analysis by Western Blot, or 2) since in wt conditions, *Lgr5* only starts to be expressed at E13.5 (the same day when the analysed cells were collect) – it could be that other proteins that play a role in its transcription are still not active, and thus, do not potentiate a more significant expression of this gene.

Genes involved in cell proliferation – *Wnt6* and *Wnt11* – are upregulated in the cells expressing the DT receptor. *Wnt11* was shown to be involved in cell proliferation and migration in the mouse intestinal cell line IEC6[54] and *Wnt6* is one of the major Wnt ligands expressed in the small intestine[142]. *Rspo1* and *Rspo3*, known Wnt agonists, are also overexpressed in the iDTR$^+$ condition. As stated before, it could be that the analyzed cells are Id2$^+$ labeled cells descendants, and thus their proliferative character, in order to reverse the cell loss. On the other hand, *Sfrp5* – a Wnt antagonist, this is, it interferes with Wnts in a negative manner – has an inverse expression profile compared with the Wnt genes analyzed, emphasizing the proliferative character of these cells.

Regarding stemness, genes associated with this property are also overexpressed in high-red epithelial iDTR$^+$ cells, namely *Smoc2*, an instestinal stem cell marker[18,143], and *Snai2*. In adult mice, *Smoc2* expression by ISC was reported by Muñoz *et al.* (2012) to be a probable physiological way to block BMP signaling in the stem cell niche[143]. *Snai2*, also known as *Slug*, is a Snail family member reported to promote cells to adopt stem cells properties and to maintain their stem cell activity[144]. *Id1* gene, that encodes a protein that plays a key role in the self-renewal of stem cells[145], is also upregulated in high-red epithelial iDTR+ cells. This gene is a target of the BMP pathway[146] and is reported to be able to maintain the self-renewal and pluripotency properties of embryonic stem cells in the absence of BMP[145]. To note that BMP was proposed to be a target of *Snai2*, since the overexpression of this gene cause the downregulation of BMP[147].

These results point to the downregulation of BMP caused by the overexpression of *Snai2* and, together with the high expression levels of Wnt genes, they evidence the high proliferative profile of this high-red cell population.

Results also show a significant statistical difference of *Kcnq1* expression on iDTR$^+$ cells. *Kcnq1* gene encodes for the pore-forming subunit of a voltage-gated potassium channel, enabling a K^+ current after electrical depolarization of the cell membrane. Together with *Kcne3*, they form a channel complex known to mediate the cAMP-activated basolateral K^+ current, essential for luminal Cl^- secretion[148]. Due to this, both genes play a critical role in ion homeostasis[149]. In acidic media, DT forms ion-conducting channels across the plasma membrane, conducting to a loss of cell potassium and the entrance of sodium and protons, which leads to a consequent rapid decrease of the membrane potential[150]. Given this, the upregulation of *Kcnq1* in DT-sensitive cells might indicate that the cells are trying to reverse the loss of potassium by creating more K^+ channels in order to increase the potassium uptake. Also, although both genes co-localize in the basolateral membranes of crypt cells in small intestine and colon, their expression levels differ – *Kcnq1* is prominently expressed in both of the organs, while *Kcne3* is expressed in lower levels in the small intestine[151] –, which might explain the low expression of *Kcne3*.

TPB is a key component of the transcription initiation machinery in eukaryotes, being involved in transcription by RNA polymerases I, II and III[152]. The overexpression of this gene increases the transcription from TATA-containing promoter[153], indicating that high-red iDTR$^+$ cells are expressing more genes, probably essential to maintain the homeostasis given their progenitors were under the effect of DT.

Non-red epithelial cells were also analyzed for the panel of genes mentioned above (**Figures 4.34 and 4.35**), in order to evaluate how the neighboring cells would respond to the ablation of the Id2$^+$ cells.

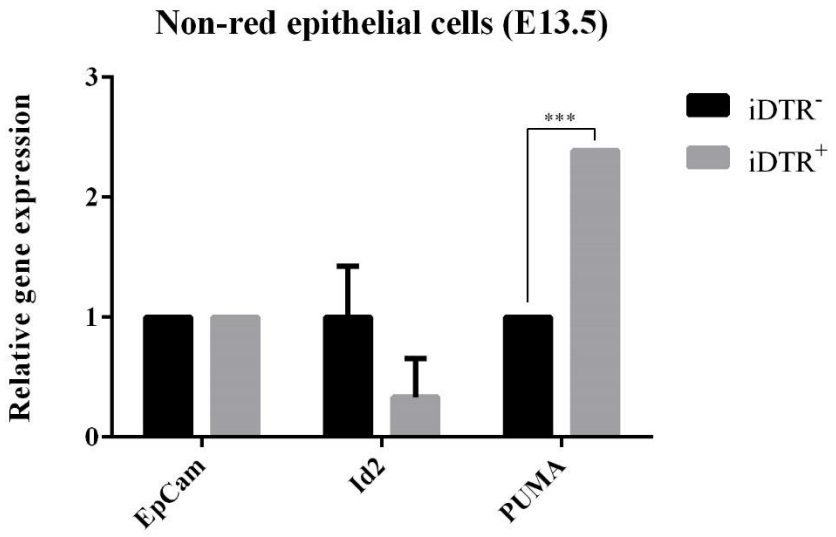

Figure 4. 34. Gene expression analysis of *Id2* and *PUMA* in non-red intestinal epithelial cells collected at E13.5. Results are shown as mean ± SEM, with N=3. Statistical significance was evaluated with Student's t test. *** corresponds to $p<0.0001$.

When compared to **figure 4.32**, results portrayed in the figure above show that the *Id2* expression levels are the same both in non-red and high-red epithelial cells. Regarding *PUMA*, this gene is about 10x less expressed in non-red epithelial $iDTR^+$ cells than in high-red epithelial cells in the same condition. This could be due to the fact that homologous recombination was quite efficient and gave origin mostly to triple positive cells ($Id2^+iDTR^+dsRed^+$) and thus there are less non-red $Id2^+iDTR^+$ cells sensitive do the toxin's action and, as a consequence, less *PUMA* expression detected.

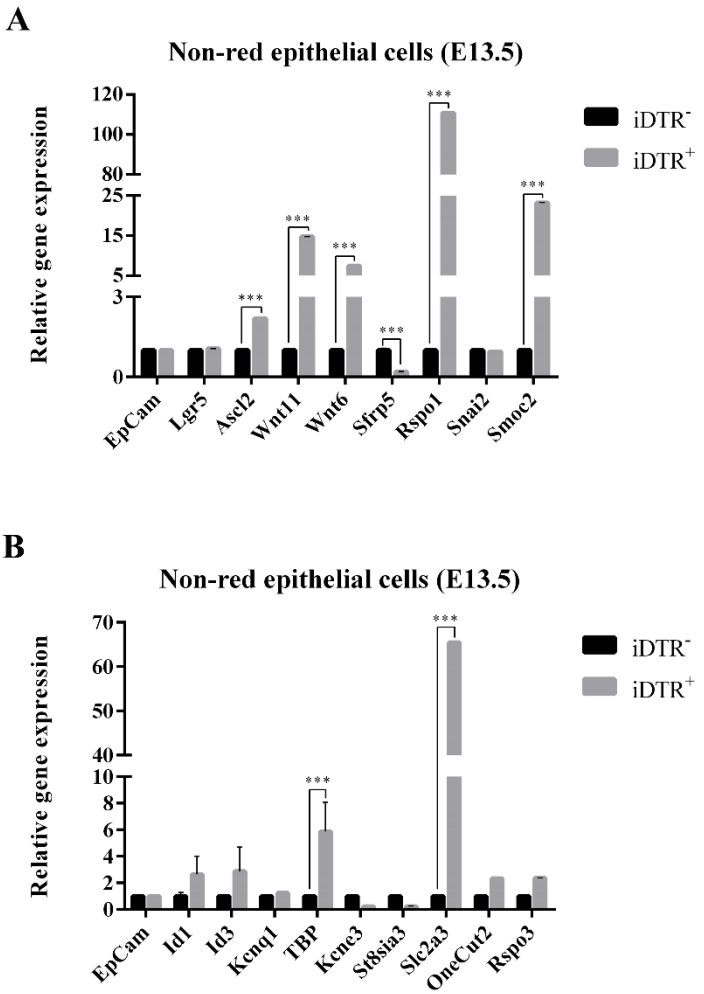

Figure 4. 35. Gene expression analysis of (A) *Lgr5, Ascl2, Wnt11, Wtn6, Sfrp5, Rspo1, Snai2, Smoc2*, (B) *Id1, Id3, Kcnq1, TBP, Kcne3, St8sia3, Slc2a3, OneCut* and *Rspo3* in non-red intestinal epithelial cells collected at E13.5. Results are shown as mean ± SEM, with N=3. Statistical significance was evaluated with Student's t test. * corresponds to $p<0.1$ and *** to $p<0.0001$.

When comparing the gene expression levels between the epithelial red cells (**Figure 4.33**) with the non-red (**Figure 4.35**), the latter show a different genetic profile. In the non-red epithelial cells, even though the expression of *Ascl2*, *Wnt11*, *Wnt6*, *Rspo1* and *Smoc2* (**Figure 4.35 A**) is statistically different between both conditions (iDTR$^-$ and iDTR$^+$) – similarly to the results shown previously for high-red epithelial intestinal cells –, their expression levels are much lower. Only *Rspo1* shows an increase in the expression levels, of about 2 times.

Besides *TBP*, *Slc2a3* expression level is also upregulated and statistically different between both conditions – iDTR$^-$ and iDTR$^+$ – in non-red epithelial cells (**Figure 4.35 B**). Also known as *Glut3*, *Slc2a3* encodes a protein that belongs to a family of integral proteins and plays a role in the transport of monosaccharides and other small carbon compounds across eukaryotic

cell's membranes[154]. When undergoing differentiation, the glycolytic flux in embryonic stem cells increases dramatically[155] and it is known that metabolic pathways might affect both homeostasis and quiescence[156], so this gene upregulation might be related to the glucose metabolism.

Taken together, these results also point to a proliferative character in this population, probably to compensate molecular signals that, in normal conditions, should be sent by the $Id2^{+}$ cell population.

5. CONCLUSIONS

The work here presented allowed to gain some insight about the overall efficiency of the DT-mediated cell ablation system in mouse embryos, since this methodology is mainly described in adult organisms.

This study aimed to establish a DT-mediated conditional ablation system within the embryonic small intestine in mouse cells expressing *Id2*. This gene, an inhibitor of DNA binding and differentiation, is known to play a role in several biological processes and is also involved in the lineage specific differentiation of intestinal cells.

The results presented in this report showed that the DT-mediated ablation system implemented triggered the specific apoptosis of the $Id2^+$ cells upon treatment with the toxin, since they are the only ones that express the DT receptor at their surface, thus being sensitive to the toxin's action. The apoptosis of $Id2^+$ cells was confirmed by immunostaining and histological analysis. Complementary analysis on this cell population performed by FACS, in a mouse strain where $Id2^+$ cells present red fluorescence, showed that upon treatment of the $iDTR^+$ cells with DT there is a reduction on the red $Id2^+$ cells. Also, FACS analysis on $iDTR^+$ mouse embryo epithelial cells suggest a correlation between $Id2^+$ and $Lgr5^+$ cells. The results showed that embryos expressing the DT receptor had a decrease of $Lgr5^+$ cells.

The genetic profile of the isolated high-red and non-red $Id2^+$ cells of $iDTR^-$ and $iDTR^+$ mouse embryos were evaluated, showing a partial ablation of *Id2* in $iDTR^+$ mouse embryos. Further analysis by qPCR showed an upregulation in genes involved in cell proliferation – such as *Wnt6*, *Wnt11* and their agonists *Rspo1* and *Rspo3* –, together with genes responsible for stem cell properties, as *Smoc2* and *Snai2*. In non-red cells, the same genes were upregulated, but at lower levels, suggesting a proliferative response in this population upon the ablation of $Id2^+$ cells.

With this study is was possible to conclude that cell ablation mediated by DT is a good technique to study the role of the $Id2^+$ cell population in the development of the mouse small intestine. Nevertheless, further optimization is needed, namely TAM and DT administration and dissection time points, to ensure that the time of dissection is near the time when the $Id2^+$ cells start to die. Also, more crossings to obtain $Id2^{Cre}dsRed^{+/+}Lgr5^{GFP}iDTR$ progeny should be done, in order to have a bigger population, and ensure that the results are indeed representative.

6. FUTURE PERSPECTIVES

Even though the data present in this report is indicative of efficiency of the DT-mediated ablation system, further optimization is needed and there are some aspects that need to be taken in consideration.

This system depends on blood circulation and on the presence of biological barriers, such as the placenta and the blood-brain barrier, and DT is only reported to cross the blood-brain barrier in adult mice[104]. Even though the work developed showed that the DT is able to take action in embryos, one of the future approaches could be the evaluation of this system in the absence of the potential limiting factors described, using a 3D cell culture technology, derived from epithelial embryonic cells collected from embryos, in which the resulting organoids would present the structural and functional main properties of the embryonic small intestine[157].

Also, because of the high toxicity of the fragment A of DT, one strategies to minimize potential risks to the embryos would be to repeat these experiments with the Id2^{Cre}DTA mice strain. Instead of having the DT receptor being expressed at the target cells – which will only be ablated upon DT treatment –, this stain harbors the gene that encodes for DT-A and, as a consequence, only the target cells will synthetize the DT subunit and die. Compared with the system used in this work, the DT-A ablation system requires only treatment with TAM in order to induce the homologous recombination, and thus it would be a good approach to eliminate the time points problems discussed here, allowing a better comprehension of the system.

7. REFERENCES

1. van der Flier LG, Clevers H. Stem cells, self-renewal, and differentiation in the intestinal epithelium. *Annu. Rev. Physiol.* 2009;71:241-260. doi:10.1146/annurev.physiol.010908.163145.

2. Spence JR, Lauf R, Shroyer NF. Vertebrate intestinal endoderm development. *Dev. Dyn.* 2011;240(3):501-520. doi:10.1002/dvdy.22540.

3. Clevers H, Loh KM, Nusse R. An integral program for tissue renewal and regeneration: Wnt signaling and stem cell control. *Science (80-.).* 2014;346(6205):1248012. doi:10.1126/science.1248012.

4. Zhang Z, Huang J. Intestinal stem cells - types and markers. *Cell Biol. Int.* 2013;37(5):406-414. doi:10.1002/cbin.10049.

5. Krausova M, Korinek V. Wnt signaling in adult intestinal stem cells and cancer. *Cell. Signal.* 2014;26(3):570-579. doi:10.1016/j.cellsig.2013.11.032.

6. Rao JN, Wang J-Y. Intestinal Architecture and Development. 2010. Available at: http://www.ncbi.nlm.nih.gov/books/NBK54098/. Accessed April 11, 2016.

7. Heath JK. *Transcriptional Networks and Signaling Pathways That Govern Vertebrate Intestinal Development*. Elsevier Inc.; 2010. doi:10.1016/S0070-2153(10)90004-5.

8. Rizk P, Barker N. Gut stem cells in tissue renewal and disease: methods, markers, and myths. *WIREs Syst Biol Med* 2012;4(October):475-496. doi:10.1002/wsbm.1176.

9. Medical Illustration Portfolio: Laurie O'Keefe: Medical Illustration Source Book. Available at: http://www.medillsb.com/ArtistPortfolioLarge.aspx?IID=43038&AID=342.

10. Bowcutt R, Forman R, Glymenaki M, Carding SR, Else KJ, Cruickshank SM. Heterogeneity across the murine small and large intestine. *World J. Gastroenterol.* 2014;20(41):15216-15232. doi:10.3748/wjg.v20.i41.15216.

11. Umar S. Intestinal Stem Cells. *Curr Gastroenterol Rep* 2010;12(5):340-348. doi:10.1007/s11894-010-0130-3.Intestinal.

12. Crosnier C, Stamataki D, Lewis J. Organizing cell renewal in the intestine: stem cells, signals and combinatorial control. *Nat. Rev. Genet.* 2006;7(5):349-359. doi:10.1038/nrg1840.

13. Yen T, Wright NA. The Gastrointestinal Tract Stem Cell Niche. *Stem Cell Rev.* 2006:203-212.

14. Moran GW, Leslie FC, Levison SE, Worthington J, McLaughlin JT. Enteroendocrine cells: neglected players in gastrointestinal disorders? *Therap. Adv. Gastroenterol.* 2008;1(1):51-60. doi:10.1177/1756283X08093943.

15. Clevers HC, Bevins CL. Paneth cells: maestros of the small intestinal crypts. *Annu. Rev. Physiol.* 2013;75:289-311. doi:10.1146/annurev-physiol-030212-183744.

16. Stange DE. Intestinal Stem Cells. *Dig. Dis.* 2013;31(3-4):293-298. doi:10.1159/000355231.

17. Barker N, Van Oudenaarden A, Clevers H. Identifying the stem cell of the intestinal crypt: Strategies and pitfalls. *Cell Stem Cell* 2012;11(4):452-460. doi:10.1016/j.stem.2012.09.009.

18. Tan DW, Barker N. *Intestinal Stem Cells and Their Defining Niche*. 1st ed. Elsevier Inc.; 2014. doi:10.1016/B978-0-12-416022-4.00003-2.

19. Sancho R, Cremona CA, Behrens A. Stem cell and progenitor fate in the mammalian intestine: Notch and lateral inhibition in homeostasis and disease. *EMBO Rep.* 2015;16(5):571-81. doi:10.15252/embr.201540188.

20. Howell JC, Wells JM. Generating intestinal tissue from stem cells: potential for research and

therapy. *Regen Med.* 2012;6(6):743-755. doi:10.2217/rme.11.90.Generating.

21. Noah TK, Donahue B, Shroyer NF. Intestinal development and differentiation. *Exp Cell Res.* 2011;317(19):2702-2710. doi:10.1242/dev.065789.

22. Hauck AL, Swanson KS, Kenis PJA, Leckband DE, Gaskins HR, Schook LB. Twists and Turns in the Development and Maintenance of the Mammalian Small Intestine Epithelium. *Birth Defects Res.* 2005;75(Part C):58-71. doi:10.1002/bdrc.20032.

23. Grosse AS, Pressprich MF, Curley LB, et al. Cell dynamics in fetal intestinal epithelium: implications for intestinal growth and morphogenesis. *Development* 2011;138:4423-4432. doi:10.1242/dev.065789.

24. Pirvulet V. Gastrointestinal stem cell up-to-date. *J. Med. Life* 2015;8(2):245-249.

25. Demitrack ES, Samuelson LC. Notch regulation of gastrointestinal stem cells. *J. Physiol.* 2016. doi:10.1113/JP271667.

26. Sancho R, Cremona CA, Behrens A. Stem cell and progenitor fate in the mammalian intestine: Notch and lateral inhibition in homeostasis and disease. *EMBO Rep.* 2015;16(5):571-81. doi:10.15252/embr.201540188.

27. Takashima S, Gold D, Hartenstein V. Stem cells and lineages of the intestine : a developmental and evolutionary perspective. *Dev Genes Evol* 2013;223:85-102. doi:10.1007/s00427-012-0422-8.

28. Sangiorgi E, Capecchi MR. Bmi1 is expressed in vivo in intestinal stem cells. *Nat. Genet.* 2008;40(7):915-20. doi:10.1038/ng.165.

29. Chia LA, Kuo CJ. The Intestinal Stem Cell. *Prog Mol Biol Transl Sci* 2010;96:157-173. doi:10.1016/B978-0-12-381280-3.00007-5.The.

30. Potten CS, Gandara R, Mahida YR, Loeffler M, Wright NA. The stem cells of small intestinal crypts: where are they? 2009:731-750. doi:10.1111/j.1365-2184.2009.00642.x.

31. Barker N, Bartfeld S, Clevers H. Tissue-resident adult stem cell populations of rapidly self-renewing organs. *Cell Stem Cell* 2010;7(6):656-670. doi:10.1016/j.stem.2010.11.016.

32. Date S, Sato T. Mini-Gut Organoids : Reconstitution of the Stem Cell Niche. 2015:269-292. doi:10.1146/annurev-cellbio-100814-125218.

33. De Mey JR, Freund J. Understanding epithelial homeostasis in the intestine: An old battlefield of ideas, recent breakthroughs and remaining controversies. *Tissue barriers* 2013;1(2):e24965. doi:10.4161/tisb.24965.

34. King SL, Dekaney CM. Small intestinal stem cells. *Curr. Opin. Gastroenterol.* 2013;29(2):140-5. doi:10.1097/MOG.0b013e32835cf253.

35. Barker N, Van Oudenaarden A, Clevers H. Identifying the stem cell of the intestinal crypt: Strategies and pitfalls. *Cell Stem Cell* 2012;11(4):452-460. doi:10.1016/j.stem.2012.09.009.

36. Yeung TM, Kuo CJ. Regulation of self-renewal and differentiation by the intestinal stem cell niche. *Cell Mol Life Sci.* 2011;68(15):2513-2523. doi:10.1007/s00018-011-0687-5.Regulation.

37. Barker N. Adult intestinal stem cells : critical drivers of epithelial homeostasis and regeneration. *Nat. Publ. Gr.* 2013;(December). doi:10.1038/nrm3721.

38. Montgomery RK, Breault DT. Small intestinal stem cell markers. *J. Anat.* 2008;213(1):52-58. doi:10.1111/j.1469-7580.2008.00925.x.

39. Barker N, van Es JH, Kuipers J, et al. Identification of stem cells in small intestine and colon by marker gene Lgr5. *Nature* 2007;449(7165):1003-1007. doi:10.1038/nature06196.

40. Batlle E. A new identity for the elusive intestinal stem cell. *Nat. Genet.* 2008;40(7):818-9. doi:10.1038/ng0708-818.

41. Reinisch C, Kandutsch S, Uthman A, Pammer J. BMI-1: A protein expressed in stem cells, specialized cells and tumors of the gastrointestinal tract. *Histol. Histopathol.* 2006;21(10-12):1143-1149.

42. Tian H, Biehs B, Warming S, et al. A reserve stem cell population in small intestine renders Lgr5-positive cells dispensable. *Nature* 2012;482(7383):120-120. doi:10.1038/nature10788.

43. Yan K, Chia L, Li X. The intestinal stem cell markers Bmi1 and Lgr5 identify two functionally distinct populations. *PNAS* 2012;109(2):466-471. doi:10.1073/pnas.1118857109/-/DCSupplemental.www.pnas.org/cgi/doi/10.1073/pnas.1118857109.

44. Ema H, Suda T. Two anatomically distinct niches regulate stem cell activity. *Blood* 2012;120(11):2174-2182. doi:10.1182/blood-2012-04-424507.

45. Sailaja BS, He XC, Li L. Regulatory niche in intestinal stem cells. *J. Physiol.* 2016;594(17):4827-36. doi:10.1113/JP271931.This.

46. Moore KA, Lemischka IR. Stem cells and their niches. *Science* 2006;311(5769):1880-1885. doi:10.1126/science.1110542.

47. Lane SW, Williams D a, Watt FM. Modulating the stem cell niche for tissue regeneration. *Nat. Biotechnol.* 2014;32(8):795-803. doi:10.1038/nbt.2978.

48. Sato T, van Es JH, Snippert HJ, et al. Paneth cells constitute the niche for Lgr5 stem cells in intestinal crypts. *Nature* 2011;469(7330):415-8. doi:10.1038/nature09637.

49. Bjerknes M, Cheng H. Modulation of specific intestinal epithelial progenitors by enteric neurons. *Proc. Natl. Acad. Sci. U. S. A.* 2001;98(22):12497-502. doi:10.1073/pnas.211278098.

50. Aoki R, Shoshkes-carmel M, Gao N, et al. Foxl1-Expressing Mesenchymal Cells Constitute the Intestinal Stem Cell Niche. *Cell. Mol. Gastroenterol. Hepatol.* 2016;2(2):175-188. doi:10.1016/j.jcmgh.2015.12.004.

51. Kühl SJ, Kühl M. On the role of Wnt/β-catenin signaling in stem cells. *Biochim. Biophys. Acta - Gen. Subj.* 2013;1830(2):2297-2306. doi:10.1016/j.bbagen.2012.08.010.

52. Jin YR, Yoon JK. The R-spondin family of proteins: Emerging regulators of WNT signaling. *Int. J. Biochem. Cell Biol.* 2012;44(12):2278-2287. doi:10.1016/j.biocel.2012.09.006.

53. Sokol SY. Spatial and temporal aspects of Wnt signaling and planar cell polarity during vertebrate embryonic development. 2016:78-85. doi:10.1016/j.semcdb.2015.05.002.Spatial.

54. Walters JRF. Recent findings in the cell and molecular biology of the small intestine. *Curr. Opin. Gastroenterol.* 2005;21(2):135-40. doi:10.1097/01.mog.0000153309.13080.8b.

55. Vincan E. *Wnt Signaling. Volume 1: Pathways, Methods and Mammal Models*.; 2008. doi:10.1007/978-1-59745-249-6.

56. Pinto D, Clevers H. Wnt control of stem cells and differentiation in the intestinal epithelium. *Exp. Cell Res.* 2005;306(2):357-363. doi:10.1016/j.yexcr.2005.02.022.

57. Reya T, Clevers H. Wnt signalling in stem cells and cancer. *Nature* 2005;434(7035):843-50. doi:10.1038/nature03319.

58. Vanuytsel T, Senger S, Fasano A, Shea-Donohue T. Major Signaling Pathways in Intestinal Stem Cells. *Biochim. Biophys. Acta* 2013;1830(2):2410-2426. doi:10.1016/j.bbagen.2012.08.006.Major.

59. Pinto D, Clevers H. Wnt, stem cells and cancer in the intestine. *Biol. Cell* 2005;97(3):185-196.

doi:10.1042/BC20040094.

60. Gao B. *Wnt Regulation of Planar Cell Polarity (PCP)*. 1st ed. Elsevier Inc.; 2012. doi:10.1016/B978-0-12-394592-1.00008-9.

61. Komiya Y, Habas R. Wnt signal transduction pathways. *Organogenesis* 2008;4(2):68-75. doi:10.4161/org.4.2.5851.

62. Farin HF, Jordens I, Mosa MH, et al. Visualization of a short-range Wnt gradient in the intestinal stem-cell niche. *Nature* 2016;530(7590):340-3. doi:10.1038/nature16937.

63. Garcia MI, Ghiani M, Lefort A, Libert F, Strollo S, Vassart G. LGR5 deficiency deregulates Wnt signaling and leads to precocious Paneth cell differentiation in the fetal intestine. *Dev. Biol.* 2009;331(1):58-67. doi:10.1016/j.ydbio.2009.04.020.

64. Gregorieff A, Clevers H. Wnt signaling in the intestinal epithelium: from endoderm to cancer. 2005:877-890. doi:10.1101/gad.1295405.

65. Kumar KK, Burgess AW, Gulbis JM. Structure and function of LGR5: An enigmatic G-protein coupled receptor marking stem cells. *Protein Sci.* 2014;23(5):551-565. doi:10.1002/pro.2446.

66. de Lau W, Peng WC, Gros P, Clevers H. The R-spondin/Lgr5/Rnf43 module: Regulator of Wnt signal strength. *Genes Dev.* 2014;28(4):305-316. doi:10.1101/gad.235473.113.

67. Bragdon B, Moseychuk O, Saldanha S, King D, Julian J, Nohe A. Bone Morphogenetic Proteins: A critical review. *Cell. Signal.* 2011;23(4):609-620. doi:10.1016/j.cellsig.2010.10.003.

68. Wang RN, Green J, Wang Z, et al. Bone Morphogenetic Protein (BMP) signaling in development and human diseases. *Genes Dis.* 2014;1(1):87-105. doi:10.1016/j.gendis.2014.07.005.

69. Yang J, Shi P, Tu M, et al. Bone morphogenetic proteins: Relationship between molecular structure and their osteogenic activity. *Food Sci. Hum. Wellness* 2014;3(3-4):127-135. doi:10.1016/j.fshw.2014.12.002.

70. Rahman MS, Akhtar N, Jamil HM, Banik RS, Asaduzzaman SM. TGF-β/BMP signaling and other molecular events: regulation of osteoblastogenesis and bone formation. *Bone Res.* 2015;3(November 2014):15005. doi:10.1038/boneres.2015.5.

71. Vrijens K, Lin W, Cui J, et al. Identification of Small Molecule Activators of BMP Signaling. *PLoS One* 2013;8(3). doi:10.1371/journal.pone.0059045.

72. Bandyopadhyay A, Yadav PS, Prashar P. BMP signaling in development and diseases: A pharmacological perspective. *Biochem. Pharmacol.* 2013;85(7):857-864. doi:10.1016/j.bcp.2013.01.004.

73. Dyer LA, Pi X, Patterson C. The role of BMPs in endothelial cell function and dysfunction. *Trends Endocrinol. Metab.* 2014;25(9):472-80. doi:10.1016/j.tem.2014.05.003.

74. Bray S. Notch signalling: a simple pathway becomes complex. *Nat. Rev. Mol. Cell Biol.* 2006;7(September):678-689. doi:10.1038/nrm2009.

75. Andersson ER, Sandberg R, Lendahl U. Notch signaling: simplicity in design, versatility in function. *Development* 2011;138(17):3593-3612. doi:10.1242/dev.063610.

76. Koch U, Lehal R, Radtke F. Stem cells living with a Notch. *Development* 2013;140(4):689-704. doi:10.1242/dev.080614.

77. Yuan X, Wu H, Xu H, et al. Notch signaling: An emerging therapeutic target for cancer treatment. *Cancer Lett.* 2015;369(1):20-27. doi:10.1016/j.canlet.2015.07.048.

78. Hori K, Sen A, Artavanis-Tsakonas S. Notch signaling at a glance. *J. Cell Sci.* 2013;126(Pt 10):2135-40. doi:10.1242/jcs.127308.

79. Schweisguth F. Regulation of Notch Signaling Activity. *Curr. Biol.* 2004;14(3):129-138. doi:10.1016/S0960-9822(04)00038-7.

80. Chillakuri CR, Sheppard D, Lea SM, Handford PA. Notch receptor-ligand binding and activation: Insights from molecular studies. *Semin. Cell Dev. Biol.* 2012;23(4):421-428. doi:10.1016/j.semcdb.2012.01.009.

81. Noah TK, Shroyer NF. Notch in the intestine: regulation of homeostasis and pathogenesis. *Annu Rev Physiol* 2013;75:263-288. doi:10.1146/annurev-physiol-030212-183741.

82. Madison BB, Nakagawa H. Delta force in intestinal crypts. *Gastroenterology* 2011;140(4):1135-1139. doi:10.1053/j.gastro.2011.02.030.

83. Saqui-Salces M, Merchant JL. Hedgehog signaling and gastrointestinal cancer. *Biochim. Biophys. Acta* 2010;1803(7):786-795. doi:10.1016/j.bbamcr.2010.03.008.

84. Takebe N, Miele L, Harris PJ, et al. Targeting Nothc, HEdgehog, and Wnt Pathways in cancer stem cells: clinical update. *Nat Rev Clin Oncol* 2015;12(8):445-464. doi:10.1038/nrclinonc.2015.61.Targeting.

85. Cochrane C, Szczepny A, Watkins D, Cain J. Hedgehog Signaling in the Maintenance of Cancer Stem Cells. *Cancers (Basel).* 2015;7(3):1554-1585. doi:10.3390/cancers7030851.

86. Watkins DN, Peacock CD. Hedgehog signalling in foregut malignancy. *Biochem. Pharmacol.* 2004;68(6):1055-1060. doi:10.1016/j.bcp.2004.04.025.

87. Varjosalo M, Taipale J. Hedgehog: Functions and mechanisms. *Genes Dev.* 2008;22(18):2454-2472. doi:10.1101/gad.1693608.

88. Xie J, Bartels CM, Barton SW, Gu D. Targeting hedgehog signaling in cancer: Research and clinical developments. *Onco. Targets. Ther.* 2013;6:1425-1435. doi:10.2147/OTT.S34678.

89. Brink GR. Hedgehog Signaling in Development and Homeostasis of the Gastrointestinal Tract. *Physiol Rev* 2007;87:1343-1375. doi:10.1152/physrev.00054.2006.

90. Herath NI, Boyd AW. The role of Eph receptors and ephrin ligands in colorectal cancer. *Int. J. Cancer* 2010;126(9):2003-2011. doi:10.1002/ijc.25147.

91. Kania A, Klein R. Mechanisms of ephrin-Eph signalling in development, physiology and disease. *Nat. Rev. Mol. Cell Biol.* 2016;17(4):240-56. doi:10.1038/nrm.2015.16.

92. Pasquale EB. Eph receptors and ephrins in cancer: bidirectional signalling and beyond. *Nat Rev Cancer.* 2010;10(3):165-180. doi:10.1038/nrc2806.Eph.

93. Lisabeth EM, Falivelli G, Pasquale EB. Eph Receptor Signaling and Ephrins. *Cold Spring Harb Perspect Biol* 2013;5:1-20.

94. Holder N, Klein R. Eph receptors and ephrins: effectors of morphogenesis. *Development* 1999;126(10):2033-2044.

95. Pasquale EB. Eph receptor signalling casts a wide net on cell behaviour. *Nat. Rev. Mol. Cell Biol.* 2005;6(6):462-75. doi:10.1038/nrm1662.

96. Stent GS. The role of cell lineage in development. *Philos. Trans. R. Soc. London B Biol. Sci.* 1985;312(1153):3-19. doi:10.1098/rstb.1985.0174.

97. Kretzschmar K, Watt FM. Lineage tracing. *Cell* 2012;148(1-2):33-45. doi:10.1016/j.cell.2012.01.002.

98. Fink J, Koo B. Clonal Evolution of Stem Cells in the Gastrointestinal Tract. In: Jansen M,

Wright NA, eds. *Stem Cells, Pre-Neoplasia, and Early Cancer of the Upper Gastrointestinal Tract, Advances in Experimental Medicine and Biology 908*.Vol 908. Springer International Publishing; 2016:11-25. doi:10.1007/978-3-319-41388-4.

99. Saito M, Iwawaki T, Taya C, et al. Diphtheria toxin receptor-mediated conditional and targeted cell ablation in transgenic mice. *Nat. Biotechnol.* 2001;19(8):746-750. doi:10.1038/90795.

100. Villalon E, Schulz DJ, Waters ST. Mouse Molecular Embryology. 2014;1092:81-94. doi:10.1007/978-1-60327-292-6.

101. Saxe MD, Battaglia F, Wang J-W, et al. Ablation of hippocampal neurogenesis impairs contextual fear conditioning and synaptic plasticity in the dentate gyrus. *Proc. Natl. Acad. Sci. U. S. A.* 2006;103(46):17501-6. doi:10.1073/pnas.0607207103.

102. Dupret D, Revest JM, Koehl M, et al. Spatial relational memory requires hippocampal adult neurogenesis. *PLoS One* 2008;3(4). doi:10.1371/journal.pone.0001959.

103. Murphy JR. Mechanism of diphtheria toxin catalytic domain delivery to the eukaryotic cell cytosol and the cellular factors that directly participate in the process. *Toxins (Basel).* 2011;3(3):294-308. doi:10.3390/toxins3030294.

104. Buch T, Heppner FL, Tertilt C, et al. A Cre-inducible diphtheria toxin receptor mediates cell lineage ablation after toxin administration. *Nat. Methods* 2005;2(6):419-426. doi:10.1038/nmeth762.

105. Zhang J, Wei H, Guo X, et al. Functional verification of the diphtheria toxin A gene in a recombinant system. *J. Anim. Sci. Biotechnol.* 2012;3(1):29. doi:10.1186/2049-1891-3-29.

106. Wisnieskisll J. Characterization of the Deoxyribonuclease Activity of Diphtheria Toxin. *J. Biol. Chem.* 1990;265(9):5237-5241.

107. Chang MP, Baldwin RL, Bruce C, Wisnieski BJ. Second cytotoxic pathway of diphtheria toxin suggested by nuclease activity. *Science* 1989;246(4934):1165-1168. doi:10.1126/science.2531465.

108. Lee JW, Nakamura LT, Chang MP, Wisnieski BJ. Mechanistic aspects of the deoxyribonuclease activity of diphtheria toxin. *Biochim. Biophys. Acta - Proteins Proteomics* 2005;1747(1):121-131. doi:10.1016/j.bbapap.2004.10.003.

109. Higashiyama S, Abraham JA, Miller J, Fiddes JC, Klagsburn M. A heparin-binding growth factor secteted by macrophage-like cells that is related to EGF. *Science (80-.).* 1991;251(October):936-939.

110. Oyagi A, Hara H. Essential roles of heparin-binding epidermal growth factor-like growth factor in the brain. *CNS Neurosci. Ther.* 2012;18(10):803-810. doi:10.1111/j.1755-5949.2012.00371.x.

111. Miyamoto S, Yagi H, Yotsumoto F, Kawarabayashi T, Mekada E. Heparin-binding epidermal growth factor-like growth factor as a novel targeting molecule for cancer therapy. *Cancer Sci.* 2006;97(5):341-347. doi:10.1111/j.1349-7006.2006.00188.x.

112. Luetteke NC. Targeted inactivation of the EGF and amphiregulin genes reveals distinct roles for EGF receptor ligands in mouse mammary gland development. *Development* 1999;126:2739-2750.

113. Iwamoto R, Yamazaki S, Asakura M, et al. Heparin-binding EGF-like growth factor and ErbB signaling is essential for heart function. *Proc. Natl. Acad. Sci. U. S. A.* 2003;100(6):3221-6. doi:10.1073/pnas.0537588100.

114. Iwamoto R, Mekada E. ErbB and HB-EGF signaling in heart development and function. *Cell Struct. Funct.* 2006;31(1):1-14. doi:10.1247/csf.31.1.

115. Ling F, Kang B, Sun XH. *Id Proteins: Small Molecules, Mighty Regulators*. 1st ed. Elsevier Inc.; 2014. doi:10.1016/B978-0-12-405943-6.00005-1.

116. Kurooka H, Yokota Y. Nucleo-cytoplasmic shuttling of Id2, a negative regulator of basic helix-loop-helix transcription factors. *J. Biol. Chem.* 2005;280(6):4313-4320. doi:10.1074/jbc.M412614200.

117. Lasorella A, Benezra R, Iavarone A. The ID proteins: master regulators of cancer stem cells and tumour aggressiveness. *Nat. Rev. Cancer* 2014;14(2):77-91. doi:10.1038/nrc3638.

118. Jen Y, Manova K, Benezra R. Expression patterns of Id1, Id2, and Id3 are highly related but distinct from that of Id4 during mouse embryogenesis. *Dev. Dyn.* 1996;207(3):235-252. doi:10.1002/(SICI)1097-0177(199611)207:3<235::AID-AJA1>3.0.CO;2-I.

119. Id2 inhibitor of DNA binding 2 [Mus musculus (house mouse)] - Gene - NCBI. Available at: http://www.ncbi.nlm.nih.gov/gene/15902. Accessed April 10, 2016.

120. Matsuura R, Kogo H, Ogaeri T, et al. Crucial transcription factors in endoderm and embryonic gut development are expressed in gut-like structures from mouse ES cells. *Stem Cells* 2006;24(3):624-30. doi:10.1634/stemcells.2005-0344.

121. Russell RG, Lasorella A, Dettin LE, Iavarone A. Id2 Drives Differentiation and Suppresses Tumor Formation in the Intestinal Epithelium. *Cancer Res.* 2004;(64):7220-7225.

122. Glick B, Pasternak J. *Molecular Biotechnology: Principles and Applications of Recombinant DNA*. 4th ed. ASM Press; 2010.

123. Maity B, Sheff D, Fisher RA. *Immunostaining. Detection of Signaling Protein Location in Tissues, Cells and Subcellular Compartments.* Elsevier; 2013. doi:10.1016/B978-0-12-407239-8.00005-7.

124. Fischer AH, Jacobson KA, Rose J, Zeller R. Hematoxylin and eosin staining of tissue and cell sections. *Cold Spring Harb. Protoc.* 2008;3(5):3-5. doi:10.1101/pdb.prot4986.

125. Cardiff RD, Miller CH, Munn RJ. Manual hematoxylin and eosin staining of mouse tissue sections. *Cold Spring Harb. Protoc.* 2014;2014(6):655-658. doi:10.1101/pdb.prot073411.

126. Long Range PCR | NEB. Available at: https://www.neb.com/applications/dna-amplification-and-pcr/specialty-pcr/long-range-pcr. Accessed April 12, 2016.

127. 12 things you don't know about Cre-lox. 2013. Available at: https://www.jax.org/news-and-insights/jax-blog/2013/september/a-dozen-facts-you-didnt-know-about-cre-lox. Accessed August 18, 2016.

128. Cre-lox myths busted. 2013. Available at: https://www.jax.org/news-and-insights/jax-blog/2013/september/cre-lox-myths-busted. Accessed August 16, 2016.

129. Aktories K, Just I, eds. *Bacterial Protein Toxins*. Springer Science & Business Media; 2000.

130. Atale N, Gupta S, Yadav UCS, Rani V. Cell-death assessment by fluorescent and nonfluorescent cytosolic and nuclear staining techniques. *J. Microsc.* 2014;255(1):7-19. doi:10.1111/jmi.12133.

131. Huang X, Darzynkiewicz Z. Cytometric Assessment of Histone H2AX Phophorylation: A Reporter of DNA Damage. *Methods Mol Biol.* 2006;314:73-80.

132. Sharma A, Singh K, Almasan A. Histone H2AX Phosphorylation: A Marker for DNA Damage. In: *DNA Repair Protocols*.Vol 920.; 2012:613-626. doi:10.1007/978-1-61779-998-3.

133. Torihashi S, Kuwahara M, Ogaeri T, Zhu P, Kurahashi M, Fujimoto T. Gut-like structures from mouse embryonic stem cells as an in vitro model for gut organogenesis preserving developmental potential after transplantation. *Stem Cells* 2006;24(12):2618-26.

doi:10.1634/stemcells.2006-0148.

134. Danielian P, Muccino D, Rowitch D, Michael S, McMahon A. Modification of gene activity in mouse embryos in utero by a tamoxifen-inducible form of Cre recombinase. *Curr Biol.* 1198;Dec 3(8):1323-6. Available at: http://www.ncbi.nlm.nih.gov/pubmed/9843687.

135. Nakamura E, Nguyen M-T, Mackem S. Kinetics of tamoxifen-regulated Cre activity in mice using a cartilage-specific CreER(T) to assay temporal activity windows along the proximodistal limb skeleton. *Dev. Dyn.* 2006;235(9):2603-12. doi:10.1002/dvdy.20892.

136. Robinson SP, Langan-Fahey SM, Johnson DA, Jordan VC. Metabolites, pharmacodynamics, and pharmacokinetics of tamoxifen in rats and mice compared to the breast cancer patient. *Drug Metab. Dispos.* 19(1):36-43. Available at: http://www.ncbi.nlm.nih.gov/pubmed/1673419. Accessed July 25, 2016.

137. Hikisz P, Kiliańska ZM. PUMA, a critical mediator of cell death--one decade on from its discovery. *Cell. Mol. Biol. Lett.* 2012;17(4):646-69. doi:10.2478/s11658-012-0032-5.

138. Meijer L, Guidet S, Vogel L, eds. Apoptosis and Cell Cycle. In: *Progress in Cell Cycle Research, Volume 2*. Springer US; 1996:155. doi:10.1007/978-1-4615-5873-6.

139. Yan KS, Kuo CJ. Ascl2 reinforces intestinal stem cell identity. *Cell Stem Cell* 2015;16(2):105-106. doi:10.1016/j.stem.2015.01.014.

140. Mustata RC, Vasile G, Fernandez-Vallone V, et al. Identification of Lgr5-Independent Spheroid-Generating Progenitors of the Mouse Fetal Intestinal Epithelium. *Cell Rep.* 2013;5(2):421-432. doi:10.1016/j.celrep.2013.09.005.

141. Schuijers J, Junker JP, Mokry M, et al. Ascl2 acts as an R-spondin/Wnt-responsive switch to control stemness in intestinal crypts. *Cell Stem Cell* 2015;16(2):158-170. doi:10.1016/j.stem.2014.12.006.

142. Richmond CA, Breault DT. Regulation of Gene Expression in the Intestinal Epithelium. *Prog Mol Biol Transl Sci* 2010;96:207-229. doi:10.1016/B978-0-12-381280-3.00009-9.REGULATION.

143. Muñoz J, Stange DE, Schepers AG, et al. The Lgr5 intestinal stem cell signature: robust expression of proposed quiescent "+4" cell markers. *EMBO J.* 2012;21(14):3079-3091. doi:10.1038/emboj.2012.166.

144. Horvay K, Jardé T, Casagranda F, et al. Snai 1 regulates cell lineage allocation and stem cell maintenance in the mouse intestinal epithelium. *EMBO J.* 2015;34(10):1319-1336. doi:10.15252/embj.201490881.

145. Zhang N, Yantiss RK, Hyung-song N, et al. ID1 is a Functional Marker for Intestinal Stem and Progenitor Cells Required for Normal Response to Injury. *Stem Cell Reports* 2014;3(5):716-724. doi:10.1016/j.stemcr.2014.09.012.

146. Zhang N, Yantiss RK, Nam H, et al. ID1 Is a Functional Marker for Intestinal Stem and Progenitor Cells Required for Normal Response to Injury. *Stem Cell Reports* 2014;3(5):716.

147. Nieto MA. The Snail Superfamily of Zinc-Finger Transcription Factors. *Nat. Rev. Mol. Cell Biol.* 2002;3(3):155-166. doi:10.1038/nrm757.

148. Grahammer F, Warth R, Barhanin J, Bleich M, Hug MJ. The Small Conductance K+ Channel, KCNQ1. Expression, function, and subunit composition in murine trachea. *J. Biol. Chem.* 2001;276(45):42268-42275. doi:10.1074/jbc.M105014200.

149. Than BLN, Goos JACM, Sarver AL, et al. The role of KCNQ1 in mouse and human gastrointestinal cancers. *Oncogene* 2014;33(29):3861-8. doi:10.1038/onc.2013.350.

150. Papini E, Sandoná D, Rappuoli R, Montecucco C. On the membrane translocation of diphtheria

toxin: at low pH the toxin induces ion channels on cells. *EMBO J.* 1988;7(11):3353-9. Available at: http://www.pubmedcentral.nih.gov/articlerender.fcgi?artid=454832&tool=pmcentrez&rendertype=abstract.

151. Dedek K, Waldegger S. Colocalization of KCNQ1/KCNE channel subunits in the mouse gastrointestinal tract. *Pflügers Arch. Eur. J. Physiol.* 2001;442(6):896-902. Available at: http://www.ncbi.nlm.nih.gov/pubmed/11680623. Accessed September 5, 2016.

152. Akhtar W, Veenstra GJC. TBP-related factors: a paradigm of diversity in transcription initiation. *Cell Biosci.* 2011;1(1):23. doi:10.1186/2045-3701-1-23.

153. Müller F, Demény MA, Tora L. New problems in RNA polymerase II transcription initiation: Matching the diversity of core promoters with a variety of promoter recognition factors. *J. Biol. Chem.* 2007;282(20):14685-14689. doi:10.1074/jbc.R700012200.

154. Mueckler M, Thorens B. The SLC2 (GLUT) Family of Membrane Transporters. *Mol Asp. Med.* 2013;34(0):121-138. doi:10.1126/scisignal.2001449.Engineering.

155. Shyh-Chang N, Daley GQ, Cantley LC. Stem cell metabolism in tissue development and aging. *Development* 2013;140(12):2535-2547. doi:10.1242/dev.091777.

156. Ito K, Suda T. Metabolic requirements for the maintenance of self-renewing stem cells. *Nat. Rev. Mol. Cell Biol.* 2014;15(4):243-56. doi:10.1038/nrm3772.

157. Clevers H. Modeling Development and Disease with Organoids. *Cell* 2016;165(7):1586-1597. doi:10.1016/j.cell.2016.05.082.

158. Sherwood RI, Maehr R, Mazzoni EO, Melton DA. Wnt signaling specifies and patterns intestinal endoderm. *Mech. Dev.* 2011;128(7-10):387-400. doi:10.1016/j.mod.2011.07.005.

ANNEXES

Annex 1: Construction of Id2^{Cre}iDTR mouse strain

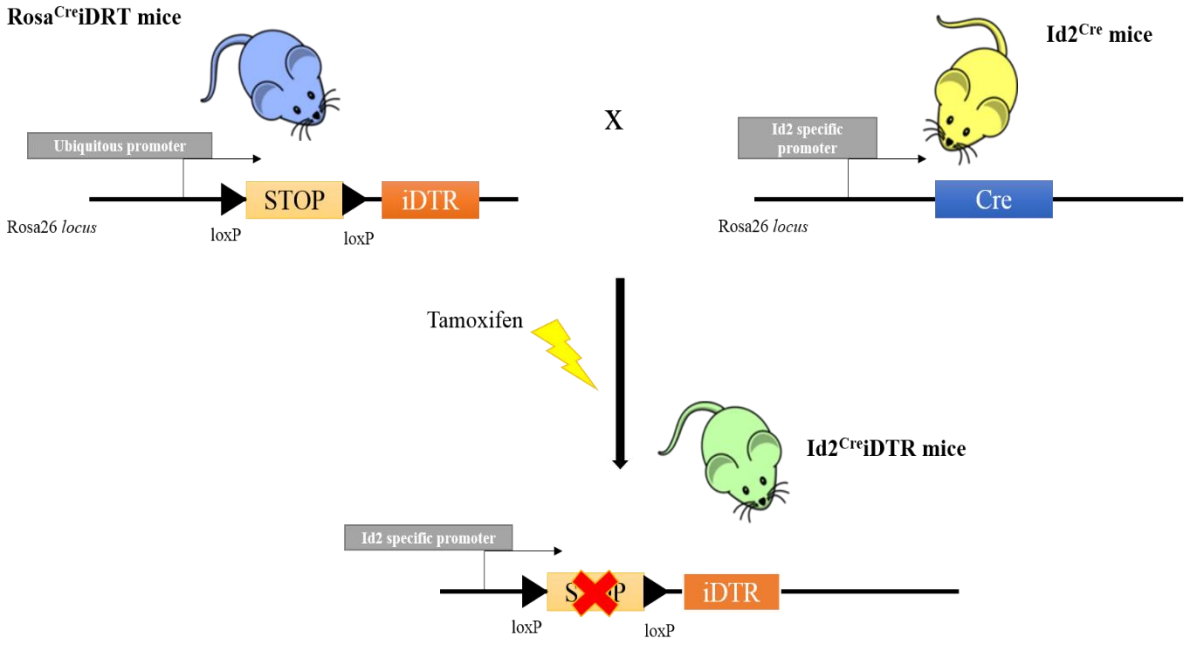

Annex 2: Anterior and posterior portions of the embryonic small intestine

Image adapted from Sherwood *et al*. (2011)[158].

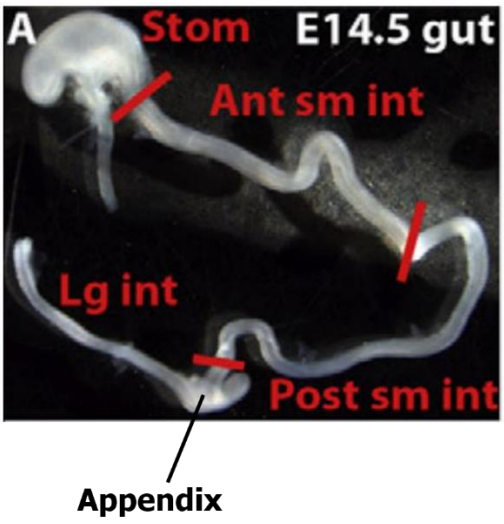

Stom: Stomach
Ant sm int: Anterior small intestine
Post sm int: Posterior small intestine
Lg int: Large intestine

Annex 3: Construction of Id2^{Cre}dsRed$^{+/-}$ iDTR